MONASH University

On Resource Allocation in Machine-Type Communication Networks

Ivana Nikoloska
M. Sci., Ss. Cyril and Methodius University, 2016
Dipl. Eng., Ss. Cyril and Methodius University, 2014

A thesis submitted for the degree of *Doctor of Philosophy* at
Monash University in 2020
Department of Electrical and Computer System Engineering

Copyright Notice

Abstract

Due to an ever increasing demand for data (and high data rates), the devices in the latest generations of wireless networks must be able to operate in places that are dangerous or hard to reach, with little or no human intervention, for prolonged periods of time. This raises many interesting questions, one of which is how to power an uninterrupted, perpetual operation for these machine-type devices, in cases when battery replacement/replenishment is not feasible or is not sustainable over time. Recently, the research community started exploring the potential of renewable energy sources, such as radio-frequency energy, which gives rise to the so called wirelessly powered communication networks (WPCNs). To deliver data with high data rates, the devices in WPCNs must make use of spectrally efficient technologies on the physical layer, such as full-duplex (FD) operation. For these FD networks, new communication protocols which are ultimately able to reach the limits of information flow in the network, i.e., the Shannon capacity, must be developed. A natural first step is to investigate the fundamental building blocks of these networks, and then exploit the obtained insights to design protocols for more complex networks.

Another pressing problem is how to allow a massive number of such machine-type devices access to the shared wireless channel in order for the devices to transmit their data. Most medium access control protocols have been primarily designed and optimised to support older generations of human to human communication networks. Thereby, new access protocols that accommodate the distinctive traffic demands of machine-type communication (MTC) networks need to be developed in order to scale the networks to massive number of devices.

This thesis is divided into two parts. In the first part, we propose new com-

munication protocols for the most basic building block of FD WPCNs. The first protocol is able to achieve the capacity of the network, whilst the second significantly improves the secrecy rate. In the second part, we propose a novel medium access control protocol for MTC networks with a massive number of devices. As a more indirect way to tackle medium access control, we consider semantic and effectiveness problems in MTC networks and we propose data selection and filtering schemes which achieve high inference precision, whilst preserving the already scarce resources of the MTC devices.

Publications During Enrolment

The following publications have arisen from the research reported in this thesis.

1 I. Nikoloska, N. Zlatanov, and Z. Hadzi-Velkov, ”Capacity of a Full-Duplex Wirelessly Powered Communication System with Self-Interference and Processing Cost”, IEEE Transactions on Wireless Communications, vol. 17, no. 11, pp. 7648 - 7660, 2018.

2 I. Nikoloska, N. Zlatanov, and Z. Hadzi-Velkov, ”On the Capacity of a Full-Duplex Wirelessly Powered Communication System with Self-Interference and Processing Cost”, in proceedings, IEEE ICC, Kansas City, MO, USA, May 2018.

3 I. Nikoloska, N. Zlatanov, Z. Hadzi-Velkov, and R. Zhang ”On the Secrecy Capacity of a Full-Duplex Wirelessly Powered Communication System”, IEEE Transactions on Wireless Communications, vol.18, no. 11, pp. 5424 - 5439, 2019.

4 I. Nikoloska, N. Zlatanov, Z. Hadzi-Velkov, and R. Zhang ”On the Secrecy Capacity of a Full-Duplex Wirelessly Powered Communication System”, in proceedings, IEEE ISWCS, Oulu, Finland, August 2019.

5 I. Nikoloska, and N. Zlatanov, ”Deep Reinforcment Learning Random Access”, submitted to the IEEE Transactions on Wireless Communications.

6 I. Nikoloska, and N. Zlatanov, ”Data Selection Scheme for Energy Efficient Supervised Learning at IoT Nodes”, IEEE Communication Letters, 2020.

Thesis Including Published Works Declaration

This thesis includes 3 original papers published in peer reviewed journals and 2 original papers published in conference proceedings. The core theme of the thesis is resource allocation in wirelessly powered communication networks and machine-type communication networks. The ideas, development and writing up of all the papers in the thesis were the principal responsibility of myself, the student, working within the Department of Electrical and Computer Systems Engineering under the supervision of Dr. Nikola Zlatanov.

The inclusion of co-authors reflects the fact that the work came from active collaboration between researchers and acknowledges input into team-based research.

In the case of Chapters 2, 3 and 5 my contribution to the work involved the following:

Thesis Chapter	Publication Title	Status	Nature and % of student contribution	Co-author name(s) Nature and % of Co-author's contribution	Co-author(s), Monash student Y/N
2	Capacity of a Full-Duplex Wirelessly Powered Communication System with Self-Interference and Processing Cost	Published	75%, deriving the results, numerical evaluation of the results, and writing the paper	20% NZ, input into the manuscript; 5% ZHV, input into the manuscript	No
3	On the Secrecy Capacity of a Full-Duplex Wirelessly Powered Communication System	Published	75%, defining the system model, deriving the results, numerical evaluation of the results, and writing the paper	15% NZ, input into the manuscript; 5% ZHV, input into the manuscript; 5% RZ, input into the manuscript	No
5	Data Selection Scheme For Energy Efficient Supervised Learning At IoT nodes	Published	80%, defining the system model, constructing and evaluating the algorithm, and writing the paper	20% NZ, input into the manuscript;	No

I have not renumbered sections of submitted or published papers in order to generate a consistent presentation within the thesis.

Student name: Ivana Nikoloska

Student signature: **Date:**

I hereby certify that the above declaration correctly reflects the nature and extent of the student's and co-authors' contributions to this work. In instances where I am not the responsible author I have consulted with the responsible author to agree on the respective contributions of the authors.

Main Supervisor name: Dr. Nikola Zlatanov

Main Supervisor signature: **Date:**

Acknowledgements

This thesis deals with enabling machines with rudimentary capabilities to communicate, learn and think. In a way, this premise is also a good analogy for my experience in the last three years. During this time, I did indeed acquire many technical skills, but I also learnt how to communicate clearly. I learnt how to learn new concepts. Most importantly, I learnt how to think critically when approaching the unknown.

In the process, I've accumulated an extensive list of gratitude debts, which I will attempt to compress in the following few paragraphs. However, as any information theorist will readily tell you, compression can be lossy, and whilst some entries in this list might not be mentioned here, all are sincerely appreciated.

First, I would like to acknowledge the role luck played in getting this far. I was incredibly lucky to have Dr. Nikola Zlatanov as my doctoral supervisor. I will forever be grateful for his steady guidance, invaluable advice, and relentless critical feedback. Dr. Zlatanov encouraged independence in research, whilst providing constant support, and this thesis wouldn't be possible without him.

I would also like to gratefully acknowledge the hospitality of Prof. Petar Popovski, and the entire Section on Connectivity during my stay at Aalborg University.

Thanks to all of my colleagues and friends at ECSE for your support and entertainment. These years have been much more colorful because of your company.

Lastly, I certainly wouldn't be where I am today without the unwavering support and unconditional love of my mother Vasa, my father Vito, and my brother Jane, who live 15226 km away, but somehow never felt distant. Thank you for teaching me to be endlessly curious, for never letting me be blind to my blindness,

and for reminding me that most of the time, we suffer more in imagination, than in reality.

To my Family.

Table of Contents

List of Tables

List of Figures

Chapter 1

Introduction

Since the 1940s, communication engineers have been tirelessly working on solving *technical problems*, namely finding ways to reliably transmit information from a sender to a recipient [1]. Traditionally the senders and receivers of information have been humans. The latest generations of communication networks include a different paradigm, namely networks where the end user is the machine itself, commonly refereed to as (massive) machine-type communication (MTC). As the foundation of the Internet of Things (IoT), MTC networks are expected to be crucial in next generation smart cities, smart homes, automated factories, automated health management systems, and many other applications, some of which can not even be foreseen today [2]. The current trajectory of the number of devices being deployed implies that eventually trillions of things will be connected to the Internet. For reference, the number of connected devices to the Internet surpassed the human population in 2010 and 75 billion connected devices are expected by 2025. As the scale of MTC networks continues to increase, it is a near certainty that we will experience a data-driven society, enabled by near instant and unlimited wireless connectivity.

Concurrently, green technologies, such as green radio communications and energy harvesting (EH) [3] have also been gaining popularity in the wireless communication community. Whilst the former aims at minimizing the use of precious radio resources, the latter relies on harvesting energy from renewable and environmentally friendly sources such as solar, thermal, vibration or wind, to support the

transmission of information [4]. Thereby, EH promises a perpetual operation of communication networks. Moreover, EH completely eliminates the need for battery replacement and/or using power cords, making it a highly convenient option for communication networks with nodes which are hard or dangerous to reach, such as MTC networks. However, EH communication networks are subjected to their own set of challenges. For example, ambient energy sources are often intermittent and scarce, which can threaten the continuous reliability of the communication session. A possible solution to this problem is harvesting radio frequency (RF) energy from a dedicated energy transmitter, which gives rise to the so called wireless powered communication networks (WPCNs) [5], [6].

Due to the sporadic sensing and communication activity of MTC nodes, the average power requirement of these devices is in the order of microwatts to milliwatts. This can easily be met by harvesting RF energy, making MTC networks ideal representatives of WPCNs. However, whilst MTC devices might be the greatest beneficiaries from wireless power, the technology is much broader in scope. Indeed, numerous studies have ascertained the feasibility of using RF EH in backscattering networks [7], device-to-device networks [8], mmwave networks [9] and even cellular networks and HetNets [10]. The devices in these networks (as well as their requirements) are fundamentally different, and yet all can benefit from utilizing wireless power to prolong or supplement their operation. Thereby, WPCNs deserve to be considered as a device agnostic, umbrella solution, instead of being exclusively associated with MTC networks.

A logical first step in investigating WPCNs is to explore the theoretical limits of information flow in the fundamental building block of the network. Based on the derived rate, i.e., the Shannon capacity, one can design a practical code that attempts to achieve (or at least come close to) the capacity. Moreover, these fundamental results can be used as guidelines when investigating more complex networks of a massive number of devices. By all means, under certain assumptions, the derived results hold for the building blocks of MTC networks powered by RF EH.

This thesis is divided into two parts. The first part will focus on the fundamental limits of WPCNs, and the second part is specific to MTC networks. In this chapter, we provide the motivation and contribution for Part 1 in Section 1.1.

The motivation and contribution of Part 2 is provided in Section 1.2. Finally, the organisation of this thesis is given in Section 1.3.

1.1 Part 1: Capacity and Secrecy Capacity of FD WPCNs

In this section we provide the motivation for Part 1, as well as the contributions.

1.1.1 Motivation

Full-duplex (FD) modes of operation have recently become a viable alternative to the traditional half-duplex (HD) transmissions, due to many advancements in antenna and digital baseband technologies, as well as interference cancellation techniques. The later is imperative for FD communication, since to accomplish FD communication, a radio has to reduce the inevitable self-interference significantly. Otherwise, the self-interference increases the amount of noise at the receiver-end and thereby reduces the achievable rate. To tackle this problem, both active and passive cancellation methods have been proposed. The former, refers to techniques which introduce attenuation of the signal that propagates from the transmit antenna to the receiver one [11], [12]. The latter exploits the knowledge of the transmit symbols by the FD node in order to partially cancel the self-interference [13],[14]. Combinations of both methods have also been considered [15]. The result of these advancements is a practically applicable FD mode of operation, that can lead to doubling (or even tripling [16]) of the spectral efficiency of the network, especially in the low transmit power domain, which is where WPCNs typically reside.

Whilst improving the spectral efficiency in WPCNs is certainly desirable, delivering data in a secure manner is critical in today's society. Considering the constraints of WPCNs, exploitation of the physical properties of the wireless channel is an attractive option to ensure confidentiality [17]. The presence of fading, interference, and path diversity in the wireless channel, all of which are usually a source of many headaches for a communication engineer, can now be exploited in order to degrade the ability of potential intruders to gain information about the confidential messages sent through the wireless channel. The core idea can be condensed to encoding the message into a codeword such that it is useful for the legitimate receiver

to reliably recover the transmitted message and at the same time, the same codeword is useless for the intruder. These two requirements appear to be contradictory at first glance and it is difficult to see if both can be achieved at the same time. However, it is indeed possible to do so, and the so-called secrecy capacity characterizes the maximal data rate at which both requirements are met. These results are based on information theoretic characterizations of secrecy, which originate in some of Shannon's and Wyner's early works on communication and information theory [17], [18]. Whilst the fundamental concepts might be ripe, physical layer security is highly applicable to novel WPCNs, due to its low complexity, and lack of need for certificate authorities or key distributors.

Motivated by the above discussion, in Chapter 2, we derive the capacity of the fundamental building blocks of any FD WPCN. In Chapter 3, we derive the upper bound on the secrecy capacity, as well as an achievable secrecy rate of the network in the presence of a passive eavesdropper.

1.1.2 Contribution

- We derive the capacity of a FD point-to-point WPCN of an energy transmitter (ET) and an energy harvesting user (EHU), assuming a processing cost at the EHU and additive white Gaussian noise channel with block fading. In addition we show that the capacity achieving scheme is relatively simple and therefore applicable to devices with limited resources. The numerical results indicate that the proposed scheme can achieve higher rate, compared to its HD counterpart.

  The results have been disclosed in the following.

  - I. Nikoloska, N. Zlatanov, and Z. Hadzi-Velkov, "Capacity of a Full-Duplex Wirelessly Powered Communication System with Self-Interference and Processing Cost", IEEE Transactions on Wireless Communications, vol. 17, no. 11, pp. 7648 - 7660, 2018.
  - I. Nikoloska, N. Zlatanov, and Z. Hadzi-Velkov, "On the Capacity of a Full-Duplex Wirelessly Powered Communication System with Self-Interference and Processing Cost", in proceedings, IEEE ICC, Kansas City, MO, USA, May 2018.

- We derive an upper bound on the secrecy capacity, as well as an achievable secrecy rate of a more complex network, where in addition to the ET and the EHU, a passive eavesdropper (EVE) is present. We propose a simple coding scheme capable of achieving the secrecy rate which is comparable to the upper bound on the secrecy capacity. In addition, the numerical results indicate that the achievable secrecy rate is higher than its HD counterpart.

  The results have been disclosed in the following.

  - I. Nikoloska, N. Zlatanov, Z. Hadzi-Velkov, and R. Zhang "On the Secrecy Capacity of a Full-Duplex Wirelessly Powered Communication System", IEEE Transactions on Wireless Communications, vol.18, no. 11, pp. 5424–5439, 2019.
  - I. Nikoloska, N. Zlatanov, Z. Hadzi-Velkov, and R. Zhang "On the Secrecy Capacity of a Full-Duplex Wirelessly Powered Communication System", in proceedings, IEEE ISWCS, Oulu, Finland, August 2019.

1.2 Part 2: Resource Allocation in MTC Networks

In this section we provide the motivation for Part 2, as well as the contributions.

1.2.1 Motivation

MTC networks are expected to scale up to a massive number of devices. This creates an entirely different set of problems, the most severe of which is medium access control. The state of the art communication schemes and medium access control mechanisms are based on assumptions that do not necessarily apply to MTC traffic patterns, as these are primarily designed to support human-to-human communication. For example, the amount of data that is usually generated by the devices is small and the activation of the devices is heterogeneous [19]. Some devices report periodic updates, whilst others report when triggered by random, external events. As per the current state of the art access protocol, in order for a MTC device to obtain exclusive rights to the channel to transmit information, it performs a contention based access procedure, known as Random Access (RA)

[20]. However, RA relies on a heavy exchange of signalling messages which becomes exacerbated when the number of devices in the cell is large, which is usually the case in MTC cells [21]. As a result, MTC networks would benefit greatly from novel medium access control, designed to accommodate for such unique traffic characteristics.

One way to improve the existing medium access control protocols is via artificial intelligence (AI), which after a long "AI winter" enjoys a new wave of success. AI appears to be a distinctive tool as it can help us tackle technical problems in wireless networks both directly and indirectly. To elaborate, as an extensive subject, communication also encompasses two higher levels of problems [22], in addition to technical problems (such as medium access control or energy efficiency). The second level of problems, *semantic problems*, concern extracting meaning from the (reliably) received bits of information. The third level of problems, *effectiveness problems*, concern the success with which the extracted meaning by the receiver leads to the desired conduct on his part. Because of the general difficulty of these problems, up until recently each group has been approached in isolation. However, AI provides a unique opportunity to tackle technical problems by solving higher level problems instead. Indeed, if one could find a way to process the information on device, in order to extract semantic information and respond to the extracted information, e.g., via the relevant actuators, then the associated technical problems of transmitting the data would be avoided (or at least it would be far less severe). This makes the solution of the semantic/effectiveness problem a meta-solution to the associated technical problems. However, because of the severe hardware constraints of MTC devices, approaching higher level problems on-device in MTC cells is equally challenging. In fact, the memory required to store a deep neural network and its energy consumption may exceed the memory size and battery level of a MTC device [23]. As a result, only simple neural networks can be deployed in such constrained nodes, which leads to relatively inaccurate on-device inferences.

Motivated by the above discussion, in Chapter 4, we propose a novel AI-aided medium access control protocol that is capable of achieving higher packet rates than the conventional RA procedure. In addition, in Chapter 5 we present novel selection strategies for data transmission that are capable of improving the inference

reliability in MTC networks, whilst indirectly mitigating the underlying technical problems.

1.2.2 Contribution

- We propose a deep reinforcement learning (DRL)-aided RA scheme, where an intelligent DRL agent learns to predict the activity of the IoT nodes[1] in each time slot and grants time-frequency resource blocks to the IoT nodes predicted as active. The IoT nodes that are missclassified as non-active by the DRL agent, as well as unseen or newly arrived nodes in the cell, employ the standard RA scheme in order to obtain time-frequency resource blocks. In addition, we speed up the training procedure of the DRL agent by leveraging expert knowledge. We also derive closed-form, analytical expressions for the average packet rate. Our analytical and numerical results show significant improvements in terms of average packet rate when the proposed DRL-aided RA scheme is implemented compared to the existing solution used in practice, the standard RA scheme.

  The results have been disclosed in the following.

  - I. Nikoloska, and N. Zlatanov "Deep Reinforcement Learning-aided Random Access", submitted, IEEE Transactions on Wireless Communications.

- We propose a data selection scheme for supervised learning that the IoT device can employ to select the data samples that would likely lead to inaccurate inferences if processed locally so that those data samples are transmitted to the cloud. As a result, local inferences are made only from data samples that would likely lead to accurate inferences. Thereby, the overall inference precision of the system is significantly improved for a given energy cost compared to the case when the inference is always made locally at the IoT device. Further, the proposed scheme can reach the inference accuracy of the cloud, but only with a fraction of the energy cost.

  The results have been disclosed in the following.

[1] The terms *IoT device* and *MTC device* are used interchangeably in the thesis.

– I. Nikoloska, and N. Zlatanov, "Data Selection Scheme for Energy Efficient Supervised Learning at IoT Nodes", submitted to the IEEE Communication Letters.

1.3 Organisation of the thesis

The organization of the thesis is given below.

In Chapter 2, we derive the capacity of the fundamental building block of any FD WPCN. We first present the system model and formally define the channel model and the EH model. Then, we formalise an optimization problem which yields the capacity achieving distribution. We prove that the derived capacity expression satisfies the converse and we provide an explicit channel coding scheme which is able to achieve the capacity. We also investigate the capacity for the special cases when the channel is impaired by Rayleigh fading. The capacity results are then numerically evaluated, and conclusions are drawn.

In Chapter 3, we derive the bounds on the secrecy capacity of FD WPCN in the presence of a passive eavesdropper. First, we present the system and channel models, as well as the EH model. We proceed to defining an optimization problem and we prove that the resulting upper bound on the secrecy capacity is not achievable. Next, we derive an achievable secrecy rate, and we provide an explicit coding scheme. The upper bound on the secrecy capacity and the achievable rate are then numerically evaluated against their HD counterpart.

In Chapter 4, we present the novel DRL-aided RA scheme. We first introduce the system model and we formalise the resource allocation problem. Next, we present the existing solution, namely the RA scheme, which is followed by the proposed DRL-aided RA scheme. We also show how to speed up the training procedure of the DRL agent by leveraging expert knowledge. Next, a closed form, analytical expression for the average packet rate is provided. The proposed scheme is then numerically evaluated against the RA scheme both on synthetic and real-world data sets.

In Chapter 5, the data selection strategy for supervised learning is presented. First, we present the system model and we formalize the considered selection problem. Next, we present the data selection strategy, and we evaluate it against multi-

ple benchmarks.

Chapter 6 provides the concluding remarks, as well as ideas for future research directions.

Chapter 2

Capacity of a Full-Duplex Wirelessly Powered Communication Network with Self-Interference and Processing Cost

The aim of this study is to investigate the capacity of the fundamental building block of FD WPCNs. To this end, we consider a system model of an energy transmitter (ET) and an energy harvesting user (EHU), which operates in the FD mode. The ET transmits energy toward the EHU. The EHU harvests this energy and uses it to transmit information back to the ET. As a result of the FD mode, both nodes are affected by self-interference. The self-interference has different effects at the two nodes. In particular, the self-interference impairs the decoding of the received information signal at the ET, whereas it serves as an additional source of energy at the EHU. In this chapter, we derive the capacity of the adopted system model assuming a processing cost at the EHU and an additive white Gaussian noise channel with block fading. In addition, we show that the coding scheme that achieves the capacity is relatively simple and therefore applicable to devices with limited

resources.
The initial results have been presented and published in the proceedings of the IEEE ICC, Kansas City, MO, USA, May 2018.

- I. Nikoloska, N. Zlatanov, and Z. Hadzi-Velkov, "On the Capacity of a Full-Duplex Wirelessly Powered Communication System with Self-Interference and Processing Cost", in proceedings, IEEE ICC, Kansas City, MO, USA, May 2018.

The complete study, which includes detailed proofs of theorems, as well as the coding scheme that achieves the capacity have been published in the IEEE Transactions on Wireless Communications, vol. 17, no. 11, pp. 7648 - 7660, 2018, and this paper is included in this chapter.

- I. Nikoloska, N. Zlatanov, and Z. Hadzi-Velkov, "Capacity of a Full-Duplex Wirelessly Powered Communication System with Self-Interference and Processing Cost", IEEE Transactions on Wireless Communications, vol. 17, no. 11, pp. 7648 - 7660, 2018. Reprinted with permission from IEEE.

Capacity of a Full-Duplex Wirelessly Powered Communication System With Self-Interference and Processing Cost

Ivana Nikoloska, *Student Member, IEEE*, Nikola Zlatanov, *Member, IEEE*, and Zoran Hadzi-Velkov, *Senior Member, IEEE*

***Abstract*— In this paper, we investigate the capacity of a point-to-point, full-duplex (FD) wirelessly powered communication system impaired by self-interference. This system is comprised of an energy transmitter (ET) and an energy harvesting user (EHU), which operates in the FD mode. The ET transmits energy toward the EHU. The EHU harvests this energy and uses it to transmit information back to the ET. As a result of the FD mode, both nodes are affected by self-interference. The self-interference has different effects at the two nodes. In particular, the self-interference impairs the decoding of the received information signal at the ET, whereas it serves as an additional source of energy at the EHU. In this paper, we derive the capacity of the adopted system model assuming a processing cost at the EHU and an additive white Gaussian noise channel with block fading. Thereby, we show that the capacity achieving scheme is relatively simple and therefore applicable to devices with limited resources. Moreover, our numerical results show significant improvements in terms of data rate when the capacity achieving strategy is employed compared to half-duplex transmission, even for very high self-interference at the ET. Moreover, we show the positive effects of the self-interference at the EHU, as well as the crippling effect of the processing cost.**

***Index Terms*— Channel capacity, energy harvesting.**

I. Introduction

IN RECENT years, wireless communication, among many others, has been highly affected by emerging green technologies, such as green radio communications and energy harvesting (EH). Whilst the former aims at minimizing the use of precious radio resources, the latter relies on harvesting energy from renewable and environmentally friendly sources such as, solar, thermal, vibration or wind, [2], [3], to support the transmission of information. Thereby, EH promises a perpetual operation of communication networks. Moreover, EH completely eliminates the need for battery replacement and/or using power cords, making it a highly convenient option for communication networks with nodes which are hard or dangerous to reach. However, EH communication networks are subjected to their own set of challenges. For example, ambient energy sources are often intermittent and scarce, which can put in danger the continuous reliability of the communication session. Possible solution to this problem is harvesting radio frequency (RF) energy from a dedicated energy transmitter, which gives rise to the so called wireless powered communication networks (WPCNs) [4], [5].

EH technology and WPCNs are also quite versatile, and have been studied in many different contexts. Specifically, the capacity of the EH additive white Gaussian noise (AWGN) channel, where the transmitter has no battery for energy storage, was studied in [6]. Transmitters with finite-size batteries have been considered in [7] and [8]. Mao and Hassibi [7] leverage stationarity and ergodicity to derive a series of computable capacity upper and lower bounds for the general discrete EH channel. EH binary symmetric channels with deterministic energy arrival processes have been considered in [8]. Both small and large battery regimes have been adopted in [9] and [10]. The capacity of a sensor node with an infinite-size battery has been investigated in [11]. Infinite-size batteries have also been adopted in [12] and [13]. Ozel and Ulukus [12] derive the capacity of the EH AWGN channel without processing cost or storage inefficiencies, whilst the authors in [13] take into account the processing cost as well as the energy storage inefficiencies. Capacity achieving schemes for the AWGN channel with random energy arrivals at the transmitter have been provided in [14]. The outage capacity of a practical EH circuit model with primary and secondary energy storage devices has been studied in [15]. The authors in [16] derive the minimum transmission outage probability for delay-limited information transfer and the maximum ergodic capacity for delay-unlimited information transfer. The capacity of the Gaussian multiple access channel (MAC) has been derived in [17] and [18]. Relaying (i.e., cooperative) networks with wireless energy transfer have also been extensively analyzed due to their ability to guarantee longer distance communication than classical point-to-point EH links [19], [20]. Information theory has also been paired with queuing theory in order to

Manuscript received February 28, 2018; revised July 7, 2018; accepted August 28, 2018. Date of publication September 14, 2018; date of current version November 9, 2018. This work was supported by the Australian Research Council's DECRA Scheme under Project DE180101134. This paper was presented in part at the IEEE ICC, Kansas City, MO, USA, May 2018 [1]. The associate editor coordinating the review of this paper and approving it for publication was X. Zhou. *(Corresponding author: Ivana Nikoloska.)*

I. Nikoloska and N. Zlatanov are with the Department of Electrical and Computer Systems Engineering, Monash University, Melbourne, VIC 3800, Australia (e-mail: ivana.nikoloska@monash.edu; nikola.zlatanov@monash.edu).

Z. Hadzi-Velkov is with the Faculty of Electrical Engineering and Information Technologies, Ss. Cyril and Methodius University, 1000 Skopje, Macedonia (e-mail: zoranhv@feit.ukim.edu.mk).

Color versions of one or more of the figures in this paper are available online at http://ieeexplore.ieee.org.

Digital Object Identifier 10.1109/TWC.2018.2869139

derive throughput optimal energy management policies for a point-to-point EH communication system in [21].

The above presented system models are assumed to operate in the half-duplex (HD) mode. However, many papers in the literature have shown that full-duplex (FD) communication is feasible. To accomplish FD communication, a radio has to reduce the inevitable self-interference significantly. Otherwise, the self-interference increases the amount of noise at the receiver-end and thereby reduces the achievable rate. Research efforts have made significant progress in tackling the problem of self-interference cancelation and both active and passive cancelation methods have been proposed. The former, refers to techniques which introduce attenuation of the signal that propagates from the transmit antenna to the receiver one [22], [23]. The latter exploits the knowledge of the transmit symbols by the FD node in order to partially cancel the self-interference [24]–[26]. Combinations of both methods have also been considered [27]. When it comes to WPCNs, it has been shown that the self-interference can also play the role of an enabler of communication, rather than a deleterious factor. In fact, the self-interference can be considered as an additional energy source for the nodes in the WPCNs, as proposed by the authors in [28]–[31].

Motivated by the notion of self-energy recycling [28]–[31], in this work, we investigate the capacity of a FD wirelessly powered communication system comprised of an energy transmitter (ET) and an energy harvesting user (EHU) that operate in an AWGN block-fading environment. In this system, the ET sends RF energy to the EHU, whereas, the EHU harvests this energy and uses it to transmit information back to the ET. Both the ET and the EHU work in the FD mode, hence, both nodes transmit and receive RF signals in the same frequency band and at the same time. As a result, both are affected by self-interference. The self-interference has opposite effects at the ET and the EHU. Specifically, the self-interference signal has a negative effect at the ET since it hinders the decoding of the information signal received from the EHU. However, at the EHU, the self-interference signal has a positive effect since it increases the amount of energy that can be harvested by the EHU. For the considered system model, we derive the capacity and we present a simple achievability scheme. Our results show great improvements in terms of rate when the proposed scheme is employed compared to HD schemes, even for very high self-interference at the ET. In addition, our results illustrate the positive influence of the self-interference at the EHU as well as the effect of the processing cost on the overall performance. We note that the considered FD communication system with self-interference and processing cost is important since it represents the fundamental building block of all other FD wirelessly powered communication systems. Hence, by deriving the capacity of this system, we gain insights into the design of future FD wirelessly powered communication systems. To the best of the authors' knowledge, this is the first paper that investigates and derives the capacity of this system model.

The rest of the paper is organized as follows. Section II provides the system and channel models as well as a model for energy harvesting at the EHU. Section III presents the capacity and provides the corresponding optimal input probability distributions at the EHU and the ET. Section IV provides the converse of the capacity and a capacity achieving scheme. In Section V, we provide numerical results and a short conclusion concludes the paper in Section VI. Proofs of theorems are provided in the Appendix.

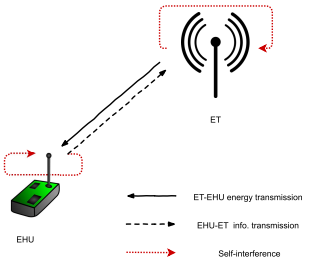

Fig. 1. System model comprised of an ET and an EHU impaired by self-interference.

II. System Model and Problem Formulation

We consider a system comprised of an EHU and an ET, c.f. Fig. 1. The ET transmits RF energy to the EHU and simultaneously receives information from the EHU. On the other hand, the EHU harvests the energy transmitted from the ET and uses it to transmit information back to the ET.

In order to improve the spectral efficiency of the considered system, both the EHU and the ET are assumed to operate in the FD mode, i.e., both nodes transmit and receive RF signals simultaneously and in the same frequency band. Thereby, the EHU receives energy signals from the ET and simultaneously transmits information signals to the ET using the same frequency band. Similarly, the ET transmits energy signals to the EHU and simultaneously receives information signals from the EHU using the same frequency band. Due to the FD mode of operation, both the EHU and the ET are impaired by self-interference. The self-interference has opposite effects at the ET and the EHU. More precisely, the self-interference signal has a negative effect at the ET since it hinders the decoding of the information signal received from the EHU. As a result, the ET should be designed with a self-interference suppression apparatus, which can suppress the self-interference at the ET. On the other hand, at the EHU, the self-interference signal has a positive effect since it increases the amount of energy that can be harvested by the EHU. Hence, the EHU should be designed without a self-interference suppression apparatus, i.e., the EHU should perform energy recycling as proposed in [28].

A. Channel Model

We assume that both the EHU and the ET are impaired by AWGNs, with variances σ_1^2 and σ_2^2, respectively. Let H_{12i} and H_{21i} model the fading channel gains of the EHU-ET and ET-EHU channels in channel use i, respectively. We assume that the channel gains, H_{12i} and H_{21i}, follow a block-fading

model, i.e., they remain constant during all channel uses in one block, but change from one block to the next. Each block consists of (infinitely) many channel uses. Due to the FD mode of operation, the channel gains H_{12i} and H_{21i} are assumed to be identical, i.e., $H_{12i} = H_{21i} = H_i$. We assume that the EHU and the ET are able to estimate the channel gain H_i perfectly.

In the i-th channel use, let the transmit symbols at the EHU and the ET be modeled as random variables (RVs), denoted by X_{1i} and X_{2i}, respectively. Moreover, in channel use i, let the received symbols at the EHU and the ET be modeled as RVs, denoted by Y_{1i} and Y_{2i}, respectively. Furthermore, in channel use i, let the RVs modeling the AWGNs at the EHU and the ET be denoted by N_{1i} and N_{2i}, respectively, and let the RVs modeling the additive self-interferences at the EHU and the ET by denoted by I_{1i} and I_{2i}, respectively. As a result, Y_{1i} and Y_{2i} can be written as

$$Y_{1i} = H_i X_{2i} + I_{1i} + N_{1i}, \tag{1}$$

$$Y_{2i} = H_i X_{1i} + I_{2i} + N_{2i}. \tag{2}$$

A general model for the self-interference at the EHU and the ET is given by [28]

$$I_{1i} = \sum_{m=1}^{M} \tilde{G}_{1,m}(i) X_{1i}^m, \tag{3}$$

$$I_{2i} = \sum_{m=1}^{M} \tilde{G}_{2,m}(i) X_{2i}^m, \tag{4}$$

where $M < \infty$ is an integer and $\tilde{G}_{1,m}(i)$ and $\tilde{G}_{2,m}(i)$ model the self-interference channels between the transmitter- and the receiver-ends at the EHU and the ET in channel use i, respectively. As shown in [28], the components in (3) and (4) for which m is odd carry non-negligible energy and the remaining components can be ignored. Furthermore, the higher order components carry less energy than the lower order terms. As a result, we can justifiably adopt the first order approximation of the self-interference in (3) and (4) and approximate I_{1i} and I_{2i} as

$$I_{1i} = \tilde{G}_{1i} X_{1i}, \tag{5}$$

$$I_{2i} = \tilde{G}_{2i} X_{2i}, \tag{6}$$

where $\tilde{G}_{1i}$ and $\tilde{G}_{2i}$ denote the self-interference channel gains in channel use i. The self-interference channel gains, $\tilde{G}_{1i}$ and $\tilde{G}_{2i}$, are time-varying and the statistical properties of these variations are dependent of the hardware configuration and the adopted self-interference suppression scheme. Inserting (5) and (6) into (1) and (2), respectively, yields

$$Y_{1i} = H_i X_{2i} + \tilde{G}_{1i} X_{1i} + N_{1i}, \tag{7}$$

$$Y_{2i} = H_i X_{1i} + \tilde{G}_{2i} X_{2i} + N_{2i}. \tag{8}$$

In this paper, we are interested in studying the worst-case performance resulting from the linear self-interference given by (5) and (6). To model the worst-case of linear self-interference, we note the following. Since the ET knows which symbol it has transmitted in channel use i, the ET knows the outcome of the RV X_{2i}, x_{2i}. As a result of this knowledge, the noise that the ET "sees" is $\tilde{G}_{2i} x_{2i} + N_{2i}$, where x_{2i} is a constant. Hence, the noise that the ET "sees", $\tilde{G}_{2i} x_{2i} + N_{2i}$, will represent the worst-case of noise, under a second moment constraint, if and only if $\tilde{G}_{2i}$ is an independent and identically distributed (i.i.d.) Gaussian RV.[1] Thereby, we obtain that the worst-case performance in terms of self-interference is obtained when $\tilde{G}_{2i}$ is an i.i.d Gaussian RV. As a result, in the rest of the paper we assume that $\tilde{G}_{2i} \sim \mathcal{N}\{\bar{g}_2, \alpha_2\}$, where $\mathcal{N}\{\bar{g}, \alpha\}$ denotes a Gaussian distribution with mean $\bar{g}$ and variance α. Meanwhile, $\tilde{G}_{1i}$ is distributed according to an arbitrary probability distribution with mean $\bar{g}_1$ and variance α_1.

Now, since $\tilde{G}_{1i}$ and $\tilde{G}_{2i}$ can be written equivalently as $\tilde{G}_{1i} = G_{1i} + \bar{g}_1$ and $\tilde{G}_{2i} = G_{2i} + \bar{g}_2$, respectively, where $G_{2i} \sim \mathcal{N}\{0, \alpha_2\}$, without loss of generality, (7) and (8) can also be written equivalently as

$$Y_{1i} = H_i X_{2i} + \bar{g}_1 X_{1i} + G_{1i} X_{1i} + N_{1i} \tag{9}$$

and

$$Y_{2i} = H_i X_{1i} + \bar{g}_2 X_{2i} + G_{2i} X_{2i} + N_{2i}, \tag{10}$$

respectively.

Since the ET knows the outcome of X_{2i} in each channel use i, and since given sufficient time it can always estimate the mean of its self-interference channel, $\bar{g}_2$, the ET can remove $\bar{g}_2\ X_{2i}$ from its received symbol Y_{2i}, given by (10), and thereby reduce its self-interference. In this way, the ET obtains a new received symbol, denoted again by Y_{2i}, as

$$Y_{2i} = H_i X_{1i} + G_{2i} X_{2i} + N_{2i}. \tag{11}$$

Note that since G_{2i} in (11) changes i.i.d. randomly from one channel use to the next, the ET cannot estimate and remove $G_{2i} X_{2i}$ from its received symbol. Thus, $G_{2i} X_{2i}$ in (11) is the residual linear self-interference at the ET. On the other hand, since the EHU benefits from the self-interference, it does not remove $\bar{g}_1\ X_{1i}$ from its received symbol Y_{1i}, given by (9), in order to have a self-interference signal with a much higher energy. Hence, the received symbol at the EHU is given by (9).

In this paper, we investigate the capacity of a channel given by the input-output relations in (9) and (11), where we are only interested in the mutual-information between the transmitted codeword at the EHU, $X_1^n = (X_{11}, X_{12}, \ldots, X_{1n})$, and the received codeword at the ET, $Y_2^n = (Y_{21}, Y_{22}, \ldots, Y_{2n})$, subject to an average power constraint on the transmitted codeword at the ET $X_2^n = (X_{21}, X_{22}, \ldots, X_{2n})$. Note that, the notation a^n is used to denote the vector $a^n = (a_1,\ a_2,\ \ldots, a_n)$. An equivalent block diagram of the considered system model is presented in Fig 2.

B. Energy Harvesting Model

We assume that the energy harvested by the EHU in channel use i is given by [28]

$$E_{\text{in},i} = \eta (H_i X_{2i} + \bar{g}_1 X_{1i} + G_{1i} X_{1i})^2, \tag{12}$$

[1]This is due to the fact that the Gaussian distribution has the largest entropy under a second moment constraint, see [35].

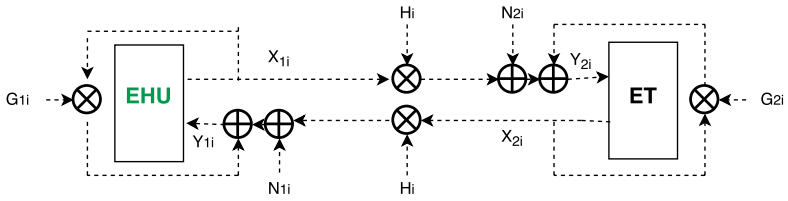

Fig. 2. Block diagram of the system model.

where $0 < \eta < 1$ is the energy harvesting inefficiency coefficient. The EHU stores $E_{\text{in},i}$ in its battery, which, for simplicity, is assumed to be infinitely large. Let B_i denote the amount of harvested energy in the battery of the EHU in the i-th channel use. Moreover, let $E_{\text{out},i}$ be the extracted energy from the battery in the i-th channel use. Then, B_i, can be written as

$$B_i = B_{i-1} + E_{\text{in},i} - E_{\text{out},i}. \tag{13}$$

Since in channel use i the EHU cannot extract more energy than the amount of energy stored in its battery during channel use $i-1$, the extracted energy from the battery in channel use i, $E_{\text{out},i}$, can be obtained as

$$E_{\text{out},i} = \min\{B_{i-1}, X_{1i}^2 + P_p\}, \tag{14}$$

where X_{1i}^2 is the transmit energy of the desired transmit symbol in channel use i, X_{1i}, and P_p is the processing cost of the EHU. The processing cost, P_p, is the energy spent for processing and the energy spent due to the inefficiency and the power consumption of the electrical components in the electrical circuit such as AC/DC convertors and RF amplifiers.

Therefore, the input-output relations of the EHU's battery are given by combining (13) and (14).

Remark 1: Note that the ET also requires energy for processing. However, the ET is assumed to be equipped with a conventional power source which is always capable of providing the processing energy without interfering with the energy required for transmission.

We now use the results in [12] and [32], where it was proven that if

- the total number of channel uses satisfies $n \to \infty$,

- the battery of the EHU has an unlimited storage capacity, and

- the average harvested energy at the EHU is larger than or equal to the average transmit energy plus the processing cost, i.e.,

$$\mathcal{E}\{E_{\text{in},i}\} \geq \mathcal{E}\{X_{1i}^2\} + P_p \tag{15}$$

holds, then the number of channel uses in which the extracted energy from the battery is insufficient and thereby $E_{\text{out},i} = B_{i-1}$ holds in (14) is negligible, compared to the number of channel uses when the extracted energy from the battery is sufficient and thereby $E_{\text{out},i} = X_{1i}^2 + P_p$ holds in (14). In other words, when the above three conditions hold, in almost all channel uses there will be enough energy to be extracted from the EHU's battery for both processing, P_p, and for the transmission of the desired transmit symbol X_{1i}, X_{1i}^2.

III. Capacity

The channel in Fig. 2, modeled by (9) and (11), is a discrete-time channel with inputs X_1 and X_2, and outputs Y_2 and Y_1. Furthermore, the probability of observing Y_2 or Y_1 is dependent on the input X_1 and/or X_2 at channel use i and is conditionally independent of previous channel inputs and outputs, making the considered channel a discrete-time memoryless channel [34]. For this channel, we propose the following theorem which establishes its capacity.

Theorem 1: Assuming that the average power constraint at the ET is P_{ET}, the capacity of the considered EHU-ET communication channel is given by

$$\begin{aligned} C &= \max_{\substack{p(x_1|x_2,h),\\ p(x_2|h)}} \sum_{x_2\in\mathcal{X}_2}\sum_{h\in\mathcal{H}} I(X_1;Y_2|X_2=x_2,H=h)p(x_2|h)p(h) \\ &\quad \text{Subject to} \\ &\quad \text{C1}: \sum_{x_2\in\mathcal{X}_2}\sum_{h\in\mathcal{H}} x_2^2\, p(x_2|h)p(h) \leq P_{ET} \\ &\quad \text{C2}: \int_{x_1}\sum_{x_2\in\mathcal{X}_2}\sum_{h\in\mathcal{H}} (x_1^2+P_p) \\ &\qquad \times p(x_1|x_2,h)p(x_2|h)p(h)dx_1 \\ &\qquad \leq \int_{x_1}\sum_{x_2\in\mathcal{X}_2}\sum_{h\in\mathcal{H}} E_{\text{in}}p(x_1|x_2,h)p(x_2|h) \\ &\qquad \times p(h)dx_1 \\ &\quad \text{C3}: \sum_{x_2\in\mathcal{X}_2} p(x_2|h) = 1 \\ &\quad \text{C4}: \int_{x_1} p(x_1|x_2,h)dx_1 = 1, \end{aligned} \tag{16}$$

where $I(;|)$ denotes the conditional mutual information between X_1 and Y_2 when the EHU knows the transmit symbols of the ET and both the EHU and the ET have full channel state information (CSI). In (16), lower case letters x_2 and h represent realizations of the random variables X_2 and H and their support sets are denoted by $\mathcal{X}_2$ and $\mathcal{H}$, respectively. Constraint C1 in (16) constrains the average transmit power of the ET to P_{ET}, and C2 is due to (15). The maximum in the objective function is taken over all possible conditional probability distributions of x_1 and x_2, given by $p(x_1|x_2,h)$ and $p(x_2|h)$, respectively.

Proof: The proof is in two parts. In Subsection IV-A we prove the converse and in Subsection IV-B we provide the achievability of the capacity. ■

In the following, we provide the solution of (16).

A. Optimal Input Distribution and Simplified Capacity Expression

The optimal input distributions at the EHU and the ET which achieve the capacity in (16) and the resulting simplified capacity expression are provided by the following theorem.

Theorem 2: We have two cases for the channel capacity and the optimal input distributions.

Case 1: If

$$\sum_{h\in\mathcal{H}} \frac{1}{2}\log\left(1+\frac{h^2\ P_{EHU}\left(\sqrt{P_{ET}},h\right)}{\sigma_2^2+P_{ET}\alpha_2}\right)p(h) = \lambda_1\ P_{ET}+\mu_1 +\lambda_2\left(\left(1-\eta(\bar{g}_1^2+\alpha_1)\right)\sum_{h\in\mathcal{H}} P_{EHU}\left(\sqrt{P_{ET}},h\right)p(h) -\eta P_{ET}\sum_{h\in\mathcal{H}} h^2p(h)\right) \quad (17)$$

holds, where λ_1, λ_2, and μ_1 are the Lagrangian multipliers associated with constraints C1, C2, and C3 in (16), respectively, the optimal input distribution at the EHU is zero-mean Gaussian with variance $P_{EHU}\left(\sqrt{P_{ET}},h\right)$, i.e., $p(x_1|x_2,h)\sim\mathcal{N}\left(0,P_{EHU}\left(\sqrt{P_{ET}},h\right)\right)$, where

$$P_{EHU}\left(\sqrt{P_{ET}},h\right)=\left[\frac{1}{\lambda_2(1-\eta(\bar{g}_1^2+\alpha_1))}-\frac{\sigma_2^2+P_{ET}\alpha_2}{h^2}\right]^+, \quad (18)$$

and λ_2 and is chosen such that

$$\left(1-\eta(\bar{g}_1^2+\alpha_1)\right)\sum_{h\in\mathcal{H}} P_{EHU}\left(\sqrt{P_{ET}},h\right)p(h)+P_p = \eta P_{ET}\sum_{h\in\mathcal{H}} h^2p(h) \quad (19)$$

holds.

On the other hand, the optimal input distribution at the ET is degenerate and given by

$$p(x_2|h)=\delta\left(x_2-\sqrt{P_{ET}}\right), \quad (20)$$

where $\delta(\cdot)$ denotes the Dirac delta function. Finally, for this case the capacity in (16) simplifies to

$$C=\sum_{h\in\mathcal{H}}\frac{1}{2}\log\left(1+\frac{h^2P_{EHU}\left(\sqrt{P_{ET}},h\right)}{\sigma_2^2+P_{ET}\alpha_2}\right)p(h). \quad (21)$$

Case 2: If (17) does not hold, the optimal input distribution at the EHU is zero-mean Gaussian with variance $P_{EHU}(x_0(h),h)$, i.e, $p(x_1|x_2,h)\sim\mathcal{N}\left(0,P_{EHU}\left(x_0(h),h\right)\right)$, where

$$P_{EHU}(x_0(h),h)=\left[\frac{1}{\lambda_2(1-\eta(\bar{g}_1^2+\alpha_1))}-\frac{\sigma_2^2+x_0^2(h)\alpha_2}{h^2}\right]^+, \quad (22)$$

where $x_0(h)$ is given by

$$x_0(h)=\sqrt{\left[\frac{h^2W\left(\frac{2\ln 2\left(\left(\lambda_1-\lambda_2\eta h^2\right)\frac{h^2}{\lambda_2(1-\eta(\bar{g}_1^2+\alpha_1))\alpha_2}-1\right)}{e^{2\ln 2\left(1+(\lambda_2\eta h^2-\lambda_1)\frac{\sigma_2^2}{\alpha_2}+\mu_1\right)}}\right)}{2\ln 2((\lambda_1-\lambda_2\eta h^2)h^2-\lambda_2(1-\eta(\bar{g}_1^2+\alpha_1))\alpha_2)}-\frac{\sigma_2^2}{\alpha_2}\right]^+} \quad (23)$$

and λ_2 is chosen such that

$$\left(1-\eta(\bar{g}_1^2+\alpha_1)\right)\sum_{h\in\mathcal{H}} P_{EHU}(x_0(h),h)p(h)+P_p = \eta\sum_{h\in\mathcal{H}} x_0^2(h)h^2p(h) \quad (24)$$

holds. In (23), $W(\cdot)$ denotes the Lambert W function.

On the other hand, the optimal input distribution at the ET is again degenerate and is given by

$$p(x_2|h)=\delta(x_2-x_0(h)). \quad (25)$$

Finally, the capacity in (16) for this case simplifies to

$$C=\sum_{h\in\mathcal{H}}\frac{1}{2}\log\left(1+\frac{h^2P_{EHU}\left(x_0(h),h\right)}{\sigma_2^2+x_0^2(h)\alpha_2}\right)p(h). \quad (26)$$

Proof: Please refer to Appendix. ■

Essentially, depending on the average fading power, i.e., on the quality of the wireless channel, we have two cases. Case 1 holds when the average quality of the channel is sufficient. When Case 1 does hold, the ET transmits the symbol $\sqrt{P_{ET}}$ in each channel use and in all fading blocks. Meanwhile, the EHU transmits a Gaussian codeword whose average power depends on the fading realization of the given fading block. Thereby, the stronger the fading channel, h, the stronger the average transmit power of the EHU during that fading realization. Conversely, the weaker the fading channel, h, the lower the average transmit power of the EHU during that fading realization. In cases when the fading channel is too weak, the EHU remains silent during that fading realization and only harvests the energy transmitted by the ET. On the other hand, Case 2 holds when the average quality of the channel is not sufficient. In that case, the ET transmits the same symbol $x_0(h)$ during all channel uses of the fading block with fading realization h. Note that now the symbol transmitted by the ET, $x_0(h)$ also depends on the fading realization, c.f. Fig. 3. Hence, the ET transmits different symbols in fading blocks with different fading realizations. In particular, if there is a strong fading gain h, $x_0(h)$ is higher, and if h is low so is $x_0(h)$. When h is very low, then $x_0(h)=0$ which means the ET becomes silent during that fading block. On the other hand, the EHU in this case transmits a Gaussian codeword with an average power $P_{EHU}(x_0(h),h)$, where $P_{EHU}(x_0(h),h)$ is again adapted to the fading gain in that fading block. If the fading gain is strong, $P_{EHU}(x_0(h),h)$ is higher and if the fading gain is weak, $P_{EHU}(x_0(h),h)$ is low. If the fading gain is too low, $P_{EHU}(x_0(h),h)=0$, i.e., the EHU becomes silent.

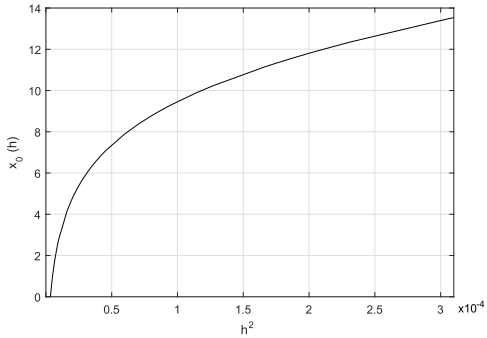

Fig. 3. ET's transmit symbol $x_0(h)$, given by (23), as a function of the fading realization h.

Note that since λ_2 is chosen such that constraint C2 in (16) holds, the expressions in (18), (22), and (23) are dependent on the processing cost P_p. This means that the capacity as well as the input distribution at the EHU are implicitly dependent on the processing cost P_p via λ_2. In particular, the capacity is a decreasing function of P_p. The impact of the processing cost is particularly important for WPCNs in practice for accurately estimating the performance in terms of achievable rates. In fact, such an estimation can be easily inflated by ignoring the processing cost P_p, as shown in the numerical examples, cf. Fig. 8.

B. Special Cases

Corollary 1 (Rayleigh Fading): When the channel fading gain H follows a Rayleigh probability distribution, the probability density function of H is given by

$$p_H(h) = \frac{h}{2\Omega_h} e^{-\frac{h^2}{\Omega_h}}. \tag{27}$$

In this case, after replacing $\sum_h(\cdot)p(h)$ in (21) with $\int_h(\cdot)p(h)dh$, where $p(h)$ is given by (27), the channel capacity has a closed-form solution as

$$C = \frac{1}{\ln 2}\left(E_1\left(\frac{\lambda_2(1-\eta(\bar{g}_1^2+\alpha_1))(\sigma_2^2+P_{ET}\alpha_2)}{\Omega_h}\right) + e^{-\frac{\lambda_2(1-\eta(\bar{g}_1^2+\alpha_1))(\sigma_2^2+P_{ET}\alpha_2)}{\Omega_h}} \ln\left(\frac{1}{\Omega_h}\right)\right), \tag{28}$$

where λ_2 can be found from the following equation

$$\frac{1}{\lambda_2(1-\eta(\bar{g}_1^2+\alpha_1))} e^{-\frac{\lambda_2(1-\eta(\bar{g}_1^2+\alpha_1))(\sigma_2^2+P_{ET}\alpha_2)}{\Omega_h}} - (\sigma_2^2+P_{ET}\alpha_2)E_1\left(\frac{\lambda_2(1-\eta(\bar{g}_1^2+\alpha_1))(\sigma_2^2+P_{ET}\alpha_2)}{\Omega_h}\right) = \frac{\eta P_{ET}\Omega_h - P_p}{(1-\eta(\bar{g}_1^2+\alpha_1))}. \tag{29}$$

In (29), E_1 denotes the exponential integral function given by $E_1(x) = \int_x^\infty \frac{e^{-t}}{t}dt$. When Case 1 does not hold, the channel capacity can be evaluated numerically using software such as Mathematica.

Corollary 2 (No Fading): When the channel is not impaired by fading, the capacity has a closed-form solution as

$$C = \frac{1}{2}\log\left(1 + \frac{P_{EHU}(\sqrt{P_{ET}})}{\sigma_2^2 + P_{ET}\alpha_2}\right), \tag{30}$$

where $P_{EHU}(\sqrt{P_{ET}})$ is given by

$$P_{EHU}(\sqrt{P_{ET}}) = \frac{\eta P_{ET}}{1-\eta(\bar{g}_1^2+\alpha_1)}. \tag{31}$$

The capacity in (30) is achieved when X_1 follows a Gaussian probability distribution as $p(x_1|x_2) = p(x_1) \sim \mathcal{N}\left(0, P_{EHU}\left(\sqrt{P_{ET}}\right)\right)$ and the probability distribution of X_2 is degenerate and given by $p(x_2) = \delta\left(x_2 - \sqrt{P_{ET}}\right)$.

In the following, we prove that the rate presented in Theorem 1 is the channel capacity. To this end, we follow a common approach by providing the two necessary elements for the proof, the converse on the capacity and a capacity achievability scheme.

IV. Converse and Achievability of the Channel Capacity

In this section, we prove the converse and the achievability of the channel capacity established in Theorem 1.

A. Converse of the Channel Capacity

Let W be the message that the EHU wants to transmit to the ET. Let this message be uniformly selected at random from the message set $\{1, 2, \ldots, 2^{nR}\}$, where $n \to \infty$ is the number of channel uses that will be used for transmitting W from the EHU to the ET, and R denotes the data rate of message W. We assume a priori knowledge of the CSI, i.e., H_i is known for $i = 1 \ldots n$ before the start of the communication session at both nodes. Then, we have

$$\begin{aligned} nR &\leq H(W|H^n) \\ &= H(W|H^n) - H(W|H^n, Y_2^n, X_2^n) + H(W|H^n, Y_2^n, X_2^n) \\ &= I(W; Y_2^n, X_2^n|H^n) + H(W|H^n, Y_2^n, X_2^n), \end{aligned} \tag{32}$$

which follows from the definition of the mutual information. By Fano's inequality we have

$$H(W|H^n, Y_2^n, X_2^n) \overset{(a)}{\leq} H(W|Y_2^n, H^n) \leq P_e nR + 1, \tag{33}$$

where (a) follows from the fact that conditioning reduces entropy and P_e is the average probability of error of the message W. Inserting (33) into (32) and dividing both sides by n, we have

$$R \leq \frac{1}{n} I(W; Y_2^n, X_2^n|H^n) + P_e R + 1/n. \tag{34}$$

Assuming that $n \to \infty$ and assuming that $P_e \to 0$ as $n \to \infty$, (34) can be written as

$$R \leq \frac{1}{n} I(W; Y_2^n, X_2^n|H^n). \tag{35}$$

We represent the right hand side of (35) as

$$I(W;Y_2^n,X_2^n|H^n)=I(W;Y_2^n|X_2^n,H^n)+I(W;X_2^n|H^n). \tag{36}$$

Now, since the transmit message W is uniformly drawn from the message set $\{1,\,2,\,\ldots,2^{nR}\}$ at the EHU, and the ET does not know which message the EHU transmits, the following holds

$$I(W;X_2^n|H^n)=0. \tag{37}$$

Inserting (37) into (36), we have

$$\begin{aligned}
&I(W;Y_2^n,X_2^n|H^n)\\
&=\;I(W;Y_2^n|X_2^n,H^n)\\
&\overset{(a)}{\leq}\sum_{i=1}^{n}I(W;Y_{2i}|Y_2^{i-1},X_2^n,H^n)\\
&\overset{(b)}{=}\sum_{i=1}^{n}H(Y_{2i}|Y_2^{i-1},X_2^n,H^n)-\sum_{i=1}^{n}H(Y_{2i}|Y_2^{i-1},X_2^n,H^n,W)\\
&\overset{(c)}{\leq}\sum_{i=1}^{n}H(Y_{2i}|X_2^n,H^n)-\sum_{i=1}^{n}H(Y_{2i}|Y_2^{i-1},X_2^n,H^n,W)\\
&\overset{(d)}{\leq}\sum_{i=1}^{n}H(Y_{2i}|X_2^n,H^n)-\sum_{i=1}^{n}H(Y_{2i}|Y_2^{i-1},X_{1i},X_2^n,H^n,W),
\end{aligned} \tag{38}$$

where (a) follows from the fact that the entropy of a collection of random variables is less than the sum of their individual entropies [34], (b) is a consequence of the chain rule, and (c) and (d) follow from the fact that conditioning reduces entropy. Now, due to the memoryless assumption, it easy to see that Y_{2i} is independent of all elements in the vectors X_2^n and H^n except the elements X_{2i} and H_i. Thereby, the following holds

$$H(Y_{2i}|X_2^n,H^n)=H(Y_{2i}|X_{2i},H_i). \tag{39}$$

Moreover, from the memoryless channel assumption, we have that Y_{2i} is independent of Y_2^{i-1}, of all elements in the vector X_2^n except the element X_{2i}, and of all the elements of the vector H^n except H_i. Thereby, the following holds

$$H(Y_{2i}|Y_2^{i-1},X_{1i},X_2^n,H^n,W)=H(Y_{2i}|X_{1i},X_{2i},H_i,W). \tag{40}$$

Using (11), we can see that given X_{1i}, X_{2i} and H_i, the RV Y_{2i} is conditionally independent of W. As a result the following holds

$$H(Y_{2i}|X_{1i},X_{2i},H_i,W)=H(Y_{2i}|X_{1i},X_{2i},H_i). \tag{41}$$

Inserting (39) and (41) into (38), we obtain

$$\begin{aligned}
&I(W;Y_2^n,X_2^n|H^n)\\
&\quad\leq\sum_{i=1}^{n}H(Y_{2i}|X_{2i},H_i)-\sum_{i=1}^{n}H(Y_{2i}|X_{1i},X_{2i},H_i)\\
&\quad=\sum_{i=1}^{n}I(X_{1i};Y_{2i}|X_{2i},H_i).
\end{aligned} \tag{42}$$

Now, inserting (42) into (35), we have

$$R\leq\frac{1}{n}\sum_{i=1}^{n}I(X_{1i};Y_{2i}|X_{2i},H_i)=I(X_1;Y_2|X_2,H). \tag{43}$$

Hence, an upper bound on the capacity is given by (43) when no additional constraints on X_1 and X_2 exist. However, in our case, we have two constraints on X_1 and X_2. One constraint is that $\mathcal{E}\{X_2^2\}\leq P_{ET}$, expressed by C1 in (16). The other constraint is given by (15), expressed by C2 in (16), which limits the average power of the EHU to be less than the maximum average harvested power. Constraints C3 and C4 in (16) come from the definitions of probability distributions. Hence, by inserting C1, C2, C3, and C4 from (16) into (43) and maximizing with respect to $p(x_1,x_2|h)=p(x_1|x_2,h)p(x_2|h)$, we obtain that the capacity is upper bounded by (16). This proves the converse. In Subsection IV-B, we prove that this upper bound can be achieved. Thus, the capacity of the considered channel is given by (16).

B. Achievability of the Channel Capacity

The capacity achieving coding scheme for this channel is similar to the coding scheme for the AWGN fading channel with EH given in [13]. The proposed scheme is outlined in the following.

The EHU wants to transmit message W to the ET using the harvested energy from the ET. Message W is assumed to be drawn uniformly at random from the message set $\{1,2\ldots2^{nR}\}$. Thereby, message W carries nR bits of information, where $n\to\infty$.

In the following, we describe a method for transferring nR bits of information from the EHU to the ET in $n+b$ channel uses, where $R=C-\epsilon$, and $\epsilon\to0$ and $n/(n+b)\to1$ hold as $n\to\infty$. As a result, the information from the EHU to the ET is transferred at rate $R=C$, as $n\to\infty$.

For the proposed achievability scheme, we assume that the transmission is carried out in $N+B$ time slots, where $N/(N+B)\to1$ as $N\to\infty$. In each time slot, we use the channel k times, where $k\to\infty$. Moreover, we assume that the fading is constant during one time slot and changes from one time slot to the next. The numbers N, B, and k are chosen such that $n=Nk$ and $b=Bk$ hold. Moreover, we assume that message W is represented in a binary form as a sequence of bits that is stored at the EHU.

1) Transmissions at the ET: In each time slot, the ET transmits the same symbol x_2 during the k channel uses of the considered time slot. The value of the symbol x_2 depends only on the fading gain of the channel h during the corresponding time slot, and it can be found in Theorem 2.

2) Receptions and Transmissions at the EHU: During the first few time slots, the EHU is silent and only harvests energy from the ET. The EHU will transmit for the first time only when it has harvested enough energy both for processing and transmission, i.e., only when its harvested energy accumulates to a level which is higher than $P_p+P_{\mathrm{EHU}}(x_2,h)$, where h is the fading gain in the time slot considered for transmission. In that case, the EHU extracts $kR(h)$ bits from its storage, maps them to a Gaussian codeword with rate

$R(h)$ and transmits that codeword to the ET in the considered time slot. The symbols in the transmitted codeword are derived independently according to the Gaussian distribution $\mathcal{N}(0, P_{EHU}(x_0(h), h))$. When (17) holds, $P_{EHU}(x_0(h), h) = P_{EHU}(\sqrt{P_{ET}}, h)$ which is given by (18), whereas the rate of the transmitted codeword $R(h)$ is given by

$$R(h) = \frac{1}{2}\log\left(1 + \frac{h^2 P_{EHU}\left(\sqrt{P_{ET}}, h\right)}{\sigma_2^2 + P_{ET}\alpha_2}\right) - \epsilon. \quad (44)$$

Otherwise, if (17) does not hold, $P_{EHU}(x_0(h), h)$ is given by (22) and the rate of the transmitted codeword, $R(h)$, is given by

$$R(h) = \frac{1}{2}\log\left(1 + \frac{h^2 P_{EHU}\left(x_0(h), h\right)}{\sigma_2^2 + x_0^2(h)\alpha_2}\right) - \epsilon. \quad (45)$$

3) Receptions at the ET: The ET is able to decode the transmitted codeword from the EHU in a time slot with fading realization h since it is received via an AWGN channel with total AWGN variance of $\sigma_2^2 + P_{ET}\alpha_2$ and $\sigma_2^2 + x_0^2(h)\alpha_2$ for the rates in (44) and (45), respectively.

The EHU and the ET repeat the above procedure for all $N + B$ time slots.

Let $\mathcal{N}$ denote a set comprised of the time slots during which the EHU has enough energy harvested and thereby transmits a codeword and let $\mathcal{B}$ denote a set comprised of the time slots during which the EHU does not have enough energy harvested and thereby it is silent. Let $N = |\mathcal{N}|$ and $B = \mathcal{B}$, where $|\cdot|$ denotes the cardinality of a set. Moreover, let $h(i)$ denote the outcome of the RV H in the i-th time slot. Using the above notations, the rate achieved during the $N + B$ time slots is given by

$$\begin{aligned} R &= \lim_{(N+B)\to\infty} \frac{1}{N+B}\left[\sum_{i\in\mathcal{N}} R(h(i)) + \sum_{i\in\mathcal{B}} 0\right] \\ &= \lim_{(N+B)\to\infty} \frac{1}{N+B}\sum_{i\in\mathcal{N}} R(h(i)). \end{aligned} \quad (46)$$

Now, it is proven in [32] that when the EHU is equipped with a battery with an unlimited storage capacity and when (15) holds, then $N \to \infty$ as $(N + B) \to \infty$. As a result, (46) simplifies to

$$R = \lim_{(N+B)\to\infty} \frac{N}{N+B}\sum_{h\in\mathcal{H}} R(h)p(h). \quad (47)$$

Moreover, it was also proven in [32] that when the EHU is equipped with a battery with an unlimited storage capacity and when (15) holds, then $N/(N + B) \to 1$ as $(N + B) \to \infty$. Using this, R in (47) simplifies to

$$R = \sum_{h\in\mathcal{H}} R(h)p(h), \quad (48)$$

which is the channel capacity.

V. Numerical Results

In this section, we illustrate examples of the capacity of the considered system model, and compare it with the achievable rate of a chosen benchmark scheme. In the following, we outline the system parameters, than we introduce the benchmark scheme, and finally we provide the numerical results.

TABLE I
Simulation Parameters

Parameter	Value
Speed of light c	299 792 458 m / s
Carrier frequency f_c	2.4 GHz
Bandwidth B	100 kHz
Noise power σ^2	-160 dBm per Hz
EH efficiency η	0.8
Path loss exponent γ	3
Distance d	10 m $\vee$ 20 m
Processing cost P_p	$-\infty \sim$ 10 dBm
ET transmit power P_{ET}	0 dBm ~ 35 dBm

A. System Parameters

We use the standard path loss model given by

$$\mathcal{E}\{H^2\} = \Omega_H = \left(\frac{c}{f_c 4\pi}\right)^2 d^{-\gamma} \quad (49)$$

in order to compute the average power of the channel fading gains of the ET-EHU/EHU-ET link, where c denotes the speed of light, f_c is the carrier frequency, d is the length of the link, and γ is the path loss exponent. We assume that $\gamma = 3$. The carrier frequency is equal to 2.4 GHz, a value used in practice for sensor networks, and $d = 10$ m or $d = 20$ m. We assume a bandwidth of $B = 100$ kHz and noise power of -160 dBm per hertz, which for 100 kHz adds-up to a total noise power of 10^{-14} Watts. The energy harvesting efficiency coefficient η is assumed to be equal to 0.8. The system parameters are summarized in Table I. Throughout this section, we assume Rayleigh fading with average power Ω_H given by (49).

B. Benchmark Schemes

Since communication schemes for the considered FD wirelessly powered communication system are not available in the literature, we exploit a HD communication scheme as a benchmark scheme. Thereby, we divide the transmission time into slots of length T. We assume that the EHU is silent and only harvests energy during a portion of the time slot, denoted by t. In the remainder of the time slot, $(T - t)$, the EHU only transmits information to the ET and does not harvest energy. Similarly, the ET transmits energy during t, but remains silent and receives information during $T - t$. In other words, both the EHU and the ET work in a HD mode. In this mode, the nodes are not impaired by self-interference, thus the harvested energy at the EHU in channel use i is given by

$$E_i = t\eta(H_i X_{2i})^2. \quad (50)$$

Again, we assume CSI knowledge at the ET and at the EHU, and in addition the EHU is also equipped with a battery with an unlimited storage capacity. Therefore, as per [32], the EHU can also choose any amount of power for information transmission as long as its average extracted energy from the battery is smaller than $\mathcal{E}\{E_i\}$, where E_i is given by (50). Considering the HD nature of this channel model, the maximum rate that the EHU can achieve is given by

$$R_{HD} = \max_t \ (T - t)\log\left(1 + \frac{h^2 P_{EHU}(h)}{\sigma_2^2}\right), \quad (51)$$

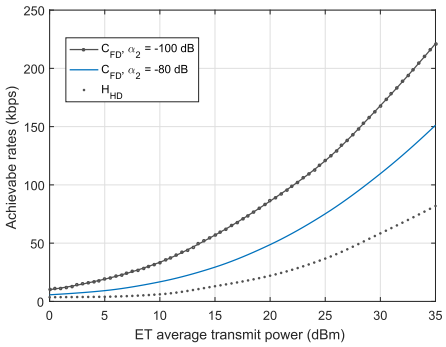

Fig. 4. Comparison of the capacity and the achievable rates of the benchmark scheme as a function of the ET average transmit power for a link distance of $d = 10$m.

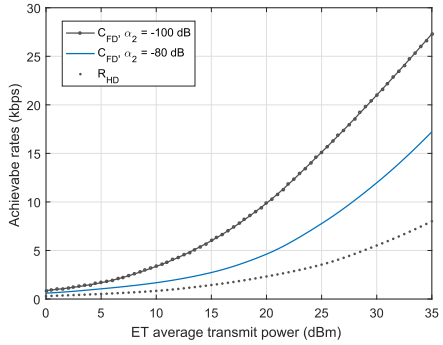

Fig. 5. Comparison of the capacity and the achievable rates of the benchmark scheme as a function of the ET average transmit power for a link distance of $d = 20$m.

where

$$P_{EHU}(h) = \max\left\{0, \frac{1}{\lambda} - \frac{\sigma^2}{h^2}\right\}, \tag{52}$$

where λ is found such that

$$(T-t)\left(P_p + \left[\frac{e^{-\frac{\lambda\sigma^2}{\Omega_H}}}{\lambda} - \frac{\sigma^2 E_1\left(\frac{\lambda\sigma^2}{\Omega_H}\right)}{\Omega_H}\right]\right) = t\eta P_{ET}\Omega_H \tag{53}$$

holds.

C. Numerical Examples

Figs. 4 and 5 illustrate the data rates achieved with the proposed capacity achieving scheme and the benchmark scheme for link distances of 10 m and 20 m, respectively, and average power of the ET that ranges from 0 dBm to 35 dBm. The processing cost at the EHU is set to $P_p = -10$ dBm. It can be clearly seen from Figs. 4 and 5 that the achievable rates of the HD benchmark scheme are much lower than the derived channel capacity. The poor performance of the HD benchmark scheme is a consequence of the following facts. Firstly, self-interference energy recycling in the HD mode is impossible at the EHU since there is no self-interference. Secondly, the FD mode of operation is much more spectrally efficient than the HD mode, i.e., using part of the time purely for energy harvesting without transmitting information has a big impact on the system's performance. In addition, as it can be seen from comparing Figs. 4 and 5, doubling the distance between the nodes, has a severe effect on performance due to the increased signal attenuation.

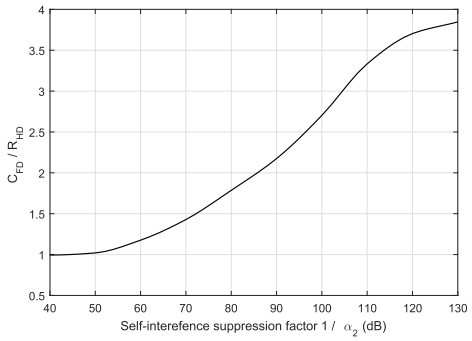

Fig. 6. C_{FD}/R_{HD} ratio as a function of the self-interference suppression factor.

In Fig. 6, we present the ratio between the capacity and the rate of the benchmark scheme, C_{FD}/R_{HD}, as a function of the self-interference suppression factor at the ET. The distance between the ET and the EHU is set to $d = 10$ m and the average transmit power of the ET is set to $P_{ET} = 30$ dBm. The self-interference suppression factor at the ET can be found as the reciprocial of the self-interference amplification factor α_2, i.e., as $1/\alpha_2$. The ratio C_{FD}/R_{HD} can be interpreted as the gain in terms of data rate obtained by using the proposed capacity achieving scheme compared to the data rate obtained by using the benchmark scheme. When the self-interference suppression factor is very small, i.e., around 40 dB, the self-interference cripples the FD capacity and the FD capacity converges to the HD rate. Naturally, as the self-interference is more efficiently suppressed, i.e., ≥ 50 dB the FD capacity becomes significantly larger than the HD rate. An interesting observation can be made for suppression factor around 70 dB, which are available in practice. In this case, the capacity achieving scheme results in a rate which is approximately 50% larger than the HD rate. Another interesting result is that for self-interference suppression of more than 85 dB, which is also available in practice, the proposed FD system model achieves a rate which is more than double the rate of the HD system. This effect is a result of the energy recycling at the EHU.

Fig. 7 presents the derived capacity as a function of the mean and the variance of the self-interference channel at the

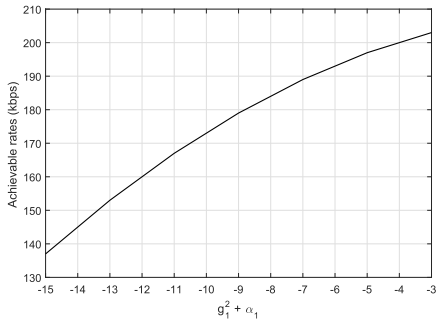

Fig. 7. Capacity as a function of $(\alpha_1 + g_1^2)$.

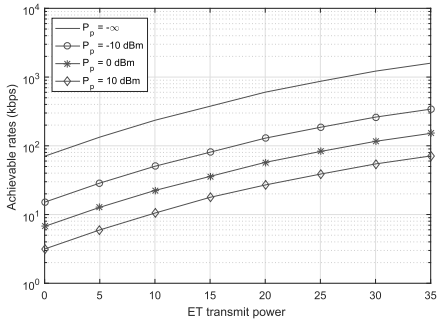

Fig. 8. Comparison of the capacity for different processing costs as a function of the ET's average transmit power for a link distance of $d = 10$m.

EHU, $(\alpha_1 + g_1^2)$. For this figure, the distance between the ET and the EHU is $d = 10$ m and the average transmit power of the ET is $P_{ET} = 30$ dBm. The self-interference suppression factor at the ET is 100 dB. As the average self-interference channel gain at the EHU increases, i.e., $(\alpha_1 + g_1^2)$ increases, the EHU can recycle a larger amount of its transmit energy. As a consequence, this results in a capacity increase. Figs. 6 and 7, reaffirm the idea that the self-interference at the EHU can be transformed from a deleterious factor, to an aide, or even an enabler of communication.

To illustrate the effect the processing energy cost has on the capacity, in Fig. 8, we present the capacity for the case when the processing cost is zero and non-zero, for a distance of $d = 10$ m. The Y axes in Fig. 8 is given in the logarithmic scale in order to better observe the discrepancy between the two scenarios. It can clearly be seen from Fig. 8 that when the processing cost is high, it has a detrimental effect on the capacity. This confirms that the energy processing cost must be considered in EH networks. Failing to do so might result in overestimating the achievable rates, which in reality would only represent very loose upper bounds that can never be achieved.

VI. Conclusion

We studied the capacity of the point-to-point FD wirelessly powered communication system, comprised of an ET and an EHU. Because of the FD mode of operation, both the EHU and the ET experience self-interference, which impairs the decoding of the information-carrying signal at the ET, whilst serving as an additional energy source at the EHU. We showed that the capacity is achieved with a relatively simple scheme, where the input probability distribution at the EHU is zero-mean Gaussian and where the ET transmits only one symbol. Numerical results showed significant gains in terms of data rate when the proposed capacity achieving scheme is employed compared to HD transmission even for very high self-interference at the ET. Moreover, we show the indisputable effect that the processing cost and the self-interference have on the performance.

Appendix
Proof of Theorem 2

Let us assume that the optimal $p(x_2|h)$ is a discrete probability distribution and that the optimal $p(x_1|x_2, h)$ is a continuous probability distribution, which will turn out to be valid assumptions. In order to find both input distributions, in the following, we solve the optimization problem given by (16).

Since $I(X_1; Y_2|X_2 = x_2, H = h)$ is the mutual information of an AWGN channel with channel gain h and AWGN with variance $\sigma_2^2 + x_2^2\alpha_2$, the optimal input distribution at the EHU, $p(x_1|x_2, h)$, is Gaussian with mean zero and variance $P_{EHU}(x_2, h)$, which has to satisfy constraint C2 in (16). Thereby, $I(X_1; Y_2|X_2 = x_2, H = h) = \frac{1}{2}\log\left(1 + \frac{h^2\ P_{EHU}(x_2,h)}{\sigma_2^2 + x_2^2\alpha_2}\right)$. Now, since G_1 and X_1 are zero-mean Gaussian RVs, the left-hand side of constraint C2 can be transformed into

$$\int_{x_1} \sum_{x_2\in\mathcal{X}_2} \sum_{h\in\mathcal{H}} (x_1^2 + P_p)p(x_1|x_2, h)p(x_2|h)p(h)dx_1 = \sum_{x_2\in\mathcal{X}_2} \sum_{h\in\mathcal{H}} P_{EHU}(x_2, h)p(x_2|h)p(h) + P_p. \quad (54)$$

Whereas, the right-hand side of C2 can be rewritten as

$$\begin{aligned}
&\int_{x_1} \sum_{x_2\in\mathcal{X}_2} \sum_{h\in\mathcal{H}} E_{\text{in}}p(x_1|x_2, h)p(x_2|h)p(h)dx_1 \\
&= \int_{g_1}\int_{x_1} \sum_{x_2\in\mathcal{X}_2} \sum_{h\in\mathcal{H}} \eta(hx_2 + \bar{g}_1x_1 + g_1x_1)^2 \\
&\quad \times p(x_1|x_2, h)p(x_2|h)p(h)p(g_1)dx_1\ dg_1 \\
&= \sum_{x_2\in\mathcal{X}_2} \sum_{h\in\mathcal{H}} \eta h^2\ x_2^2\ p(x_2|h)p(h) \\
&\quad + \int_{x_1} \sum_{x_2\in\mathcal{X}_2} \sum_{h\in\mathcal{H}} \eta\bar{g}_1^2\ x_1^2\ p(x_1|x_2, h)p(x_2|h)p(h)dx_1 \\
&\quad + \int_{g_1}\int_{x_1} \sum_{x_2\in\mathcal{X}_2} \sum_{h\in\mathcal{H}} \eta g_1^2\ x_1^2 \\
&\quad \times p(x_1|x_2, h)p(x_2|h)p(h)p(g_1)dx_1\ dg_1 \\
&= \sum_{x_2\in\mathcal{X}_2} \sum_{h\in\mathcal{H}} \eta h^2\ x_2^2\ p(x_2|h)p(h)
\end{aligned}$$

$$+\eta\bar{g_1}^2 \sum_{x_2\in\mathcal{X}_2}\sum_{h\in\mathcal{H}} P_{EHU}(x_2,h)p(x_2|h)p(h)$$
$$+\eta\alpha_1 \sum_{x_2\in\mathcal{X}_2}\sum_{h\in\mathcal{H}} P_{EHU}(x_2,h)p(x_2|h)p(h), \quad (55)$$

where g_1 represents the realizations of the random variable G_1. Combining (54) and (55) transforms (16) into

$$\max_{\substack{P_{EHU}(x_2,h),\\ p(x_2|h)}} \sum_{x_2\in\mathcal{X}_\epsilon}\sum_{h\in\mathcal{H}} \frac{1}{2}\log\left(1+\frac{h^2\ P_{EHU}(x_2,h)}{\sigma_2^2+x_2^2\alpha_2}\right) \times p(x_2|h)p(h)$$

Subject to

$$\text{C1}: \sum_{x_2\in\mathcal{X}_2}\sum_{h\in\mathcal{H}} x_2^2\ p(x_2|h)p(h) \le P_{ET}$$
$$\text{C2}: \sum_{x_2\in\mathcal{X}_2}\sum_{h\in\mathcal{H}} P_{EHU}(x_2,h)p(x_2|h)p(h)+P_p \le \sum_{x_2\in\mathcal{X}_2}\sum_{h\in\mathcal{H}} \eta h^2\ x_2^2\ p(x_2|h)p(h) + \eta(\bar{g_1}^2+\alpha_1)\sum_{x_2\in\mathcal{X}_2}\sum_{h\in\mathcal{H}} P_{EHU} \times (x_2,h)p(x_2|h)p(h)$$
$$\text{C3}: \sum_{x_2\in\mathcal{X}_2} p(x_2|h) = 1.$$
$$\text{C4}: P_{EHU}(x_2,h) \ge 0. \quad (56)$$

Now, (56) can be solved in a straightforward manner using the Lagrange duality method. Thereby, we write the Lagrangian of (56) as

$$\mathcal{L} = \sum_{x_2\in\mathcal{X}_\epsilon}\sum_{h\in\mathcal{H}} \frac{1}{2}\log\left(1+\frac{h^2\ P_{EHU}(x_2,h)}{\sigma_2^2+x_2^2\alpha_2}\right)p(x_2|h)p(h) - \lambda_1\left(\sum_{x_2\in\mathcal{X}_\epsilon}\sum_{h\in\mathcal{H}} x_2^2\ p(x_2|h)p(h) - P_{ET}\right) - \mu_1\left(\sum_{x_2\in\mathcal{X}_\epsilon} p(x_2|h) - 1\right) - \mu_2\ P_{EHU}(x_2,h) - \lambda_2\Bigg((1-\eta(\bar{g_1}^2+\alpha_1))\sum_{x_2\in\mathcal{X}_2}\sum_{h\in\mathcal{H}} P_{EHU}(x_2,h)p(x_2|h)p(h) + P_p - \sum_{x_2\in\mathcal{X}_2}\sum_{h\in\mathcal{H}} \eta h^2 x_2^2 p(x_2|h)p(h)\Bigg). \quad (57)$$

In (56), we assume that $0 < \eta(\bar{g_1}^2+\alpha_1) < 1$, since $\eta(\bar{g_1}^2+\alpha_1) \ge 1$ would practically imply that the EHU recycles the same or even a larger amount of energy than what has been transmitted by the EHU, which is not possible in reality. In (57), λ_1, λ_2, μ_1, and μ_2 are the Lagrangian multipliers associated with C1, C2, C3, and C4 in (16), respectively. Differentiating (57) with respect to the optimization variables, we obtain

$$\frac{\partial\mathcal{L}}{\partial P_{EHU}(x_2,h)} = \frac{\frac{h^2}{\sigma_2^2+x_2^2\alpha_2}}{1+\frac{h^2\ P_{EHU}(x_2,h)}{\sigma_2^2+x_2^2\alpha_2}} - \lambda_2(1-\eta(\bar{g_1}^2+\alpha_1)) - \mu_2 = 0 \quad (58)$$

$$\frac{\partial L}{\partial p(x_2|h)} = \frac{1}{2}\sum_{h\in\mathcal{H}}\log\left(1+\frac{h^2\ P_{EHU}(x_2,h)}{\sigma_2^2+x_2^2\alpha_2}\right)p(h) - \lambda_1\sum_{h\in\mathcal{H}} x_2^2 p(h) - \mu_1 - \lambda_2\Bigg((1-\eta(\bar{g_1}^2+\alpha_1))\sum_{h\in\mathcal{H}} P_{EHU}(x_2,h)p(h) - \eta\sum_{h\in\mathcal{H}} h^2 x_2^2 p(h)\Bigg) = 0. \quad (59)$$

When $P_{EHU}(x_2,h) > 0$, then $\mu_2 = 0$. In consequence, we can use (58) to find $P_{EHU}(x_2,h)$ as given by Theorem 2.

When $\mu_1 > 0$, then (59) has only two possible solutions $\pm x_2^*$. In order for $p^*(x_2|h)$ to be a valid probability distribution $p(x_2^*|h) + p(-x_2^*|h) = 1$ has to hold. Furthermore, $\sum_{x_2\in\mathcal{X}_2} x_2^2\ p(x_2|h)p(h) \le P_{ET}$ also has to hold. So, one possible solution for the optimal input distribution is $p^*(x_2|h) = \frac{1}{2}\delta(x_2-x_2^*) + \frac{1}{2}\delta(x_2+x_2^*)$. However, x_2 does not need to carry any information to the EHU, thus uniformly choosing x_2 between x_2^* and $-x_2^*$ brings no benefit to the EHU. Moreover, the complexity of the ET will be reduced if it only transmits one symbol, the symbol x_2^*. Thus, $p^*(x_2|h) = \delta(x_2-x_2^*)$ is chosen. Now for $\sum_{x_2\in\mathcal{X}_2} x_2^2\ p(x_2|h)p(h) \le P_{ET}$ to hold, we can choose $x_2^* = \sqrt{P_{ET}}$. Thus, possible solution for $p^*(x_2|h)$ is given by (20) in Theorem 2. Using (59), we find the condition for $p(x_2|h) = \delta(x_2-\sqrt{P_{ET}})$ as

$$\sum_{h\in\mathcal{H}}\frac{1}{2}\log\left(1+\frac{h^2\ P_{EHU}(\sqrt{P_{ET}},h)}{\sigma_2^2+P_{ET}\alpha_2}\right)p(h) = \lambda_1\ P_{ET} + \mu_1 + \lambda_2\left(\left(1-\eta(\bar{g_1}^2+\alpha_1)\right)\sum_{h\in\mathcal{H}} P_{EHU}\left(\sqrt{P_{ET}},h\right)p(h) - \eta P_{ET}\sum_{h\in\mathcal{H}} h^2 p(h)\right). \quad (60)$$

In this case, the capacity is given by (21). On the other hand, when (60) does not hold, another possible way to satisfy $\sum_{x_2\in\mathcal{X}_2} x_2^2\ p(x_2|h)p(h) \le P_{ET}$ is to have $x_2^* = x_0(h)$, where in addition to C1 in (56), the following has to be satisfied

$$\sum_{h\in\mathcal{H}}\frac{1}{2}\log\left(1+\frac{h^2\ P_{EHU}(x_0(h),h)}{\sigma_2^2+x_0^2(h)\alpha_2}\right)p(h) = \lambda_1\sum_{h\in\mathcal{H}} x_0^2(h)p(h) + \mu_1 + \lambda_2\left(\left(1-\eta(\bar{g_1}^2+\alpha_1)\right)\sum_{h\in\mathcal{H}} P_{EHU}(x_0(h),h)p(h) - \eta\sum_{h\in\mathcal{H}} x_0^2(h)h^2 p(h)\right). \quad (61)$$

Using (61) and C3 in (56), we can find the optimal $x_0(h)$ as given by (23) in Theorem 2.

ACKNOWLEDGMENT

The authors would like to thank Prof. P. Popovski, Aalborg University, Denmark, for comments that greatly improved the manuscript.

REFERENCES

[1] I. Nikoloska, N. Zlatanov, and Z. Hadzi-Velkov, "On the capacity of a full-duplex wirelessly powered communication system with self-interference and processing cost," in *Proc. IEEE ICC*, Kansas City, MO, USA, May 2018, pp. 1–7.

[2] D. Gunduz, K. Stamatiou, N. Michelusi, and M. Zorzi, "Designing intelligent energy harvesting communication systems," *IEEE Commun. Mag.*, vol. 52, no. 1, pp. 210–216, Jan. 2014.

[3] C. K. Ho and R. Zhang, "Optimal energy allocation for wireless communications with energy harvesting constraints," *IEEE Trans. Signal Process.*, vol. 60, no. 9, pp. 4808–4818, Sep. 2012.

[4] L. R. Varshney, "Transporting information and energy simultaneously," in *Proc. IEEE ISIT*, Toronto, ON, Canada, Jul. 2008, pp. 1612–1616.

[5] H. Yu and R. Zhang, "Throughput maximization in wireless powered communication networks," in *Proc. IEEE GLOBECOM*, Atlanta, GA, USA, Dec. 2013, pp. 4086–4091.

[6] O. Ozel and S. Ulukus, "AWGN channel under time-varying amplitude constraints with causal information at the transmitter," in *Proc. IEEE ASILOMAR*, Pacific Grove, CA, USA, Nov. 2011, pp. 373–377.

[7] W. Mao and B. Hassibi, "Capacity analysis of discrete energy harvesting channels," *IEEE Trans. Inf. Theory*, vol. 63, no. 9, pp. 5850–5885, Sep. 2017.

[8] Z. Chen, G. C. Fen-Ante, H. H. Yang, and T. Q. S. Quek, "Capacity bounds on energy harvesting binary symmetric channels with finite battery," in *Proc. IEEE ICC*, Paris, France, May 2017, pp. 1–5.

[9] D. Shaviv, P.-M. Nguyen, and A. Özgür, "Capacity of the energy-harvesting channel with a finite battery," *IEEE Trans. Inf. Theory*, vol. 62, no. 11, pp. 6436–6458, Nov. 2016.

[10] M. Ashraphijuo, V. Aggarwal, and X. Wang, "On the capacity of energy harvesting communication link," *IEEE J. Sel. Areas Commun.*, vol. 33, no. 12, pp. 2671–2686, Dec. 2015.

[11] R. Rajesh, V. Sharma, and P. Viswanath, "Information capacity of energy harvesting sensor nodes," in *Proc. IEEE ISIT*, St. Petersburg, Russia, Jul./Aug. 2011, pp. 2363–2367.

[12] O. Ozel and S. Ulukus, "Achieving AWGN capacity under stochastic energy harvesting," *IEEE Trans. Inf. Theory*, vol. 58, no. 10, pp. 6471–6483, Oct. 2012.

[13] R. Rajesh, V. Sharma, and P. Viswanath, "Capacity of Gaussian channels with energy harvesting and processing cost," *IEEE Trans. Inf. Theory*, vol. 60, no. 5, pp. 2563–2575, May 2014.

[14] O. Ozel and S. Ulukus, "Information-theoretic analysis of an energy harvesting communication system," in *Proc. 21st IEEE Int. Symp. Pers., Indoor Mobile Radio Commun. Workshops*, Instanbul, Turkey, Sep. 2010, pp. 330–335.

[15] S. Luo, R. Zhang, and T. J. Lim, "Optimal save-then-transmit protocol for energy harvesting wireless transmitters," *IEEE Trans. Wireless Commun.*, vol. 12, no. 3, pp. 1196–1207, Mar. 2013.

[16] L. Liu, R. Zhang, and K.-C. Chua, "Wireless information transfer with opportunistic energy harvesting," *IEEE Trans. Wireless Commun.*, vol. 12, no. 1, pp. 288–300, Jan. 2013.

[17] Y. Dong, Z. Chen, and P. Fan, "Capacity region of Gaussian multiple-access channels with energy harvesting and energy cooperation," *IEEE Access*, vol. 5, pp. 1570–1578, 2017.

[18] H. A. Inan, D. Shaviv, and A. Ozgur, "Capacity of the energy harvesting Gaussian MAC," in *Proc. IEEE ISIT*, Barcelona, Spain, Jul. 2016, pp. 2744–2748.

[19] N. Zlatanov, D. W. K. Ng, and R. Schober, "Capacity of the two-hop relay channel with wireless energy transfer from relay to source and energy transmission cost," *IEEE Trans. Wireless Commun.*, vol. 16, no. 1, pp. 647–662, Jan. 2017.

[20] Y. Gu and S. Aïssa, "RF-based energy harvesting in decode-and-forward relaying systems: Ergodic and outage capacities," *IEEE Trans. Wireless Commun.*, vol. 14, no. 11, pp. 6425–6434, Nov. 2015.

[21] V. Sharma and R. Rajesh, "Queuing theoretic and information theoretic capacity of energy harvesting sensor nodes," in *Proc. IEEE ASILOMAR*, Pacific Grove, CA, USA, Nov. 2011, pp. 383–388.

[22] E. Everett, A. Sahai, and A. Sabharwal, "Passive self-interference suppression for full-duplex infrastructure nodes," *IEEE Trans. Wireless Commun.*, vol. 13, no. 2, pp. 680–694, Jan. 2014.

[23] C. R. Anderson *et al.*, "Antenna isolation, wideband multipath propagation measurements, and interference mitigation for on-frequency repeaters," in *Proc. IEEE SoutheastCon*, Mar. 2004, pp. 110–114.

[24] M. Duarte, C. Dick, and A. Sabharwal, "Experiment-driven characterization of full-duplex wireless systems," *IEEE Trans. Wireless Commun.*, vol. 11, no. 12, pp. 4296–4307, Dec. 2012.

[25] A. Sahai, G. Patel, C. Dick, and A. Sabharwal, "On the impact of phase noise on active cancelation in wireless full-duplex," *IEEE Trans. Veh. Technol.*, vol. 62, no. 9, pp. 4494–4510, Nov. 2013.

[26] B. P. Day, A. R. Margetts, D. W. Bliss, and P. Schniter, "Full-duplex MIMO relaying: Achievable rates under limited dynamic range," in *Proc. IEEE ASILOMAR*, Pacific Grove, CA, USA, Nov. 2012, pp. 1290–1294.

[27] M. Duarte *et al.*, "Design and characterization of a full-duplex multi-antenna system for WiFi networks," *IEEE Trans. Veh. Technol.*, vol. 63, no. 3, pp. 1160–1177, Mar. 2014.

[28] Y. Zeng and R. Zhang, "Full-duplex wireless-powered relay with self-energy recycling," *IEEE Wireless Commun. Lett.*, vol. 4, no. 2, pp. 201–204, Apr. 2015.

[29] M. Maso, C.-F. Liu, C.-H. Lee, T. Q. S. Quek, and L. S. Cardoso, "Energy-recycling full-duplex radios for next-generation networks," *IEEE J. Sel. Areas Commun.*, vol. 33, no. 2, pp. 2948–2962, Dec. 2015.

[30] Z. Hu, C. Yuan, F. Zhu, and F. Gao, "Weighted sum transmit power minimization for full-duplex system with SWIPT and self-energy recycling," *IEEE Access*, vol. 4, pp. 4874–4881, 2016.

[31] J. Chae, H. Lee, J. Kim, and I. Lee, "Self energy recycling techniques for MIMO wireless communication systems," in *Proc. IEEE ICC*, Paris, France, May 2017, pp. 1–6.

[32] D. Bharadia, E. McMilin, and S. Katti, "Full duplex radios," in *Proc. ACM SIGCOMM*, Hong Kong, 2013, pp. 375–386.

[33] N. Zlatanov, E. Sippel, V. Jamali, and R. Schober, "Capacity of the Gaussian two-hop full-duplex relay channel with residual self-interference," *IEEE Trans. Commun.*, vol. 65, no. 3, pp. 1005–1021, Mar. 2017.

[34] N. Zlatanov, R. Schober, and Z. Hadzi-Velkov, "Asymptotically optimal power allocation for energy harvesting communication networks," *IEEE Trans. Veh. Technol.*, vol. 66, no. 8, pp. 7286–7301, Aug. 2017.

[35] T. M. Cover and J. A. Thomas, *Elements of Information Theory*. Hoboken, NJ, USA: Wiley, 2012.

[36] D. Tse and P. Viswanath, *Fundamentals of Wireless Communication*. Cambridge, U.K.: Cambridge Univ. Press, 2005.

Ivana Nikoloska (S'14) received the bachelor's and master's degrees from Ss. Cyril and Methodius University, Skopje, Macedonia, in 2014 and 2016, respectively. She is currently pursuing the Ph.D. degree with Monash University, Melbourne, Australia. From 2015 to 2016, she was a Research Associate with the Faculty of Electrical Engineering and Information Technologies, Ss. Cyril and Methodius University, where she was involved in research projects funded by the Alexander von Humboldt Foundation. Her research interests include wireless communication and information theory.

Nikola Zlatanov (S'06–M'15) was born in Macedonia. He received the Dipl.-Ing. and master's degrees in electrical engineering from Ss. Cyril and Methodius University, Skopje, Macedonia, in 2007 and 2010, respectively, and the Ph.D. degree from The University of British Columbia (UBC), Vancouver, Canada, in 2015. He is currently a Lecturer (Assistant Professor) with the Department of Electrical and Computer Systems Engineering, Monash University, Melbourne, Australia. His current research interests include wireless communications and information theory. He is a TPC Member of various conferences, including Globecom, ICC, VTC, and ISWCS. He received several scholarships/awards for his research including the UBC's Four Year Doctoral Fellowship in 2010, the UBC's Killam Doctoral Scholarship and Macedonia's Young Scientist of the Year in 2011, the Vanier Canada Graduate Scholarship in 2012, the Best Journal Paper Award from the German Information Technology Society in 2014, and the Best Conference Paper Award at ICNC in 2016. He serves as an Editor for the IEEE COMMUNICATIONS LETTERS.

Zoran Hadzi-Velkov (M'97–SM'11) received the Dipl.-Ing. degree (Hons.) in electrical engineering, the Magister Ing. degree (Hons.) in communications engineering, and the Ph.D. degree in technical sciences from Ss. Cyril and Methodius University, Skopje, Macedonia, in 1996, 2000, and 2003, respectively. During 2001–2002, he was a Visiting Scholar with the IBM Watson Research Center, Yorktown Heights, NY, USA. Between 2012 and 2014, he was a Visiting Professor with the Institute for Digital Communications, University of Erlangen-Nuremberg, Germany. He is currently a Professor of telecommunications with Ss. Cyril and Methodius University. He was a recipient of the Alexander von Humboldt Fellowship for experienced researchers in 2012. He received the Annual Best Scientist Award from Ss. Cyril and Methodius University in 2014. Between 2012 and 2015, he was the Chair of the Macedonian Chapter of the IEEE Communications Society. He served on the technical program committees for numerous international conferences, including IEEE ICC and IEEE GLOBECOM. Between 2012 and 2016, he served as an Editor for the IEEE COMMUNICATIONS LETTERS.

Chapter 3

Secrecy Capacity of a Full-Duplex Wirelessly Powered Communication Network in the Presence of a Passive Eavesdropper

To ensure confidentiality in FD WPCNs, in this chapter, we extend the system model from Chapter 2, and we investigate the secrecy capacity in the presence of a passive eavesdropper (EVE). The ET is assumed to transmit radio-frequency energy, which is used for powering the EHU as well as for generating interference at the EVE. The EHU uses the energy harvested from the ET to transmit confidential messages back to the ET. As a consequence of the FD mode of operation, both the EHU and the ET are subjected to self-interference, which has different effects at the two nodes. In particular, the self-interference impairs the decoding of the received message at the ET, whilst it serves as an additional energy source at the EHU. For this system model, we derive an upper and a lower bound on the secrecy capacity. For the lower bound, we propose a simple coding scheme.
The initial results have been presented and published in the proceedings of the

IEEE ISWCS, Oulu, Finland, August 2019.

- I. Nikoloska, N. Zlatanov, Z. Hadzi-Velkov, and R. Zhang "On the Secrecy Capacity of a Full-Duplex Wirelessly Powered Communication System", in proceedings, IEEE ISWCS, Oulu, Finland, August 2019.

The complete study, which includes detailed proofs of theorems, a simple coding scheme that achieves the lower bound on the secrecy capacity, as well as a more extensive numerical analysis have been published in the IEEE Transactions on Wireless Communications, vol.18, no. 11, pp. 5424-5439, 2019, and this paper is included in this chapter.

- I. Nikoloska, N. Zlatanov, Z. Hadzi-Velkov, and R. Zhang "On the Secrecy Capacity of a Full-Duplex Wirelessly Powered Communication System", IEEE Transactions on Wireless Communications, vol.18, no. 11, pp. 5424-5439, 2019. Reprinted with permission from IEEE.

On the Secrecy Capacity of a Full-Duplex Wirelessly Powered Communication System

Ivana Nikoloska, *Student Member, IEEE*, Nikola Zlatanov, *Member, IEEE*, Zoran Hadzi-Velkov, *Senior Member, IEEE*, and Rui Zhang, *Fellow, IEEE*

***Abstract*— In this paper, we investigate the secrecy capacity of a point-to-point, full-duplex (FD) wirelesly powered communication system in the presence of a passive eavesdropper (EVE). The considered system is comprised of an energy transmitter (ET), an energy harvesting user (EHU), and a passive EVE. The ET transmits radio-frequency energy, which is used for powering the EHU as well as for generating interference at the EVE. The EHU uses the energy harvested from the ET to transmit confidential messages back to the ET. As a consequence of the FD mode of operation, both the EHU and the ET are subjected to self-interference, which has different effects at the two nodes. In particular, the self-interference impairs the decoding of the received message at the ET, whilst it serves as an additional energy source at the EHU. For this system model, we derive an upper and a lower bound on the secrecy capacity. For the lower bound, we propose a simple achievability scheme. Our numerical results show significant improvements in terms of achievable secrecy rate when the proposed communication scheme is employed against its half-duplex counterpart, even for practical self-interference values at the ET.**

***Index Terms*— Physical layer security, secrecy capacity, full-duplex communication.**

I. Introduction

THE security of wireless communication is of critical societal interest. Traditionally, encryption has been the primary method which ensures that only the legitimate receiver receives the intended message. Encryption algorithms commonly require that some information, colloquially referred to as a key, is shared only among the legitimate entities in the network. However, key management makes the encryption impractical in architectures such as radio-frequency identification (RFID) networks and sensor networks, since certificate authorities or key distributers are often not available and limitations in terms of computational complexity make the use of standard data encryption difficult [1], [2]. This problem with network security will be increasingly emphasised in the foreseeable future because of paradigms such as the Internet of Things (IoT). The IoT, as a "network of networks", will provide ubiquitous connectivity and information-gathering capabilities to a massive number of communication devices. However, the low-complexity hardware and the severe energy constraints of the IoT devices present unique security challenges. To ensure confidentiality in such networks, exploitation of the physical properties of the wireless channel has become an attractive option [2]. Essentially, the presence of fading, interference, and path diversity in the wireless channel can be leveraged in order to degrade the ability of potential intruders to gain information about the confidential messages sent through the wireless channel [2]. This approach is commonly known as physical layer security, or alternatively as information-theoretic security [3].

Shannon and Wyner have laid a solid foundation for studying secrecy of many different system models in [4], [5], including communication systems powered by energy harvesting (EH), which have attracted significant attention recently [6], [7]. EH relies on harvesting energy from ambient renewable and environmentally friendly sources such as, solar, thermal, vibration or wind, or, from dedicated energy transmitters. The latter gives rise to wirelesly powered communication networks (WPCNs) [8]. EH is often considered as a suitable supplement to IoT networks, since most IoT nodes have low power requirements on the order of microwatts to milliwatts, which can be easily met by EH. In addition, when paired with physical layer security, WPCNs can potentially offer a secure and ubiquitous operation [9]. An EH network with multiple power-constrained information sources has been studied in [10], where the authors derived an exact expression for the probability of a positive secrecy capacity. In [11] and [12], the secrecy capacity of the EH Gaussian multiple-input-multiple-output (MIMO) wire-tap channel under transmitter- and receiver-side power constraints has been derived. The secrecy outage probability of a single-input-multiple-output (SIMO) and multiple-input-single-output (MISO) simultaneous wireless information and power transfer (SWIPT) systems were characterized in [13] and [14], [15], respectively. Secrecy in SWIPT systems has also been studied in [16], [17]. Relaying networks with EH in the presence of a passive eavesdropper have been studied in [18]. Defence methods with EH friendly

Manuscript received November 28, 2018; revised May 18, 2019; accepted August 5, 2019. Date of publication August 26, 2019; date of current version November 11, 2019. This work was supported by the Australian Research Councils Discovery Early Career Researcher Award (DECRA) Scheme under Project DE180101134. This article was presented in part at the 2019 IEEE International Symposium on Wireless Communication Systems. The associate editor coordinating the review of this article and approving it for publication was S. Ma. *(Corresponding author: Ivana Nikoloska.)*

I. Nikoloska and N. Zlatanov are with the Department of Electrical and Computer Systems Engineering, Monash University, Melbourne, VIC 3800, Australia (e-mail: ivana.nikoloska@monash.edu; nikola.zlatanov@monash.edu).

Z. Hadzi-Velkov is with the Faculty of Electrical Engineering and Information Technologies, Ss. Cyril and Methodius University, 1000 Skopje, North Macedonia (e-mail: zoranhv@feit.ukim.edu.mk).

R. Zhang is with the Department of Electrical and Computer Engineering, National University of Singapore, Singapore 119077 (e-mail: elezhang@nus.edu.sg).

Color versions of one or more of the figures in this article are available online at http://ieeexplore.ieee.org.

Digital Object Identifier 10.1109/TWC.2019.2936201

jammers, have been proposed in [19] and [20], where the secrecy capacity and the secrecy outage probability have been derived.

In addition to physical layer security, another appealing option for networks with scarce resources such as WPCNs, is the full-duplex (FD) mode of operation. Recent results in the literature, e.g., [21]–[24], have shown that it is possible for transceivers to operate in the FD mode by transmitting and receiving signals simultaneously and in the same frequency band. The FD mode of operation can lead to doubling (or even tripling, see [25]) of the spectral efficiency of the network in question.

Motivated by these advances in FD communication and the applicability of physical layer security to WPCNs, in this paper, we investigate the secrecy capacity of a FD wirelessly powered communication system. Unlike our prior work in [26] which does not have an eavesdropper and therefore does not consider secrecy constraints, the network in this paper is comprised of an energy transmitter (ET) and an energy harvesting user (EHU) in the presence of a passive eavesdropper (EVE). The objective in this paper is to investigate the secrecy capacity and develop novel communication schemes capable of achieving non-zero secrecy rates. As a result, the achievability schemes presented in this paper are different than the achievability schemes in [26]. In this system, the ET sends radio-frequency (RF) energy to the EHU, whereas, the EHU harvests this energy and uses it to transmit confidential information back to the ET. The signal transmitted by the ET serves a second purpose by acting as an interference signal for EVE. Both the ET and the EHU are assumed to operate in the FD mode, hence, both nodes transmit and receive RF signals in the same frequency band and at the same time. As a result, both are subjected to self-interference. The self-interference hinders the decoding of the information signal received from the EHU at the ET. At the EHU, the self-interference resulting from the simultaneous transmission and reception increases the amount of energy that can be harvested by the EHU [27]. Meanwhile, EVE is passive and only aims to intercept the confidential message transmitted by the EHU to the ET. For the considered system model, we derive an upper and a lower bound on the secrecy capacity. Furthermore, we provide a simple achievability scheme for the lower bound on the secrecy capacity. The proposed scheme in this paper is relatively simple and therefore easily applicable in practice in wirelessly powered IoT networks which require secure information transmissions. For example, sensors which are embedded in the infrastructure, like buildings, bridges or the power grid, monitor their environment and generate measurements. The generated measurements often contain sensitive information. An Unmanned Aerial Vehicle (UAV) can fly close to the sensors in order to power them, and then receive the generated data packets from the sensors. The proposed scheme in this paper can be used in this scenario and it will guarantees that such sensitive information will never be intercepted by an illegitimate, third party.

The rest of the paper is organized as follows. Section II provides the system and channel models. Sections III and IV present the upper and the lower bounds on the secrecy capacity, respectively. In Section V, we provide numerical results and we conclude the paper in Section VI. Proofs of theorems/lemmas are provided in the Appendices.

II. System Model and Problem Formulation

We consider a system model comprised of an EHU, an ET, and an EVE. In order to improve the spectral efficiency of the considered system, both the EHU and the ET are assumed to operate in the FD mode, i.e., both nodes transmit and receive RF signals simultaneously and in the same frequency band. Thereby, the EHU receives energy signals from the ET and simultaneously transmits information signals to the ET. Similarly, the ET transmits energy signals to the EHU and simultaneously receives information signals from the EHU. The signal transmitted from the ET also serves as interference to the EVE, and thereby increases its noise floor. Due to the FD mode of operation, both the EHU and the ET are subjected to self-interference, which has opposite effects at the two nodes, respectively. More precisely, the self-interference signal has a negative effect at the ET since it hinders the decoding of the information signal received from the EHU. As a result, the ET should be designed with a self-interference suppression apparatus, which can suppress the self-interference at the ET and thereby improve the decoding of the desired signal received from the EHU. On the other hand, at the EHU, the self-interference signal is desired since it increases the amount of energy that can be harvested by the EHU. Hence, the EHU should be designed without a self-interference suppression apparatus in order for the energy contained in the self-interference signal to be harvested, i.e., the EHU should perform energy recycling as proposed in [27]. Meanwhile, EVE remains passive and only receives, thus it is not subjected to self-interference.

A. Channel Model

Let V_{12i} and V_{21i} denote random variables (RVs) which model the fading channel gains of the EHU-ET and ET-EHU channels in channel use i, respectively. Due to the FD mode of operation, the EHU-ET and the ET-EHU channels are identical and as a result the channel gains V_{12i} and V_{21i} are assumed to be identical, i.e., $V_{12i} = V_{21i} = V_i$. Moreover, let F_i and G_i denote RVs which model the fading channel gains of the EHU-EVE and ET-EVE channels in channel use i, respectively. We assume that all channel gains follow a block-fading model, i.e., they remain constant during all channel uses in one block, but change from one block to the next, where each block consists of (infinitely) many channel uses. All three nodes are assumed to have a priori knowledge of the CSI of the EHU-ET channel, i.e., V_i. In addition, EVE is assumed to have CSI of the the EHU-EVE and the ET-EVE channels, given by G_i and F_i, respectively.

In the i-th channel use, let the transmit symbols at the EHU and the ET be modeled as RVs, denoted by X_{1i} and X_{2i}, respectively. Moreover, in channel use i, let the received symbols at the EHU, the ET, and EVE be modeled as RVs, denoted by Y_{1i}, Y_{2i}, and Y_{3i}, respectively. Furthermore, in channel use i, let the RVs modeling the AWGNs at the EHU, the ET, and the EVE be denoted by N_{1i}, N_{2i}, and N_{3i},

respectively, such that $N_{1i} \sim \mathcal{N}\left(0, \sigma_1^2\right)$, $N_{2i} \sim \mathcal{N}\left(0, \sigma_2^2\right)$, and $N_{3i} \sim \mathcal{N}\left(0, \sigma_3^2\right)$, where $\mathcal{N}\left(\mu, \sigma^2\right)$ denotes a Gaussian distribution with mean μ and variance σ^2. Note that the derived results can be extended to the complex-valued channel in a straightforward manner since the complex-valued channel can be resolved in two parallel real-valued channels that use the achievability schemes that we derive here. Moreover, let the RVs modeling the additive self-interferences at the EHU and the ET in channel use i be denoted by I_{1i} and I_{2i}, respectively.

By using the notation defined above, the input-output relations describing the considered channel in channel use i can be written as

$$Y_{1i} = V_i X_{2i} + I_{1i} + N_{1i}, \tag{1}$$

$$Y_{2i} = V_i X_{1i} + I_{2i} + N_{2i}, \tag{2}$$

$$Y_{3i} = F_i X_{1i} + G_i X_{2i} + N_{3i}. \tag{3}$$

B. Self-Interference Model

A general model for the self-interference at the EHU and the ET is given by [28]

$$I_{1i} = \sum_{m=1}^{M} \tilde{Q}_{1,m}(i) X_{1i}^m, \tag{4}$$

$$I_{2i} = \sum_{m=1}^{M} \tilde{Q}_{2,m}(i) X_{2i}^m, \tag{5}$$

where $M < \infty$ is an integer and $\tilde{Q}_{1,m}(i)$ and $\tilde{Q}_{2,m}(i)$ model the m-th component of the self-interference channel between the transmitter- and the receiver-ends at the EHU and the ET in channel use i, respectively. As shown in [28], the components in (4) and (5) for which m is odd carry non-negligible energy and the remaining components carry negligible energy and therefore can be ignored. Furthermore, the higher order components carry less energy than the lower order terms. As a result, we can justifiably adopt the first-order approximation of the self-interference in (4) and (5), and model I_{1i} and I_{2i} as

$$I_{1i} = \tilde{Q}_{1i} X_{1i}, \tag{6}$$

$$I_{2i} = \tilde{Q}_{2i} X_{2i}, \tag{7}$$

where $\tilde{Q}_{1i} = \tilde{Q}_1(i)$ and $\tilde{Q}_{2i} = \tilde{Q}_2(i)$ are used for simplicity of notation. Thereby, the adopted self-interference model takes into account only the linear component of (4) and (5), i.e., the component for $m = 1$. The linear self-interference model has been widely used, e.g. in [28], [29].

By inserting (6) and (7) into (1) and (2), respectively, we obtain

$$Y_{1i} = V_i X_{2i} + \tilde{Q}_{1i} X_{1i} + N_{1i}, \tag{8}$$

$$Y_{2i} = V_i X_{1i} + \tilde{Q}_{2i} X_{2i} + N_{2i}. \tag{9}$$

To model the worst-case of linear self-interference, we note the following. Since the ET knows which symbol it has transmitted in channel use i, the ET knows the outcome of the RV X_{2i}, denoted by x_{2i}. As a result of this knowledge, the noise that the ET "sees" in its received symbol Y_{2i} given by (9), is $\tilde{Q}_{2i} x_{2i} + N_{2i}$, where x_{2i} is a constant. Hence, the noise that the ET "sees", $\tilde{Q}_{2i} x_{2i} + N_{2i}$, will represent the worst-case of noise, under a second moment constraint, if and only if $\tilde{Q}_{2i}$ is an independent and identically distributed (i.i.d.) Gaussian RV.[1] Therefore, in order to derive results for the worst-case of linear self-interference, we assume that $\tilde{Q}_{2i} \sim \mathcal{N}\{\bar{q}_{2i}, \alpha_2\}$ in the rest of the paper. Meanwhile, Q_{1i} is distributed according to an arbitrary probability distribution with mean $\bar{q}_{1i}$ and variance α_1.

Now, since $\tilde{Q}_{1i}$ and $\tilde{Q}_{2i}$ can be written equivalently as $\tilde{Q}_{1i} = Q_{1i} + \bar{q}_1$ and $\tilde{Q}_{2i} = Q_{2i} + \bar{q}_2$, where $\bar{q}_{1i}$ and $\bar{q}_{2i}$ are the means of $\tilde{Q}_{1i}$ and $\tilde{Q}_{2i}$, respectively, and Q_{1i} and Q_{2i} denote the remaining zero-mean components of $\tilde{Q}_{1i}$ and $\tilde{Q}_{2i}$, respectively, we can write Y_{1i} and Y_{2i} in (8) and (9), respectively, as

$$Y_{1i} = V_i X_{2i} + \bar{q}_{1i} X_{1i} + Q_{1i} X_{1i} + N_{1i}, \tag{10}$$

$$Y_{2i} = V_i X_{1i} + \bar{q}_{2i} X_{2i} + Q_{2i} X_{2i} + N_{2i}. \tag{11}$$

Since the ET always knows the outcome of X_{2i}, x_{2i}, and since given sufficient time it can always estimate the deterministic component of its self-interference channel, $\bar{q}_2$, the ET can remove $\bar{q}_2 X_{2i}$ from its received symbol Y_{2i}, given by (11), and thereby reduce its self-interference. In this way, the ET obtains a new received symbol, denoted again by Y_{2i}, as

$$Y_{2i} = V_i X_{1i} + Q_{2i} X_{2i} + N_{2i}. \tag{12}$$

Note that, X_{2i} travels from the transmitter-side to the receiver-side at the ET, it undergoes a random transformation which is unknown to the ET. Thereby, since Q_{2i} in (12) changes independently from one channel use to the next, the ET cannot estimate and remove $Q_{2i} X_{2i}$ from its received symbol even though the ET knows the outcome of X_{2i}. Thus, $Q_{2i} X_{2i}$ in (12) is the residual self-interference at the ET where the ET knows the outcome of X_{2i}. On the other hand, since the EHU benefits from the self-interference, it does not remove $\bar{q}_1\ X_{1i}$ from its received symbol Y_{1i}, given by (10), in order to have a self-interference signal with a much higher energy, which it can then harvest. Hence, the received symbol at the EHU is given by (10).

In this paper, we are interested in the secrecy capacity of the channel characterised by the input-output relationships given by (10), (12), and (3).

C. Energy Harvesting Model

The energy harvested by the EHU in channel use i is given by [27]

$$E_{\text{in},i} = \eta (V_i X_{2i} + \bar{q}_1 X_{1i} + Q_{1i} X_{1i})^2, \tag{13}$$

where $0 < \eta < 1$ is the energy harvesting efficiency coefficient. For convenience, we have assumed unit time and thus we use the terms power and energy interchangeably in the sequel. The EHU stores $E_{\text{in},i}$ in its battery, which is assumed to have an infinitely large storage capacity. Let B_i denote

[1] This is due to the fact that the Gaussian distribution has the largest entropy under a second moment constraint, see [30].

the amount of harvested energy in the battery of the EHU at the end of the i-th channel use. Moreover, let $E_{\text{out},i}$ be the extracted energy from the battery in the i-th channel use. Then, B_i, can be written as

$$B_i = B_{i-1} + E_{\text{in},i} - E_{\text{out},i}. \tag{14}$$

Since in channel use i the EHU cannot extract more energy than the amount of energy stored in its battery at the end of channel use $i-1$, the extracted energy from the battery in channel use i, $E_{\text{out},i}$, can be obtained as

$$E_{\text{out},i} = \min\{B_{i-1}, X_{1i}^2 + P_p\}, \tag{15}$$

where X_{1i}^2 is the transmit energy of the desired transmit symbol in channel use i, X_{1i}, and P_p is the processing energy cost of the EHU [31]. The processing cost, P_p, models the system level power consumption at the EHU, i.e., the energy spent due to the electrical components in the electrical circuit such as AC/DC convertors and RF amplifiers as well as the energy spent for processing. Note that the ET also requires energy for processing. However, the ET is assumed to be equipped with a conventional power source which is always capable of providing the processing energy without affecting the energy required for transmission.

Now, if the total number of channel uses satisfies $n \to \infty$, if the battery of the EHU has an unlimited storage capacity, and furthermore

$$\mathcal{E}\{E_{\text{in},i}\} \geq \mathcal{E}\{X_{1i}^2\} + P_p \tag{16}$$

holds, where $\mathcal{E}\{\cdot\}$ denotes statistical expectation, then the number of channel uses in which the extracted energy from the battery is insufficient and thereby $E_{\text{out},i} = B_{i-1}$ holds is negligible compared to the number of channel uses in which the extracted energy is sufficient for both transmission and processing [32]. In other words, when the above three conditions hold, in almost all channel uses, there will be enough energy to be extracted from the EHU's battery for both processing, P_p, and for the transmission of the desired transmit symbol X_{1i}, X_{1i}^2, and thereby $E_{\text{out},i} = X_{1i}^2 + P_p$ holds.

III. Upper Bound on the Secrecy Capacity

For the considered channel, we propose the following theorem which establishes an upper bound on the secrecy capacity.

Theorem 1: Assuming that the average power constraint at the ET is P_{ET}, an upper bound on the secrecy capacity of the considered channel is given by

$$\begin{aligned}
\max_{p(x_1|x_2,v),p(x_2|v)} \; & \sum_{x_2\in\mathcal{X}_2}\sum_{v\in\mathcal{V}} I(X_1;Y_2|X_2=x_2,V=v) \\
& \times p(x_2|v)p(v) \\
& - \sum_{v\in\mathcal{V}}\sum_{g\in\mathcal{G}}\sum_{f\in\mathcal{F}} I(X_1;Y_3|V=v, \\
& G=g,F=f)p(v)p(g)p(f) \\
\text{Subject to C1:} \; & \sum_{x_2\in\mathcal{X}_2}\sum_{v\in\mathcal{V}} x_2^2\, p(x_2|v)p(v) \leq P_{ET} \\
\text{C2:} \; & \int_{x_1}\sum_{x_2\in\mathcal{X}_2}\sum_{v\in\mathcal{V}} (x_1^2+P_p) \\
& \times p(x_1|x_2,v)p(x_2|v)p(v)dx_1 \\
& \leq \int_{x_1}\sum_{x_2\in\mathcal{X}_2}\sum_{v\in\mathcal{V}} E_{\text{in}} p(x_1|x_2,v) \\
& \times p(x_2|v)p(v)dx_1 \\
\text{C3:} \; & \sum_{x_2\in\mathcal{X}_2} p(x_2|v) = 1 \\
\text{C4:} \; & \int_{x_1} p(x_1|x_2,v)dx_1 = 1,
\end{aligned} \tag{17}$$

where $I(;|)$ denotes the conditional mutual information. In (17), lower-case letters x_2, v, g, and f represent realizations of the random variables X_2, V, G, and F, respectively, and their support sets are denoted by $\mathcal{X}_2$, $\mathcal{V}$, $\mathcal{G}$, and $\mathcal{F}$, respectively. Constraint C1 in (17) constrains the average transmit power of the ET to P_{ET}, and C2 is due to (16), i.e., due to the fact that EHU has to have harvested enough energy for both processing and transmission of symbol X_1. The maximum in the objective function is taken over all possible conditional probability distributions of x_1 and x_2, given by $p(x_1|x_2,v)$ and $p(x_2|v)$, respectively.

Proof: Please refer to Appendix A, where the converse is provided. ∎

A. Simplified Expression of the Upper Bound on the Secrecy Capacity

The optimal input distributions at the EHU and the ET that are the solutions of the optimization problem in (17) and the resulting simplified expressions of the upper bound on the secrecy capacity are provided by the following lemma.

Lemma 1: The optimal input distribution at the EHU, found as the solution of the optimization problem in (17), is zero-mean Gaussian with variance $P_{EHU}(x_2,v)$, i.e., $p(x_1|x_2,v) \sim \mathcal{N}(0, P_{EHU}(x_2,v))$, where $P_{EHU}(x_2,v)$ can be found as the solution of

$$\begin{aligned}
& \frac{v^2}{\sigma_2^2 + x_2^2\alpha_2} \\
& \quad + \left(1 + \frac{v^2\; P_{EHU}(x_2,v)}{\sigma_2^2 + x_2^2\alpha_2}\right) \sum_{f\in\mathcal{F}} \frac{f^2}{f^2 P_{EHU}(x_2,v) + \sigma_3^2} p(f) \\
& = \left(1 + \frac{v^2 P_{EHU}(x_2,v)}{\sigma_2^2 + x_2^2\alpha_2}\right) \lambda_2(1 - \eta(\bar{g_1}^2 + \alpha_1)),
\end{aligned} \tag{18}$$

where λ_2 is chosen such that C2 in (17) holds with equality.

On the other hand, the optimal input distribution at the ET, found as the solution of the optimization problem in (17), has the following discrete form

$$\begin{aligned}
p(x_2|v) = \; & p(x_2=0)\delta(x_2) \\
& + \frac{1}{2}\sum_{j=1}^{J} p(x_2 = x_{2j}) \\
& \times \Big(\delta(x_2 - x_{2j}) + \delta(x_2 + x_{2j})\Big),
\end{aligned} \tag{19}$$

where $\delta(\cdot)$ denotes the Dirac delta function. Finally, the simplified expression of the upper bound on the secrecy capacity

in (17), denoted by C_s^u, is given by

$$\begin{aligned}C_s^u = &\frac{1}{2}\sum_{v\in\mathcal{V}}\sum_{j=1}^{J}\log\left(1+\frac{v^2\ P_{EHU}(x_2,v)}{\sigma_2^2+x_{2j}^2\alpha_2}\right)p(x_2=x_{2j})p(v)\\ &+\sum_{v\in\mathcal{V}}\sum_{g\in\mathcal{G}}\sum_{f\in\mathcal{F}}\left[\int_{-\infty}^{\infty}\frac{1}{\sqrt{2\pi\sigma_{y_3}^2}}\sum_{j=1}^{J}p(x_2=x_{2j})\right.\\ &\times e^{-\frac{(y_3-x_{2j})^2}{2\sigma_{y_3}^2}}\\ &\times\ln\left(\frac{1}{\sqrt{2\pi\sigma_{y_3}^2}}\sum_{j=1}^{J}p(x_2=x_{2j})e^{-\frac{(y_3-x_{2j})^2}{2\sigma_{y_3}^2}}\right)dy_3\\ &-\int_{-\infty}^{\infty}\frac{1}{\sqrt{2\pi\sigma_3^2}}\sum_{j=1}^{J}p(x_2=x_{2j})e^{-\frac{(z-x_{2j})^2}{2\sigma_3^2}}\\ &\left.\times\ln\left(\frac{1}{\sqrt{2\pi\sigma_3^2}}\sum_{j=1}^{J}p(x_2=x_{2j})e^{-\frac{(z-x_{2j})^2}{2\sigma_3^2}}\right)dz_3\right]\\ &\times p(v)p(g)p(f).\end{aligned}\tag{20}$$

Proof: Please refer to Appendix B. ∎

IV. Lower Bound on the Secrecy Capacity - An Achievable Secrecy Rate

From Lemma 1, we can see that the upper bound on the secrecy capacity cannot be achieved since the EHU has to know x_{2i}^2 in each channel use i, in order for the EHU to calculate (18). In other words, the EHU can not adapt $P_{EHU}(x_2,v)$ and the data rates of its codewords accordingly. The knowledge of x_{2i}^2 at the EHU is not possible since the input distribution at the ET, given by (19), is discrete with a finite number of probability mass points. However, if we set the input distribution at the ET to be binary such that x_{2i}, $\forall i$, takes values from the set $\{x_0,-x_0\}$, then the EHU can know x_{2i}^2 in each channel use i since $x_{2i}^2=x_0^2$, $\forall i$, and therefore this rate can be achieved. Hence, to obtain an achievable lower bound on the secrecy capacity, we propose the ET to use the following input distribution

$$p(x_2|v)=\frac{1}{2}\Big(\delta(x_2-x_0(v))+\delta(x_2+x_0(v))\Big).\tag{21}$$

The value of $x_0(v)$ will be determined in the following.

A. Simplified Expression of the Lower Bound on the Secrecy Capacity

The simplified expression for the lower bound on the secrecy capacity resulting from the ET using the distribution given by (21), is provided by the following lemma.

Lemma 2: Let us define $\mathcal{I}(x)$ as

$$\mathcal{I}(x)\ =\frac{2}{\sqrt{2\pi}x}e^{-x^2/2}\int_0^{\infty}e^{-y^2/2x}\cosh(y)\ln(\cosh(y))dy.\tag{22}$$

Depending on the channel qualities, we have three cases for the achievable secrecy rate.

Case 1: If the following conditions hold

$$\begin{aligned}&\frac{1}{2}\sum_{v\in\mathcal{V}}\log\left(1+\frac{v^2\ P_{EHU}(x_2,v)}{\sigma_2^2+P_{ET}\alpha_2}\right)p(v)+\lambda_1\ P_{ET}\\ &=\lambda_2\left((1-\eta(\bar{q_1}^2+\alpha_1))\sum_{v\in\mathcal{V}}P_{EHU}(x_2,v)p(v)-\eta P_{ET}\Omega_V\right),\end{aligned}\tag{23}$$

and

$$\begin{aligned}&\frac{1}{2}\sum_{v\in\mathcal{V}}\log\left(1+\frac{v^2\ P_{EHU}(x_2,v)}{\sigma_2^2+P_{ET}\alpha_2}\right)p(v)\\ &>\sum_{v\in\mathcal{V}}\sum_{g\in\mathcal{G}}\sum_{f\in\mathcal{F}}\left[\frac{1}{2}\ln\left(2\pi e\sigma_{y_3}^2\right)\right.\\ &\quad+\frac{P_{ET}}{f^2\ P_{EHU}(x_2,v)+\sigma_3^2}-\mathcal{I}\left(\frac{\sqrt{P_{ET}}}{\sqrt{f^2\ P_{EHU}(x_2,v)+\sigma_3^2}}\right)\\ &\quad\left.-\frac{1}{2}\ln\left(2\pi e\sigma_3^2\right)-\frac{P_{ET}}{\sigma_3^2}+\mathcal{I}\left(\frac{\sqrt{P_{ET}}}{\sigma_3}\right)\right]p(v)p(g)p(f),\end{aligned}\tag{24}$$

where $P_{EHU}(x_2,v)$ is the root of (18) for $x_2=\sqrt{P_{ET}}$ and $\Omega_V=\mathcal{E}\{v^2\}$, then the input distribution at the ET has the following form

$$p(x_2|v)=\frac{1}{2}\left(\delta\left(x_2-\sqrt{P_{ET}}\right)+\delta\left(x_2+\sqrt{P_{ET}}\right)\right),\quad\forall v.\tag{25}$$

On the other hand, the input distribution at the EHU is zero-mean Gaussian with variance $P_{EHU}(\sqrt{P_{ET}},v)$, i.e., $p(x_1|x_2,v)\sim\mathcal{N}\left(0,P_{EHU}(\sqrt{P_{ET}},v)\right)$, where $P_{EHU}(\sqrt{P_{ET}},v)$ can be found as the solution of (18) for $x_2=\sqrt{P_{ET}}$.

For Case 1, the achievable secrecy rate, denoted by C_s^l, is given by

$$\begin{aligned}&C_s^l\\ &=\frac{1}{2}\sum_{v\in\mathcal{V}}\log\left(1+\frac{v^2\ P_{EHU}(\sqrt{P_{ET}},v)}{\sigma_2^2+P_{ET}\alpha_2}\right)p(v)\\ &\quad+\sum_{v\in\mathcal{V}}\sum_{g\in\mathcal{G}}\sum_{f\in\mathcal{F}}\left[\int_{-\infty}^{\infty}\frac{1}{2\sqrt{2\pi\sigma_{y_3}^2}}\left(e^{-\frac{(y_3-\sqrt{P_{ET}})^2}{2\sigma_{y_3}^2}}\right.\right.\\ &\quad\left.+e^{-\frac{(y_3+\sqrt{P_{ET}})^2}{2\sigma_{y_3}^2}}\right)\\ &\quad\times\ln\left(\frac{1}{2\sqrt{2\pi\sigma_{y_3}^2}}\left(e^{-\frac{(y_3-\sqrt{P_{ET}})^2}{2\sigma_{y_3}^2}}+e^{-\frac{(y_3+\sqrt{P_{ET}})^2}{2\sigma_{y_3}^2}}\right)\right)dy_3\\ &\quad-\int_{-\infty}^{\infty}\frac{1}{2\sqrt{2\pi\sigma_3^2}}\left(e^{-\frac{(z_3-\sqrt{P_{ET}})^2}{2\sigma_3^2}}+e^{-\frac{(z_3+\sqrt{P_{ET}})^2}{2\sigma_3^2}}\right)\\ &\quad\left.\times\ln\left(e^{-\frac{(z_3-\sqrt{P_{ET}})^2}{2\sigma_3^2}}+e^{-\frac{(z_3+\sqrt{P_{ET}})^2}{2\sigma_3^2}}\right)dz_3\right]\\ &\quad\times p(v)p(g)p(f).\end{aligned}\tag{26}$$

Case 2: If (23) does not hold, and

$$\begin{aligned}&\frac{1}{2}\sum_{v\in\mathcal{V}}\log\left(1+\frac{v^2\ P_{EHU}(x_2,v)}{\sigma_2^2+x_0^2(v)\alpha_2}\right)p(v)\\&>\sum_{v\in\mathcal{V}}\sum_{g\in\mathcal{G}}\sum_{f\in\mathcal{F}}\Bigg[\frac{1}{2}\ln\left(2\pi e\sigma_{y_3}^2\right)\\&\quad+\frac{x_0^2(v)}{f^2\ P_{EHU}(x_2,v)+\sigma_3^2}-\mathcal{I}\left(\frac{x_0(v)}{\sqrt{f^2\ P_{EHU}(x_2,v)+\sigma_3^2}}\right)\\&\quad-\frac{1}{2}\ln\left(2\pi e\sigma_3^2\right)-\frac{x_0^2(v)}{\sigma_3^2}+\mathcal{I}\left(\frac{x_0(v)}{\sigma_3}\right)\Bigg]p(v)p(g)p(f)\end{aligned}\tag{27}$$

holds, then the input distribution at the ET is given by

$$p(x_2|v)=\frac{1}{2}\Big(\delta(x_2-x_0(v))+\delta(x_2+x_0(v))\Big),\tag{28}$$

whereas the input distribution at the EHU is zero-mean Gaussian with variance $P_{EHU}(x_0(v),v)$. In this case, $P_{EHU}(x_0(v),v)$ and $x_0(v)$ are the roots of the system of equations comprised of (18) for $x_2=x_0(v)$ and the following equation

$$\begin{aligned}&\frac{1}{2}\log\left(1+\frac{v^2P_{EHU}(x_0(v),v)}{\sigma_2^2+x_0^2(v)\alpha_2}\right)-\lambda_1x_0^2(v)\\&\quad=\lambda_2\left((1-\eta(\bar{q_1}^2+\alpha_1))P_{EHU}(x_0(v),v)-\eta v^2x_0^2(v)\right).\end{aligned}\tag{29}$$

For Case 2, the achievable secrecy rate is given by

$$\begin{aligned}&C_s^l\\&=\frac{1}{2}\sum_{v\in\mathcal{V}}\log\left(1+\frac{v^2\ P_{EHU}(x_0(v),v)}{\sigma_2^2+x_0^2(v)\alpha_2}\right)p(v)\\&\quad+\sum_{v\in\mathcal{V}}\sum_{g\in\mathcal{G}}\sum_{f\in\mathcal{F}}\Bigg[\int_{-\infty}^{\infty}\frac{1}{2\sqrt{2\pi\sigma_{y_3}^2}}\left(e^{-\frac{(y_3-x_0(v))^2}{2\sigma_{y_3}^2}}\right.\\&\quad\left.+e^{-\frac{(y_3+x_0(v))^2}{2\sigma_{y_3}^2}}\right)\\&\quad\times\ln\left(\frac{1}{2\sqrt{2\pi\sigma_{y_3}^2}}\left(e^{-\frac{(y_3-x_0(v))^2}{2\sigma_{y_3}^2}}+e^{-\frac{(y_3+x_0(v))^2}{2\sigma_{y_3}^2}}\right)\right)dy_3\\&\quad-\int_{-\infty}^{\infty}\frac{1}{2\sqrt{2\pi\sigma_3^2}}\left(e^{-\frac{(z_3-x_0(v))^2}{2\sigma_3^2}}+e^{-\frac{(z_3+x_0(v))^2}{2\sigma_3^2}}\right)\\&\quad\times\ln\left(e^{-\frac{(z_3-x_0(v))^2}{2\sigma_3^2}}+e^{-\frac{(z_3+x_0(v))^2}{2\sigma_3^2}}\right)dz_3\Bigg]p(v)p(g)p(f).\end{aligned}\tag{30}$$

Case 3: If neither (24) nor (27) holds, then, the achievable secrecy rate is $C_s^l=0$.

Proof: In order for C1 in (17) to hold, or equivalently for C1 in (60) to hold, there are two possible cases for x_2. In Case 1, C1 in (60) is satisfied if x_2 is set to take values from the set $\{\sqrt{P_{ET}},-\sqrt{P_{ET}}\}$. If (63) for $x_2^2=P_{ET}$ does not hold, then x_2 is set to take values from the set $\{x_0(v),-x_0(v)\}$, where $x_0(v)$ is given by (29) in order for C1 in (60) to be satisfied. Now, since $C_s^l=\sum_{x_2\in\mathcal{X}_2}\sum_{v\in\mathcal{V}}I(X_1;Y_2|X_2=x_2,V=v)p(x_2|v)p(v)-\sum_{v\in\mathcal{V}}\sum_{g\in\mathcal{G}}\sum_{f\in\mathcal{F}}I(X_1;Y_3|V=v,G=g,F=f)p(v)p(g)p(f)$, where X_1 follows a Gaussian probability distribution, and X_2 is distributed according to (25) and (28) for Case 1 and Case 2, respectively, we obtain the expressions in (26) and (30) by using (60) and (78). ■

Lemma 2 gives insights into the achievability scheme of the derived lower bound on the secrecy capacity. When Case 1 of Lemma 2 holds, the achievability scheme is very simple. In particular, the ET only chooses between $-\sqrt{P_{ET}}$ or $\sqrt{P_{ET}}$ in every channel use. When Case 2 of Lemma 2 holds, from (29) we see that the ET adapts its transmit power to the channel fading states of the EHU-ET channel, v, and increases its transmit power when v is larger, and conversely, it lowers its transmit power when v is not as favourable. As for the EHU, we first note that, since the EHU knows the square of the transmit symbol of the ET x_2 in a given channel use, the EHU can adapt its transmit power and its rate in the given channel use according to the expected self-interference at the ET, which depends on the value of x_2^2. Secondly, the EHU also takes advantage of the better channel fading states of the EHU-ET channel, v, and increases its transmit power and rate when v is larger, and conversely, it lowers its transmit power and rate when v is not as strong. Thirdly, since λ_2 is chosen such that constraint C2 in (17) holds, the transmit power of the EHU $P_{EHU}(x_2,v)$ depends on the processing cost P_p. Thereby, when Case 2 holds, the ET also takes into account the processing cost of the EHU.

B. Achievability of the Lower Bound on the Secrecy Capacity

We set the total number of channel uses (i.e., symbols) n to $n=k(N+B)$, where $N+B$ denotes the total number of time slots used for the transmission and k denotes the number of symbols transmitted per time slot, where $n\to\infty$, $k\to\infty$, $N\to\infty$, and $(N+B)\to\infty$.

Let $\mathcal{N}$ denote a set comprised of the time slots during which the EHU has enough energy harvested and thereby transmits a codeword, and let $\mathcal{B}$ denote a set comprised of the time slots during which the EHU does not have enough energy harvested and thereby it is silent. Let $N=|\mathcal{N}|$ and $B=|\mathcal{B}|$, where $|\cdot|$ denotes the cardinality of a set.

1) Transmissions at the ET: During the k channel uses of a considered time slot with fading realisation v, the ET's transmit symbol is drawn from the probability distribution given in Lemma 2. Thus, in each channel use of the considered time slot, the ET transmits either $\sqrt{P_{ET}}$ or $-\sqrt{P_{ET}}$ with probability 1/2 if Case 1 in Lemma 2 holds, or transmits $x_0(v)$ or $-x_0(v)$ with probability 1/2 if Case 2 in Lemma 2 holds.

2) Reception of Energy and Transmission of Information at the EHU: The EHU first generates all binary sequences of length kNR_{EHU}, where

$$R_{EHU}=\frac{1}{2}\sum_{v\in\mathcal{V}}\log\left(1+\frac{v^2P_{EHU}(x_2,v)}{\sigma_2^2+x_2^2\alpha_2}\right)p(v),\tag{31}$$

where $P_{EHU}(x_2,v)$ and x_2 can be found from Lemma 2 depending on which case holds. Then the EHU

uniformly assigns each generated sequence to one of 2^{kNR_s} groups, where R_s is given by (26) for Case 1 of Lemma 2, or by (30) for Case 2 of Lemma 2. The confidential message W drawn uniformly from the set $W \in \{1, 2, \ldots, 2^{kNR_s}\}$ is then assigned to a group. Next, the EHU randomly select a binary sequence from the corresponding group to which W is assigned, according to the uniform distribution. This binary sequence is then mapped to a codeword comprised of kN symbols, which is to be transmitted in $N + B$ time slots. The symbols of the codeword are drawn according to a zero-mean, unit-variance Gaussian distribution. Next, the codeword is divided into N blocks, where each block is comprised of k symbols. The length of each block is assumed to coincide with a single fading realization, and thereby to a single time slot.

The EHU will transmit in a given time slot only when it has harvested enough energy both for processing and transmission in the given time slot, i.e., only when its harvested energy accumulates to a level which is higher than $P_p + P_{\text{EHU}}(x_2, v)$, where v is the fading gain in the time slot considered for transmission. Otherwise, the EHU is silent and only harvests energy. When the EHU transmits, it transmits the next untransmitted block of k symbols of its codeword. To this end, each symbol of this block is first multiplied by $\sqrt{P_{EHU}(x_2, v)}$, where $P_{EHU}(x_2, v)$ can be found from Lemma 2, and then the block of k symbols is transmitted over the wireless channel to the ET. The EHU repeats this procedure until it transmits all N blocks of its entire codeword for which it needs $N + B$ time slots.

3) Receptions at the ET: When the ET receives a transmitted block by the EHU, it checks if the power level of the received block is higher than the noise level at the ET or not. If affirmative, the ET places the received block in its data storage, without decoding. Otherwise the received block is discarded.

Now, in $N + B$ time slots, the ET receives the entire codeword transmitted by the EHU. In order for the ET to be able to decode the transmitted codeword, the rate of the transmitted codeword must be equal to or lower than the capacity of the EHU-ET's channel, given by

$$C_{EHU-ET} = \frac{1}{2} \sum_{v \in \mathcal{V}} \log \left(1 + \frac{v^2 P_{EHU}(x_2, v)}{\sigma_2^2 + x_2^2 \alpha_2}\right) p(v). \quad (32)$$

Note that the rate of the transmitted codeword is R_{EHU}, given by (31). Now, since $R_{EHU} = C_{EHU-ET}$, the ET is able to decode the codeword transmitted by the EHU, by using a joint topicality decoder. Next, since the ET knows the binary sequences corresponding to each group, by decoding the transmitted codeword the ET determines the group to which the transmitted codeword belongs to. As a result, the ET is able to decode the secret message W.

In the $N + B$ time slots, the achieved secrecy rate is given by $\lim_{(N+B)\to\infty} \frac{kN}{k(N+B)} R_s = \lim_{(N+B)\to\infty} \frac{N}{N+B} R_s$. It was proven in [32] that when the EHU is equipped with a battery with an unlimited storage capacity and when C2 in (17) holds, then $N/(N + B) \to 1$ as $(N + B) \to \infty$. Thereby, the achieved secrecy rate in $N + B$ time slots is given by $\lim_{(N+B)\to\infty} \frac{N}{N+B} R_s = R_s$, which is the actual lower bound of the channel secrecy capacity given by Lemma 2.

4) Receptions at the EVE: EVE receives the transmitted blocks by the EHU and the ET. Similarly to the ET, EVE places the received block in its data storage, without decoding.

In $N + B$ time slots, the EVE also receives the entire codeword transmitted by the EHU. In addition, EVE receives the signal from the ET, comprised of randomly generated symbols (see Lemma 2), which acts as noise to EVE and impairs the ability of EVE to decode the codeword from the EHU. To show that the EVE will not be able to decode the secret message, we use properties of the multiple access channel, resulting from the EHU and the ET transmitting at the same time. The multiple-access capacity region at the EVE formed by the transmission of the EHU and the ET is given by $I(X_1, X_2; Y_3|V, G, F)$. The EVE will be able to decode the EHU's codeword only if one of the following two cases holds, i.e., $R_{EHU} \leq I(X_1, Y_2|X_2, V, G, F)$ when $R_{ET} \leq I(X_2; Y_3|V, G, F)$ or $R_{EHU} \leq I(X_1, Y_2|V, G, F)$ when $R_{ET} \leq I(X_2; Y_3|X_1, V, G, F)$, where R_{ET} is the entropy of the signal generated by the ET and is given by

$$R_{ET} = -\Big[p(x_2) \log_2 p(x_2) + p(x_2) \log_2 p(x_2)\Big]. \quad (33)$$

In (33), $p(x_2) = 1/2$, see Lemma 2. As a result,

$$R_{ET} = \log 2 = 1. \quad (34)$$

Case 1: For the EHU's codeword to be decodable at the EVE in this case, $R_{EHU} \leq I(X_1, Y_2|X_2, V, G, F)$ and $R_{ET} \leq I(X_2; Y_3|V, G, F)$ have to hold. For $I(X_2; Y_3|V, G, F)$ we have

$$\begin{aligned} &I(X_2; Y_3|V, F, G) \\ &= \sum_{v \in \mathcal{V}} \sum_{g \in \mathcal{G}} \sum_{f \in \mathcal{F}} \left[\int_{-\infty}^{\infty} \frac{1}{2\sqrt{2\pi\sigma_{y_3}^2}} \left(e^{-\frac{(y_3 - x_2)^2}{2\sigma_{y_3}^2}} + e^{-\frac{(y_3 + x_2)^2}{2\sigma_{y_3}^2}} \right) \right. \\ &\quad \times \ln \left(\frac{1}{2\sqrt{2\pi\sigma_{y_3}^2}} \left(e^{-\frac{(y_3 - x_2)^2}{2\sigma_{y_3}^2}} + e^{-\frac{(y_3 + x_2)^2}{2\sigma_{y_3}^2}} \right) \right) dy_3 \\ &\quad \left. - \int_{-\infty}^{\infty} \frac{1}{2\sqrt{2\pi\sigma_{y_3}^2}} e^{-\frac{(z_3 - x_2)^2}{2\sigma_{y_3}^2}} \times \ln e^{-\frac{(z_3 - x_2)^2}{2\sigma_{y_3}^2}^2} dz_3 \right] \\ &\quad \times p(v) p(g) p(f), \end{aligned} \quad (35)$$

where x_2 is drawn from (25) or (28), depending on which case in Lemma 2 holds. According to [33], we can rewrite (35) as

$$\begin{aligned} &I(X_2; Y_3|V, F, G) \\ &= \sum_{v \in \mathcal{V}} \sum_{g \in \mathcal{G}} \sum_{f \in \mathcal{F}} \left[\frac{1}{2} \ln \left(2\pi e \sigma_{y_3}^2\right) + \frac{x_2^2}{f^2\ P_{EHU}(x_2, v) + \sigma_3^2} \right. \\ &\quad \left. - \mathcal{I}\left(\frac{x_2}{\sqrt{f^2 P_{EHU}(x_2, v) + \sigma_3^2}} \right) - \frac{1}{2} \ln \left(2\pi e \sigma_{y_3}^2\right) \right] \\ &\quad \times p(v) p(g) p(f), \end{aligned} \quad (36)$$

where $\mathcal{I}(x)$ is defined in (22). Thereby,

$$I(X_2;Y_3|V,F,G)=\sum_{v\in\mathcal{V}}\sum_{g\in\mathcal{G}}\sum_{f\in\mathcal{F}}\left[\frac{x_2^2}{f^2\ P_{EHU}(x_2,v)+\sigma_3^2}-\mathcal{I}\left(\frac{x_2}{\sqrt{f^2P_{EHU}(x_2,v)+\sigma_3^2}}\right)\right]\times p(v)p(g)p(f). \tag{37}$$

The maximum value of the term $\frac{x_2^2}{f^2\ P_{EHU}(x_2,v)+\sigma_3^2}-\mathcal{I}\left(\frac{x_2}{\sqrt{f^2\ P_{EHU}(x_2,v)+\sigma_3^2}}\right)$ in (37), for any v, f, and g is one [33]. Thereby, in order for $R_{ET}=I(X_2;Y_3|V,F,G)=1$ to hold, in which case the EVE would decode the secret message, then $\frac{x_2^2}{f^2\ P_{EHU}(x_2,v)+\sigma_3^2}-\mathcal{I}\left(\frac{x_2}{\sqrt{f^2\ P_{EHU}(x_2,v)+\sigma_3^2}}\right)$ has to be equal to one for all fading realizations v, f, g. However, since the fading realizations are outcomes of continuous RVs, the probability of that happening is zero. Thereby, $I(X_2;Y_3|V,F,G)$ is less than 1 and as a result $R_{ET}>I(X_2;Y_3|V,F,G)$. Consequently, Case 1 can not hold.

Case 2: For the EHU's codeword to be decodable at the EVE, then $R_{EHU}\leq I(X_1,Y_2|V,G,F)$ and $R_{ET}\leq I(X_2;Y_3|X_1,V,G,F)$ have to hold. For $I(X_1;Y_3|V,F,G)$ we have

$$\begin{aligned}&I(X_1;Y_3|V,F,G)\\&=\sum_{v\in\mathcal{V}}\sum_{g\in\mathcal{G}}\sum_{f\in\mathcal{F}}\left[\int_{-\infty}^{\infty}\frac{1}{2\sqrt{2\pi\sigma_{y_3}^2}}\left(e^{-\frac{(y_3-x_2)^2}{2\sigma_{y_3}^2}}+e^{-\frac{(y_3+x_2)^2}{2\sigma_{y_3}^2}}\right)\right.\\&\times\ln\left(\frac{1}{2\sqrt{2\pi\sigma_{y_3}^2}}\left(e^{-\frac{(y_3-x_2)^2}{2\sigma_{y_3}^2}}+e^{-\frac{(y_3+x_2)^2}{2\sigma_{y_3}^2}}\right)\right)dy_3\\&-\left.\int_{-\infty}^{\infty}\frac{1}{2\sqrt{2\pi\sigma_3^2}}\left(e^{-\frac{(z_3-x_2)^2}{2\sigma_3^2}}+e^{-\frac{(z_3+x_2)^2}{2\sigma_3^2}}\right)\right.\\&\times\ln\left.\left(e^{-\frac{(z_3-x_2)^2}{2\sigma_3^2}}+e^{-\frac{(z_3+x_2)^2}{2\sigma_3^2}}\right)dz_3\right]\\&\times p(v)p(g)p(f),\end{aligned} \tag{38}$$

where x_2 is drawn from (25) or (28), depending on which case in Lemma 2 holds. We can rewrite (38) as

$$\begin{aligned}&I(X_1;Y_3|V,F,G)\\&=\sum_{v\in\mathcal{V}}\sum_{g\in\mathcal{G}}\sum_{f\in\mathcal{F}}\left[\frac{1}{2}\ln\left(2\pi e\sigma_{y_3}^2\right)+\frac{x_2^2}{f^2\ P_{EHU}(x_2,v)+\sigma_3^2}\right.\\&-\mathcal{I}\left(\frac{x_2}{\sqrt{f^2\ P_{EHU}(x_2,v)+\sigma_3^2}}\right)-\frac{1}{2}\ln\left(2\pi e\sigma_3^2\right)-\frac{x_2^2}{\sigma_3^2}\\&\left.+\mathcal{I}\left(\frac{x_2}{\sigma_3}\right)\right]p(v)p(g)p(f),\end{aligned} \tag{39}$$

where $\mathcal{I}(x)$ is defined in (22). By rearranging the elements in (39), we can write

$$\begin{aligned}&I(X_1;Y_3|V,F,G)\\&=\sum_{v\in\mathcal{V}}\sum_{g\in\mathcal{G}}\sum_{f\in\mathcal{F}}\left[\frac{1}{2}\ln\left(1+\frac{f^2P_{EHU}(x_2,v)}{\sigma_3^2}\right)-\Psi\right]\\&\times p(v)p(g)p(f).\end{aligned} \tag{40}$$

In (40), $\Psi=\frac{x_2^2}{\sigma_3^2}-\mathcal{I}\left(\frac{x_2}{\sigma_3}\right)-\frac{x_2^2}{f^2\ P_{EHU}(x_2,v)+\sigma_3^2}+\mathcal{I}\left(\frac{x_2}{\sqrt{f^2\ P_{EHU}(x_2,v)+\sigma_3^2}}\right)$. Now, we can lower bound R_{EHU} as

$$\begin{aligned}&R_{EHU}\\&=\frac{1}{2}\sum_{v\in\mathcal{V}}\log\left(1+\frac{v^2\ P_{EHU}(x_2,v)}{\sigma_2^2+x_2^2\alpha_2}\right)p(v)\\&>\sum_{v\in\mathcal{V}}\sum_{g\in\mathcal{G}}\sum_{f\in\mathcal{F}}\left[\frac{1}{2}\ln\left(2\pi e\sigma_{y_3}^2\right)+\frac{x_2^2}{f^2\ P_{EHU}(x_2,v)+\sigma_3^2}\right.\\&-\mathcal{I}\left(\frac{x_2}{\sqrt{f^2\ P_{EHU}(x_2,v)+\sigma_3^2}}\right)\\&\left.-\frac{1}{2}\ln\left(2\pi e\sigma_3^2\right)-\frac{x_2^2}{\sigma_3^2}+\mathcal{I}\left(\frac{x_2}{\sigma_3}\right)\right]p(v)p(g)p(f)\\&=\sum_{v\in\mathcal{V}}\sum_{g\in\mathcal{G}}\sum_{f\in\mathcal{F}}\left[\frac{1}{2}\ln\left(1+\frac{f^2P_{EHU}(x_2,v)}{\sigma_3^2}\right)-\Psi\right]\\&\times p(v)p(g)p(f)\\&=I(X_1,Y_2|V,G,F).\end{aligned} \tag{41}$$

Thereby, $R_{EHU}>I(X_1,Y_2|V,G,F)$. As a result, Case 2 can not hold either.

As Case 1 and Case 2 show, the EHU's codeword is outside the multiple-access capacity region at the EVE, and thereby the EVE will not be able to decode the EHU's secret message.

V. Numerical Results

In this section, we illustrate numerical examples of the upper bound on the secrecy capacity as well as the derived achievable secrecy rate, and compare it with the achievable secrecy rates of a chosen benchmark scheme. To this end, we first outline the system parameters, then we introduce the benchmark scheme, and finally we provide the numerical results.

A. System Parameters

We use the standard path loss model given by

$$\Omega_j=\left(\frac{c}{f_c4\pi}\right)^2d^{-\gamma},\quad j\in\{V,F,G\} \tag{42}$$

in order to compute the average power of the channel fading gains, V, F, and G, where c denotes the speed of light, f_c is the carrier frequency, d is the length of the considered link (i.e., the length of the EHU-ET link for Ω_V, the length of the EHU-EVE link for Ω_F, and the length of the ET-E link for Ω_G), and γ is the path loss exponent. We assume that $\gamma=3$. For the carrier frequency, we adopt a value which is commonly associated with low power networks, and we set $f_c=2.4$ GHz. In addition, we assume a bandwidth of $B=100$ kHz. To account for the energy losses during the energy harvesting process, the energy harvesting efficiency coefficient η is assumed to be equal to 0.8. Throughout this section, we assume Rayleigh fading with average power Ω_V, Ω_F, and Ω_G, respectively, given by (42). To provide practical results, we chose an achievable value for the self-interference suppression factor, and we set α_2 to -100 dB. As a result, the ET needs to suppress 100 dB of the self-interference,

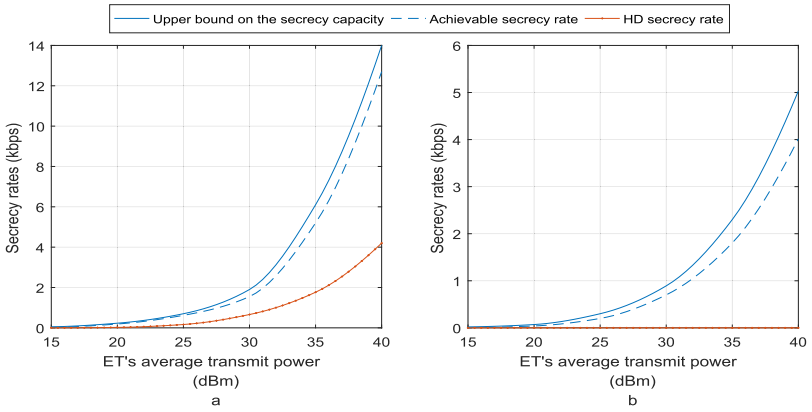

Fig. 1. Upper and lower bounds on the secrecy capacity. Fig. 1a corresponds to the case when the ET is closer to the EHU than the EVE, i.e., $d_{EHU-ET} = 10m$ and $d_{EHU-EVE} = 12m$, whilst Fig. 1b corresponds to the case when the EVE is closer to the EHU than the ET, i.e., $d_{EHU-ET} = 10m$ and $d_{EHU-EVE} = 9m$.

which is possible in practice [24]. As the EHU does not suppress the self-interference, we chose higher values for the self-interference amplification factor at the EHU and we set α_1 to -40 dB and q_1 to 0 dB. The noise power to -90 dBm.

B. Benchmark Scheme

Since to the best of the authors' knowledge there are no available communication schemes in the literature for the considered FD system model, we use the HD counterpart as a benchmark scheme, which is outlined in the following.

Time is divided into time slots with duration T. A single time slot coincides with one fading realization. A portion of each time slot, denoted by $T - t$, is used for energy transmission by the ET and for energy harvesting by the EHU and the rest of the time slot, t, is used for information transmission by the EHU, during which the ET is silent. Hence the EHU and the ET both operate in the HD mode. The EHU and the ET are assumed to have full CSI of the EHU-ET channel. Since in this case the ET stops transmitting during the information transmission by the EHU, an interference signal is not present at the EVE. The secrecy rate is thus given by

$$R_s = \max\left(0, \max_t t\left(\frac{1}{2}\sum_{v\in\mathcal{V}}\log\left(1+\frac{v^2\ P_{EHU}(v)}{\sigma_1^2}\right)p(v) - \sum_{v\in\mathcal{V}}\sum_{f\in\mathcal{F}}\log\left(1+\frac{f^2P_{EHU}(v)}{\sigma_3^2}\right)p(v)p(f)\right)\right), \tag{43}$$

where $P_{EHU}(v)$ can be found as the root of the following equation

$$\frac{v^2}{\sigma_1^2} - \left(1+\frac{v^2\ P_{EHU}(v)}{\sigma_1^2}\right)\sum_{f\in\mathcal{F}}\frac{f^2}{f^2P_{EHU}(v)+\sigma_3^2}p(f) = \left(1+\frac{v^2P_{EHU}(v)}{\sigma_1^2}\right)\lambda_2 \tag{44}$$

and λ_2 is chosen such that

$$t\left(\sum_{v\in\mathcal{V}}P_{EHU}(v)\ p(v)+P_p\right) = (T-t)\eta P_{ET}\Omega_V \tag{45}$$

holds.

C. Numerical Examples

The upper and lower bounds on the secrecy capacity are illustrated on Fig. 1, and are evaluated against the benchmark scheme. From Fig. 1 we notice that the FD scheme outperforms the HD scheme, which is a result of two factors. Firstly, energy recycling is impossible when the EHU operates as an HD node. Secondly, in HD, the ET stops acting like a jammer and an interference signal is not present at the EVE. Note that since physical layer security relies on the channel quality between the nodes in the network, distance plays a crucial role. To demonstrate this, we consider different cases for the distances between the nodes. In the case when the ET is closer to the EHU than the EVE, the EHU-ET channel is better, on average, than the EHU-EVE channel. For this case, the secrecy rate of the HD benchmark scheme is non-zero, but it is smaller than the derived achievable secrecy rate of the FD scheme, as it can be seen in Fig. 1a. When the EVE is closer to the EHU than the ET, the EHU-ET channel is worse, on average, than the EHU-EVE channel. In this case the secrecy rate of the HD benchmark scheme is zero, whereas the derived FD secrecy rate is positive, see Fig. 1b. Thereby, as a result of the interference signal generated by the ET, in these cases the proposed FD scheme offers positive secrecy rates even when the EVE is closer to the EHU than the legitimate receiver, which is impossible to achieve by employing the HD scheme. As our numerical results show, the difference between the upper bound on the secrecy capacity and the achievable rate is smaller than 1 dB. Thereby, the derived upper bound is tight in the sense that it shows that the secrecy capacity

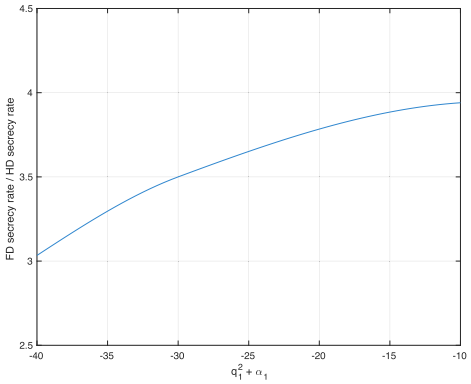

Fig. 2. FD secrecy rate / HD secrecy rate ratio as a function of the self-interference at the EHU. Fig. 2 corresponds to the case when the ET is closer to the EHU than the EVE, i.e., $d_{EHU-ET} = 10m$ and $d_{EHU-EVE} = 12m$.

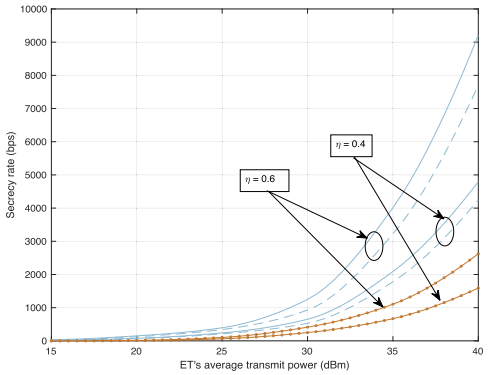

Fig. 3. Upper and lower bounds on the secrecy capacity, for different values of the energy harvesting efficiency coefficient η. Fig. 3 corresponds to the case when the ET is closer to the EHU than the EVE, i.e., $d_{EHU-ET} = 10m$ and $d_{EHU-EVE} = 12m$.

and the achievable rate differ only 1 dB, which for practical purposes is not a large gap.

In Figs. 2- 3, we show the impact of the self-recycled energy on the achieved secrecy rates. In particular, we show the ratio between the FD secrecy rate and the HD secrecy rate as a function of the self-interference at the EHU, given by $q_1^2 + \alpha_1$. As the self-interference at the EHU increases, so does the FD secrecy rate. Meanwhile, the HD secrecy rate is constant, as the HD mode does not result in self-interference. Thereby, higher self-interference at the EHU leads to higher secrecy rate. The secrecy rates are also illustrated on Fig. 3, for different values of the energy harvesting efficiency coefficient η. As the energy harvesting efficiency coefficient represents the amount of energy that is converted from harvested to operational energy (i.e., energy used for transmission and processing), lower values for η yield lower secrecy rates, both for FD and HD. However, the FD scheme again outperforms the HD scheme as a result of the previously discussed factors.

VI. Conclusion

In this paper, we have studied the secrecy capacity of a FD wirelessly powered communication system consisting of an EHU and an ET in the presence of a passive EVE. We have shown that the ET's transmit signal can act as interference against the EVE. We have derived an upper bound on the secrecy capacity and, furthermore, an achievable secrecy rate that can be achieved with relative low complexity. It has been shown that the proposed scheme achieves higher secrecy rates compared to the conventional HD-based schemes, even in the case when the channel between the EHU and the ET is worse, on average, than the channel between the EHU and EVE. In future works, it would be interesting to consider an arbitrary number of EHUs and EVEs in the network.

Appendix A
Converse

In order for us to claim that the result in (17) is indeed an upper bound on the secrecy capacity of the considered channel, we provide the following converse.

Let W be the confidential message that the EHU wants to transmit to the ET and which EVE wants to intercept. Let this message be uniformly selected at random from the message set $\{1, 2, \ldots, 2^{nR_s}\}$, where $n \to \infty$ is the number of channel uses that will be used for transmitting W from the EHU to the ET, and R_s denotes the data rate of message W. We assume a priori knowledge of the CSI of the EHU-ET channel, i.e., V_i is known for $i = 1 \ldots .n$ before the start of the communication at all three nodes. In addition, the EHU-EVE and the ET-EVE channels, given by G_i and F_i, respectively, are only known by EVE for $i = 1 \ldots .n$.

We have the following limits for the mutual information between the EHU and EVE

$$\begin{aligned} &I(W; Y_3^n | V^n, G^n, F^n) \\ &\quad = H(W|V^n, G^n, F^n) - H(W|Y_3^n, V^n, G^n, F^n) \\ &\quad \overset{(a)}{\leq} H(W|V^n) - H(W|Y_3^n, V^n, G^n, F^n) \leq n\epsilon, \end{aligned} \tag{46}$$

where (a) follows since conditioning reduces entropy and ϵ is a positive number. On the other hand, we have the following limit due to Fano's inequality [30]

$$H(W|Y_2^n, V^n) \leq P_e n R_s + 1, \tag{47}$$

where P_e is the average probability of error of the message W and R_s is the secrecy rate.

Now, for the secrecy rate, R_s, we have the following limit

$$\begin{aligned} nR_s &\leq H(W|V^n) \\ &\overset{(a)}{\leq} H(W|Y_3^n, V^n, G^n, F^n) + n\epsilon \\ &= H(W|Y_3^n, V^n, G^n, F^n) + n\epsilon + H(W|V^n) \\ &\quad - H(W|V^n) + H(W|V^n, Y_2^n, X_2^n) \\ &\quad - H(W|V^n, Y_2^n, X_2^n) \end{aligned}$$

$$\begin{aligned}
&\overset{(b)}{\leq} H(W|Y_3^n, V^n, G^n, F^n) + n\epsilon + H(W|V^n) \\
&\quad - H(W|V^n, G^n, F^n) + H(W|V^n, Y_2^n, X_2^n) \\
&\quad - H(W|V^n, Y_2^n, X_2^n) \\
&\overset{(c)}{=} I(W; Y_2^n, X_2^n|V^n) - I(W; Y_3^n|V^n, G^n, F^n) \\
&\quad + H(W|V^n, Y_2^n, X_2^n) + n\epsilon \\
&\overset{(d)}{\leq} I(W; Y_2^n, X_2^n|V^n) - I(W; Y_3^n|V^n, G^n, F^n) \\
&\quad + H(W|V^n, Y_2^n) + n\epsilon \\
&\overset{(e)}{\leq} I(W; Y_2^n, X_2^n|V^n) - I(W; Y_3^n|V^n, G^n, F^n) \\
&\quad + P_e n R_s + 1 + n\epsilon \qquad (48)
\end{aligned}$$

where (a) follows from (46), (b) follows from the fact that conditioning reduces entropy, (c) is obtained by exploiting $I(W; Y_2^n, X_2^n|V^n) = H(W|V^n) - H(W|V^n, Y_2^n, X_2^n)$ and $I(W; Y_3^n|V^n, G^n, F^n) = H(W|V^n, G^n, F^n) - H(W|Y_3^n, V^n, G^n, F^n)$, (d) results from the fact that conditioning reduces entropy, and (e) follows by Fano's inequality given by (47). Dividing both sides of (48) by n, we have

$$\begin{aligned}
R_s \leq \frac{1}{n} I(W; Y_2^n, X_2^n|V^n) - \frac{1}{n} I(W; Y_3^n|V^n, G^n, F^n) \\
+ P_e R_s + \frac{1}{n} + \epsilon. \qquad (49)
\end{aligned}$$

Assuming that $P_e \to 0$ and $\epsilon \to 0$ as $n \to \infty$, which means that we assume a zero-error probability at the ET and zero mutual information between the EHU and EVE, (49) for $n \to \infty$ can be written as

$$R_s \leq \frac{1}{n} I(W; Y_2^n, X_2^n|V^n) - \frac{1}{n} I(W; Y_3^n|V^n, G^n, F^n). \qquad (50)$$

We represent the first element of the right hand side of (50) as

$$I(W; Y_2^n, X_2^n|V^n) = I(W; Y_2^n|X_2^n, V^n) + I(W; X_2^n|V^n). \qquad (51)$$

Now, since the transmitted message W is uniformly drawn from the message set at the EHU and since the ET does not know which message the EHU transmits, the following holds

$$I(W; X_2^n|V^n) = 0. \qquad (52)$$

Inserting (52) into (51), we have

$$I(W; Y_2^n, X_2^n|V^n) = I(W; Y_2^n|X_2^n, V^n). \qquad (53)$$

Inserting (53) into (50), we have

$$\begin{aligned}
R_s \;&\leq\; \frac{1}{n} I(W; Y_2^n|X_2^n, V^n) - \frac{1}{n} I(W; Y_3^n|V^n, G^n, F^n) \\
&\overset{(a)}{\leq} \sum_{i=1}^{n} \Big(I(W; Y_{2i}|Y_2^{i-1}, X_2^n, V^n) \\
&\quad - I(W; Y_{3i}|Y_3^{i-1}, V^n, G^n, F^n) \Big) \\
&=\; \frac{1}{n} \sum_{i=1}^{n} \Big(H(Y_{2i}|Y_2^{i-1}, X_2^n, V^n) \\
&\quad - H(Y_{2i}|Y_2^{i-1}, X_2^n, V^n, W) \\
&\quad - H(Y_{3i}|Y_3^{i-1} V^n, G^n, F^n) \\
&\quad + H(Y_{3i}|Y_3^{i-1}, V^n, G^n, F^n, W) \Big) \\
&\overset{(b)}{\leq} \frac{1}{n} \sum_{i=1}^{n} \Big(H(Y_{2i}|Y_2^{i-1}, X_2^n, V^n) \\
&\quad - H(Y_{2i}|Y_2^{i-1}, X_2^n, V^n, W, X_{1i}) \\
&\quad - H(Y_{3i}|Y_3^{i-1}, V^n, G^n, F^n) \\
&\quad + H(Y_{3i}|Y_3^{i-1}, V^n, G^n, F^n, W) \Big). \qquad (54)
\end{aligned}$$

where (a) follows from the fact that the entropy between a collection of random variables is less than or equal to the sum of their individual entropies and (b) results from the fact that conditioning reduces entropy. On the other hand, because of the memoryless channel assumption, Y_{3i} is independent of Y_3^{i-1}, therefore, we can write

$$\begin{aligned}
&H(Y_{3i}|Y_3^{i-1}, V^n, G^n, F^n, W) \\
&\quad = H(Y_{3i}|V^n, G^n, F^n, W) \\
&\quad \overset{(a)}{=} H(Y_{3i}, V^n, G^n, F^n, W) - H(V^n, G^n, F^n, W) \\
&\quad \overset{(b)}{\leq} H(Y_{3i}, V^n, G^n, F^n, W, X_1^n) - H(V^n, G^n, F^n, W) \\
&\quad \overset{(c)}{=} H(Y_{3i}|V^n, G^n, F^n, W, X_1^n) + H(V^n, G^n, F^n, W, X_1^n) \\
&\qquad - H(V^n, G^n, F^n, W) \\
&\quad \overset{(d)}{=} H(Y_{3i}|V^n, G^n, F^n, W, X_1^n) + H(X_1^n|V^n, G^n, F^n, W) \\
&\qquad + H(V^n, G^n, F^n, W) - H(V^n, G^n, F^n, W) \\
&\quad = H(Y_{3i}|V^n, G^n, F^n, W, X_1^n) + H(X_1^n|V^n, G^n, F^n, W) \\
&\quad \overset{(e)}{=} H(Y_{3i}|V^n, G^n, F^n, W, X_1^n) \\
&\quad \overset{(f)}{\leq} H(Y_{3i}|V^n, G^n, F^n, X_1^n), \qquad (55)
\end{aligned}$$

where (a) follows from the chain rule for joint entropy, (b) follows from the properties of joint entropy, (c) and (d) follow from the chain rule for joint entropy, (e) follows from the fact that $H(X_1^n|W, V^n, G^n, F^n) = 0$ because of the deterministic mapping $W \to X_1^n$, and (f) follows from the fact that conditioning reduces entropy.

By inserting (55) into (54), we obtain

$$\begin{aligned}
R_s \;&\leq\; \frac{1}{n} \sum_{i=1}^{n} \Big(H(Y_{2i}|Y_2^{i-1}, X_2^n, V^n) \\
&\quad - H(Y_{2i}|Y_2^{i-1}, X_2^n, V^n, X_{1i}, W) \\
&\quad - H(Y_{3i}|Y_3^{i-1}, V^n, G^n, F^n) \\
&\quad + H(Y_{3i}|V^n, G^n, F^n, X_1^n) \Big) \\
&\overset{(a)}{=} \frac{1}{n} \sum_{i=1}^{n} \Big(H(Y_{2i}|X_{2i}, V_i) - H(Y_{2i}|X_{2i}, V_i, X_{1i}, W) \\
&\quad - (H(Y_{3i}|V_i, G_i, F_i) - H(Y_{3i}|V_i, G_i, F_i, X_{1i})) \Big) \\
&\overset{(b)}{=} \frac{1}{n} \sum_{i=1}^{n} \Big(H(Y_{2i}|X_{2i}, V_i) - H(Y_{2i}|X_{2i}, V_i, X_{1i}) \\
&\quad - (H(Y_{3i}|V_i, G_i, F_i) - H(Y_{3i}|V_i, G_i, F_i, X_{1i})) \Big) \qquad (56)
\end{aligned}$$

where (a) follows from the fact that due to the memoryless channel assumption, Y_{2i} is independent of all elements in the vectors X_2^n, V^n, and X_1^n except the elements X_{2i}, V_i, and X_{1i}, respectively, and of Y_2^{i-1}, and

thereby $H(Y_{2i}|Y_2^{i-1}, X_2^n, V^n) = H(Y_{2i}|X_{2i}, V_i)$, and $H(Y_{2i}|Y_2^{i-1}, X_2^n, V^n, X_{1i}, W) = H(Y_{2i}|X_{2i}, V_i, X_{1i}, W)$. Similarly, Y_{3i} is independent of all the elements of the vector X_1^n except X_{1i}, of all the elements of the vector V^n except V_i, of all the elements of the vector G^n except G_i, of all the elements of the vector F^n except F_i and of Y_3^{i-1}, and thereby $H(Y_{3i}|Y_3^{i-1}, V^n, G^n, F^n) = H(Y_{3i}|V_i, G_i, F_i)$ and $H(Y_{3i}|V^n, G^n, F^n, X_1^n) = H(Y_{3i}|V_i, G_i, F_i, X_{1i})$. In continuation, (b) follows from the fact that given X_{2i}, V_i, and X_{1i}, Y_{2i} is conditionally independent of the message W as it can be seen from (12), and thereby $H(Y_{2i}|X_{2i}, V_i, X_{1i}, W) = H(Y_{2i}|X_{2i}, V_i, X_{1i})$. Now, we can write (56) as

$$\begin{aligned} R_s &\leq \frac{1}{n}\sum_{i=1}^{n}\Big(I(X_{1i}; Y_{2i}|X_{2i}, V_i) - I(X_{1i}; Y_{3i}|V_i, G_i, F_i)\Big) \\ &= I(X_1; Y_2|X_2, V) - I(X_1; Y_3|V, G, F). \end{aligned} \tag{57}$$

Therefore, an upper bound on the secrecy capacity is given by (57) when no additional constraints on X_1 and X_2 exist and it is achieved by maximizing over all possible probability distributions $p(x_1, x_2|v)$, or equivalently by $\{p(x_1|x_2, v), p(x_2|v)\}$. In our case, we impose a further constraint on X_2 which limits the ET's average output power to P_{ET}, which is expressed by C1 in (17). Moreover, the second constraint, expressed by C2 in (17), concerns X_1 and it limits the average transmit power of the EHU to be less than the maximum average harvested power minus the processing cost P_p. Constraints C3 and C4 in (17) come from the definitions of probability distributions. Hence, the capacity is upper bounded by (17). This proves the converse.

APPENDIX B
PROOF OF THEOREM 2

Since the EHU-ET channel is an AWGN channel with channel gain v and AWGN with variance $\sigma_2^2 + x_2^2\alpha_2$, $I(X_1; Y_2|X_2 = x_2, V = v) = \frac{1}{2}\log\left(1 + \frac{v^2\ P_{EHU}(x_2,v)}{\sigma_2^2 + x_2^2\alpha_2}\right)$. In addition, since Q_1 and X_1 are zero-mean Gaussian RVs, the left-hand side of constraint C2 in (17) can be transformed into

$$\begin{aligned} &\int_{x_1}\sum_{x_2\in\mathcal{X}_2}\sum_{v\in\mathcal{V}}(x_1^2 + P_p)p(x_1|x_2, v)p(x_2|v)p(v)dx_1 \\ &\qquad = \sum_{x_2\in\mathcal{X}_2}\sum_{v\in\mathcal{V}} P_{EHU}(x_2, v)p(x_2|v)p(v) + P_p. \end{aligned} \tag{58}$$

where we have used $\int_{x_1}\sum_{x_2\in\mathcal{X}_2}\sum_{v\in\mathcal{V}} x_1^2\ \ p(x_1|x_2, v)\ p(x_2|v)p(v)dx_1 = \sum_{x_2\in\mathcal{X}_2}\sum_{v\in\mathcal{V}} P_{EHU}(x_2, v)p(x_2|v)p(v)$. Whereas, the right-hand side of C2 in (17) can be rewritten as

$$\begin{aligned} &\int_{x_1}\sum_{x_2\in\mathcal{X}_2}\sum_{v\in\mathcal{V}} E_{\text{in}}p(x_1|x_2, v)p(x_2|v)p(v)dx_1 \\ &= \int_{q_1}\int_{x_1}\sum_{x_2\in\mathcal{X}_2}\sum_{v\in\mathcal{V}}\eta(ex_2 + \bar{q}_1x_1 + q_1x_1)^2 \\ &\quad \times p(x_1|x_2, v)p(x_2|v)p(v)p(q_1)dx_1\ dq_1 \\ &= \sum_{x_2\in\mathcal{X}_2}\sum_{v\in\mathcal{V}}\eta v^2\ x_2^2\ p(x_2|v)p(v) \\ &\quad + \int_{x_1}\sum_{x_2\in\mathcal{X}_2}\sum_{v\in\mathcal{V}}\eta\bar{q}_1^2\ x_1^2\ p(x_1|x_2, v)p(x_2|v)p(v)dx_1 \\ &\quad + \int_{q_1}\int_{x_1}\sum_{x_2\in\mathcal{X}_2}\sum_{v\in\mathcal{V}}\eta q_1^2\ x_1^2\ p(x_1|x_2, v)p(x_2|v)p(v)p(g_1) \\ &\quad \times dx_1\ dg_1 \\ &= \sum_{x_2\in\mathcal{X}_2}\sum_{v\in\mathcal{V}}\eta e^2\ x_2^2\ p(x_2|v)p(v) \\ &\quad + \eta\bar{q}_1^2\sum_{x_2\in\mathcal{X}_2}\sum_{v\in\mathcal{V}} P_{EHU}(x_2, v)p(x_2|v)p(v) \\ &\quad + \eta\alpha_1\sum_{x_2\in\mathcal{X}_2}\sum_{v\in\mathcal{V}} P_{EHU}(x_2, v)p(x_2|v)p(v), \end{aligned} \tag{59}$$

where q_1 represents the realizations of the random variable Q_1. Combining (58) and (59) transforms (17) into

$$\begin{aligned} \max_{P_{EHU}(x_2,v),p(x_2|v)}\ & \sum_{x_2\in\mathcal{X}_\epsilon}\sum_{v\in\mathcal{V}}\frac{1}{2}\log\left(1+\frac{v^2\ P_{EHU}(x_2,v)}{\sigma_2^2+x_2^2\alpha_2}\right) \\ & \times p(x_2|v)p(v) \\ & - \sum_{v\in\mathcal{V}}\sum_{g\in\mathcal{G}}\sum_{f\in\mathcal{F}} I(X_1; Y_3|V = v, \\ & G = g, F = f)p(v)p(g)p(f) \\ \text{Subject to C1:}\ & \sum_{x_2\in\mathcal{X}_2}\sum_{v\in\mathcal{V}} x_2^2\ p(x_2|v)p(v) \leq P_{ET} \\ \text{C2:}\ & \sum_{x_2\in\mathcal{X}_2}\sum_{v\in\mathcal{V}} P_{EHU}(x_2, v)p(x_2|v) \\ & p(v) + P_p \\ & \leq \sum_{x_2\in\mathcal{X}_2}\sum_{v\in\mathcal{V}}\eta v^2\ x_2^2\ p(x_2|v)p(v) \\ & + \eta(\bar{q_1}^2 + \alpha_1) \\ & \sum_{x_2\in\mathcal{X}_2}\sum_{v\in\mathcal{V}} P_{EHU}(x_2, v)p(x_2|v) \\ & p(v) \\ \text{C3:}\ & \sum_{x_2\in\mathcal{X}_2} p(x_2|v) = 1 \\ \text{C4:}\ & P_{EHU}(x_2, v) \geq 0. \end{aligned} \tag{60}$$

Now, since the log function and the mutual information are both concave functions [34] with respect to the optimization variables, their difference, as given in the objective function of (60) is in general neither concave nor convex. Therefore, the optimization problem in (60) may not be convex so a given solution can either be a local maximum or a global maximum. However, since we are interested in finding an upper bound on the secrecy capacity, we can still apply the Lagrange duality method due to the fact that the dual function of a maximization optimization problem yields an upper bound on the optimal solution, see [35]. Thereby, we write the Lagrangian of (60) as

$$\begin{aligned} \mathcal{L} = & \sum_{x_2\in\mathcal{X}_\epsilon}\sum_{v\in\mathcal{V}}\frac{1}{2}\log\left(1 + \frac{v^2\ P_{EHU}(x_2, v)}{\sigma_2^2 + x_2^2\alpha_2}\right)p(x_2|v)p(v) \\ & - \sum_{v\in\mathcal{V}}\sum_{g\in\mathcal{G}}\sum_{f\in\mathcal{F}} I(X_1; Y_3|V = v, G = g, F = f) \\ & \times p(v)p(g)p(f) \\ & - \lambda_1\left(\sum_{x_2\in\mathcal{X}_2}\sum_{v\in\mathcal{V}} x_2^2\ p(x_2|v)p(v) - P_{ET}\right) \end{aligned}$$

$$
\begin{aligned}
&- \lambda_2 \left((1-\eta(\bar{q_1}^2+\alpha_1)) \sum_{x_2\in\mathcal{X}_2}\sum_{v\in\mathcal{V}} P_{EHU}(x_2,v) \right.\\
&\times p(x_2|v)p(v)\\
&\left. + P_p - \sum_{x_2\in\mathcal{X}_2}\sum_{v\in\mathcal{V}} \eta v^2\ x_2^2\ p(x_2|v)p(v) \right)\\
&- \mu_1 \left(\sum_{x_2\in\mathcal{X}_\epsilon} p(x_2|v) - 1 \right) - \mu_2 P_{EHU}. \qquad (61)
\end{aligned}
$$

In (60), we assume that $0 < \eta(\bar{g_1}^2+\alpha_1) < 1$, since $\eta(\bar{g_1}^2+\alpha_1) \geq 1$ would practically imply that the EHU recycles the same or even a larger amount of energy than what has been transmitted by the EHU, which is not possible in reality. In (61), λ_1, λ_2, μ_1, and μ_2 are the Lagrangian multipliers associated with C1, C2, C3, and C4 in (17), respectively. Differentiating (61) with respect to the optimization variables, we obtain

$$
\begin{aligned}
&\frac{\partial \mathcal{L}}{\partial P_{EHU}(x_2,v)}\\
&= \frac{\frac{v^2}{\sigma_2^2+x_2^2\alpha_2}}{1+\frac{v^2\ P_{EHU}(x_2,v)}{\sigma_2^2+x_2^2\alpha_2}} - \lambda_2(1-\eta(\bar{g_1}^2+\alpha_1)) - \mu_2\\
&- \frac{\partial}{\partial P_{EHU}(x_2,v)} \left(\sum_{g\in\mathcal{G}}\sum_{f\in\mathcal{F}} I(X_1;Y_3|V=v,G=g,\right.\\
&\left. F=f)p(g)p(f) \right) = 0, \qquad (62)
\end{aligned}
$$

$$
\begin{aligned}
&\frac{\partial \mathcal{L}}{\partial p(x_2|v)}\\
&= \frac{1}{2}\sum_{v\in\mathcal{V}} \log\left(1+\frac{v^2\ P_{EHU}(x_2,v)}{\sigma_2^2+x_2^2\alpha_2}\right) p(v)\\
&- \lambda_1 \sum_{v\in\mathcal{V}} x_2^2\ p(v) - \mu_1\\
&- \frac{\partial}{\partial p\,(x_2|v)} \left(\sum_{v\in\mathcal{V}}\sum_{g\in\mathcal{G}}\sum_{f\in\mathcal{F}} I(X_1;Y_3|V=v,G=g,\right.\\
&\left. F=f)p(v)p(g)p(f) \right)\\
&- \lambda_2 \left((1-\eta(\bar{q_1}^2+\alpha_1)) \sum_{v\in\mathcal{V}} P_{EHU}(x_2,v)p(v) \right.\\
&\left. - \eta \sum_{v\in\mathcal{V}} v^2 x_2^2 p(v) \right) = 0. \qquad (63)
\end{aligned}
$$

Now, when $P_{EHU} > 0$, then $\mu_2 = 0$ in (62). In consequence, we can use (62) to find $P_{EHU}(x_2,v)$ as given by Theorem 2. If the solution is negative, then $P_{EHU}(x_2,v) = 0$.

By using (63), we can prove that the optimal input probability distribution, $p(x_2|v)$, is discrete. The proof is based on ([36]), where the authors derive a methodology which identifies the capacity-achieving distribution, based on standard decompositions in Hilbert space with the Hermitian polynomials as a basis. Since

$$
\begin{aligned}
&I(X_1;Y_3|V=v,G=g,F=f)\\
&\quad = H(Y_3|E=e,G=g,F=f)\\
&\qquad - H(Y_3|X_1=x_1,V=v,G=g,F=f)\\
&\quad = I(X_1;Y_3|V=v,G=g,F=f)\\
&\quad = H(Y_3|V=v,G=g,F=f)\\
&\qquad - H(Z_3|V=v,G=g,F=f), \qquad (64)
\end{aligned}
$$

where $Z_3 = GX_2 + N_3$, first we note that

$$
\begin{aligned}
&I'(X_1;Y_3|V=v,G=g,F=f)\\
&\quad = H'(Y_3|V=v,G=g,F=f)\\
&\qquad - H'(Z_3|V=v,G=g,F=f)\\
&\quad = \int_{-\infty}^{\infty} \frac{1}{\sqrt{2\pi\sigma_{z_3}}} e^{-\frac{(z_3-x_2)^2}{2\sigma_{z_3}^2}} \times \ln\left(p(z_3)\right) dz_3\\
&\qquad - \int_{-\infty}^{\infty} \frac{1}{\sqrt{2\pi\sigma_{y_3}}} e^{-\frac{(y_3-x_2)^2}{2\sigma_{y_3}^2}} \times \log\left(p(y_3)\right) dy_3. \qquad (65)
\end{aligned}
$$

where $'$ denotes the derivative with respect to $p(x_2|v)$. Now, we decompose the integrals in (65) by using Hermitian polynomials. To this end, we define

$$
\log(p(y_3)) = \sum_{m=0}^{\infty} c_m^{(1)} H_m(y_3)
$$

and

$$
\log(p(z_3)) = \sum_{m=0}^{\infty} c_m^{(2)} H_m(z_3), \qquad (66)
$$

where $c_m^{(1)}$ and $c_m^{(2)}$ are constants and $H_m(y_3)$ and $H_m(z_3)$ are the Hermitian polynomials, $\forall m$. When (66) is used in conjunction with the generating function of the Hermitian polynomials, given by

$$
e^{-\frac{t^2}{2}+tx} = \sum_{m=0}^{\infty} H_m(x)\frac{t^m}{m!}, \qquad (67)
$$

for $H'(Y_3|E=e,G=g,F=f)$ in (65) we obtain

$$
\begin{aligned}
&H'(Y_3|E=e,G=g,F=f)\\
&= -\int_{-\infty}^{\infty} \frac{1}{\sqrt{2\pi}} e^{-\frac{(y_3-x_2)^2}{2\sigma_{y_3}^2}} \sum_{m=0}^{\infty} c_m^{(1)} H_m(y_3) dy_3\\
&= -\int_{-\infty}^{\infty} \frac{1}{\sqrt{2\pi}} e^{-\frac{y_3^2}{2}} e^{-\frac{x_2^2}{2}+x_2y_3} \sum_{m=0}^{\infty} c_m^{(1)} H_m(y_3) dy_3\\
&= -\int_{-\infty}^{\infty} \frac{1}{\sqrt{2\pi}} e^{-\frac{y_3^2}{2}} \sum_{n=0}^{\infty} H_n(x)\frac{t^n}{n!} \sum_{m=0}^{\infty} c_m^{(1)} H_m(y_3) dy_3\\
&= -\sum_{m=0}^{\infty} c_m^{(1)} x_2^m. \qquad (68)
\end{aligned}
$$

In (68), we used the ortogonality of the Hermitian polynomials with respect to the weight function $e^{-\frac{y_3^2}{2}}$ and we set $\sigma_{y_3}^2 = 1$ for simplicity. By following an analogous procedure for $H'(Z_3|E=e,G=g,F=f)$ in (65), we obtain

$$
H'(Z_3|V=v,G=g,F=f) = -\sum_{m=0}^{\infty} c_m^{(2)} x_2^m. \qquad (69)
$$

In order to identify the constants $c_m^{(1)}$ and $c_m^{(2)}$ in (66), we consider 2 scenarios.

Case 1: Let us assume $P_{EHU}(x_2, v) = 0$. The condition given by (63) can be written as

$$\sum_{m=0}^{\infty}(c_m^{(1)} - c_m^{(2)})x_2^m = \lambda_1 x_2^2 + \mu_1 + \lambda_2\left((1-\eta(\bar{q_1}^2+\alpha_1))P_{EHU} - \eta e^2 x_2^2\right). \quad (70)$$

The comparison of the exponents of x_2 in (70) yields

$$c_0^{(1)} = \mu_1, c_0^{(2)} = 0; \quad c_1^{(1)} = c_1^{(2)} = 0; \quad c_2^{(1)} = \lambda_1, \quad c_2^{(2)} = \lambda_1\eta v^2; \quad c_m^{(1)} = c_m^{(2)} = 0, \quad \forall m > 2. \quad (71)$$

Now, we can insert (71) into (66) and obtain

$$p(y_3) = e^{\ln(2)(c_0^{(1)}H_0(y_3)+c_2^{(1)}H_2(y_3))} \overset{(a)}{=} e^{\ln(2)(c_0^{(1)}-c_2^{(1)})}e^{\ln(2)c_2^{(1)}y_3^2}, \quad (72)$$

where (a) follows from the definition of Hermitian polynomials, i.e., $H_0(y_3) = 1$ and $H_2(y_3) = y_3^2 - 1$. The expression given by (72) can only be a valid probability distribution iff $c_2^{(1)} < 0$, in which case $p(y_3)$ would be distributed according to a normal distribution. Consequently, x_2 would also be a Gaussian RV. However, since $\lambda_1 \geq 0$, this would not be possible, thus $p(y_3)$ can not be a continuous probability distribution. A similar argument would follow for $p(z_3)$ in (66), and it would lead to an identical conclusion since $\lambda_1\eta v^2$ can not be negative.

Case 2: Let us assume $P_{EHU}(x_2, v) > 0$. By using a Taylor series expansion we can rewrite the $\log(.)$ function in (63) as

$$\frac{1}{2}\log\left(1 + \frac{v^2 P_{EHU}(x_2, v)}{\sigma_2^2 + x_2^2\alpha_2}\right) = \frac{1}{2}\sum_{n=0}^{\infty}(-1)^n a_n x_2^{2n}, \quad (73)$$

therefore (63) can be written as

$$\sum_{m=0}^{\infty}(c_m^{(2)} - c_m^{(1)})x_2^m = \frac{1}{2}\sum_{n=0}^{\infty}(-1)^n a_n x_2^{2n} - \lambda_1 x_2^2 - \mu_1 - \lambda_2\left((1-\eta(\bar{q_1}^2+\alpha_1))P_{EHU}(x_2, v) - \eta v^2 x_2^2\right). \quad (74)$$

In (73) and (74), $a_n > 0$ are known constants. By applying the same procedure as in Case 1, we obtain $c_m^{(2)}$ and $c_m^{(1)}$ as

$$\begin{aligned} c_0^{(1)} &= \lambda_2\ P_{EHU}(x_2, v) + \mu_1, c_0^{(2)} \\ &= \frac{1}{2}a_n + \lambda_2\eta(\bar{q_1}^2+\alpha_1)P_{EHU}(x_2, v); \quad c_1^{(1)} = c_1^{(2)} = 0; \\ c_2^{(1)} &= \lambda_1, c_2^{(2)} = \lambda_1\eta v^2; \quad c_m^{(1)} = 0, \\ c_m^{(2)} &= \frac{1}{2}a_{m/2}, \quad \forall m > 2 \wedge m \text{ is even} \\ c_m^{(1)} &= c_m^{(2)} = 0, \quad \forall m > 2 \wedge m \text{ is odd.} \end{aligned} \quad (75)$$

Consequently,

$$p(y_3) = e^{\ln(2)(c_0^{(1)}H_0(y_3)+c_2^{(1)}H_2(y_3))} \overset{(a)}{=} e^{\ln(2)(c_0^{(1)}-c_2^{(1)})}e^{\ln(2)c_2^{(1)}y_3^2}, \quad (76)$$

however, $\lambda_1 \geq 0$, so $c_2^{(1)}$ is positive, thus $p(y_3)$ can not be a valid continuous distribution. As for $p(z_3)$, we have

$$p(z_3) = e^{\ln(2)\sum_{m=0}^{\infty}c_m^{(2)}H_m(z_3)} \overset{(a)}{=} e^{\ln(2)\sum_{n=0}^{\infty}q_n z_3^{2n}} = \prod_{n=0}^{\infty}e^{\ln(2)q_n z_3^{2n}}, \quad (77)$$

where (a) follows from the fact that $c_m^{(2)} > 0$ only for even values of m and q_n are known non-zero constants, whose value is determined by the polynomials and a_n. Since $q_n > 0$ for some $n \to \infty$, $p(z_3)$ is unbounded, and as a result $p(x_2)$ can not be continues. Considering Case 1 and Case 2, we obtain that $p(x_2|v)$ has to be discrete on the entire domain of x_2. Now, we generate every discrete probability distribution satisfying C1 in (60) and settle on the probability distribution which maximizes the secrecy rate.

In order to obtain $I(X_1; Y_3|V = v, G = g, F = f)$, we use the definition of mutual information, and we can write

$$\begin{aligned} &I(X_1; Y_3|V = v, G = g, F = f) \\ &= H(Y_3|V = v, G = g, F = f) \\ &\quad - H(Y_3|X_1 = x_1, V = v, G = g, F = f) \\ &= \left(\int_{-\infty}^{\infty}\frac{1}{\sqrt{2\pi\sigma_{y_3}}}\sum_{j=1}^{J}p(x_2 = x_{2j})e^{-\frac{(y_3-x_{2j})^2}{2\sigma_{y_3}^2}}\right. \\ &\quad \times \ln\left(\frac{1}{\sqrt{2\pi\sigma_{y_3}}}\sum_{j=1}^{J}p(x_2 = x_{2j})e^{-\frac{(y_3-x_{2j})^2}{2\sigma_{y_3}^2}}\right)dy_3 \\ &\quad - \int_{-\infty}^{\infty}\frac{1}{\sqrt{2\pi\sigma_3}}\sum_{j=1}^{J}p(x_2 = x_{2j})e^{-\frac{(z-x_{2j})^2}{2\sigma_3^2}} \\ &\quad \left.\times \ln\left(\frac{1}{\sqrt{2\pi\sigma_3}}\sum_{j=1}^{J}p(x_2 = x_{2j})\ e^{-\frac{(z-x_{2j})^2}{2\sigma_3^2}}\right)dz_3\right), \end{aligned} \quad (78)$$

where the last equality is a consequence of the definition of entropy. Finally, by using (78) we obtain the upper bound as given in Theorem 2.

REFERENCES

[1] W. Saad, Z. Han, and H. V. Poor, "On the physical layer security of backscatter RFID systems," in *Proc. Int. Symp. Wireless Commun. Syst. (ISWCS)*, Aug. 2012, pp. 1092–1096.

[2] J. Choi, J. Ha, and H. Jeon, "Physical layer security for wireless sensor networks," in *Proc. IEEE 24th Annu. Int. Symp. Pers., Indoor, Mobile Radio Commun. (PIMRC)*, Sep. 2013, pp. 1–6.

[3] P. K. Gopala, L. Lai, and H. El Gamal, "On the secrecy capacity of fading channels," *IEEE Trans. Inf. Theory*, vol. 54, no. 10, pp. 4687–4698, Oct. 2008.

[4] C. E. Shannon, "Communication theory of secrecy systems," *Bell Labs Tech. J.*, vol. 28, no. 4, pp. 656–715, Oct. 1949.

[5] A. D. Wyner, "The wire-tap channel," *Bell Syst. Tech. J.*, vol. 54, pp. 1355–1387, Oct. 1975.

[6] H. Ju and R. Zhang, "Throughput maximization in wireless powered communication networks," *IEEE Trans. Wireless Commun.*, vol. 13, no. 1, pp. 418–428, Jan. 2014.

[7] D. Gunduz, K. Stamatiou, N. Michelusi, and M. Zorzi, "Designing intelligent energy harvesting communication systems," *IEEE Commun. Mag.*, vol. 52, no. 1, pp. 210–216, Jan. 2014.

[8] S. Bi, Y. Zeng, and R. Zhang, "Wireless powered communication networks: An overview," *IEEE Wireless Commun.*, vol. 23, no. 2, pp. 10–18, Apr. 2016.

[9] Y. Liu, J. Xu, and R. Zhang, "Exploiting interference for secrecy wireless information and power transfer," *IEEE Wireless Commun.*, vol. 25, no. 1, pp. 133–139, Feb. 2018.
[10] C.-N. Nguyen, P. C. Doan-Thi, D.-D. Tran, and D.-B. Ha, "Secured energy harvesting networks with multiple power-constrained information sources," in *Proc. Int. Conf. Recent Adv. Signal Process., Telecommun. Comput. (SigTelCom)*, Jan. 2017, pp. 134–138.
[11] K. Banawan and S. Ulukus, "Gaussian MIMO wiretap channel under receiver side power constraints," in *Proc. 52nd Annu. Allerton Conf. Commun., Control, Comput. (Allerton)*, Sep./Oct. 2014, pp. 183–190.
[12] K. Banawan and S. Ulukus, "MIMO wiretap channel under receiver-side power constraints with applications to wireless power transfer and cognitive radio," *IEEE Trans. Commun.*, vol. 64, no. 9, pp. 3872–3885, Sep. 2016.
[13] G. Pan, C. Tang, T. Li, and Y. Chen, "Secrecy performance analysis for SIMO simultaneous wireless information and power transfer systems," *IEEE Trans. Commun.*, vol. 63, no. 9, pp. 3423–3433, Sep. 2015.
[14] L. Liu, R. Zhang, and K.-C. Chua, "Secrecy wireless information and power transfer with MISO beamforming," in *Proc. IEEE Global Commun. Conf. (GLOBECOM)*, Dec. 2013, pp. 1831–1836.
[15] G. Pan *et al.*, "On secrecy performance of MISO SWIPT systems with TAS and imperfect CSI," *IEEE Trans. Commun.*, vol. 64, no. 9, pp. 3831–3843, Sep. 2016.
[16] M. Liu and Y. Liu, "Power allocation for secure SWIPT systems with wireless-powered cooperative jamming," *IEEE Commun. Lett.*, vol. 21, no. 6, pp. 1353–1356, Jun. 2017.
[17] M. Zhang, Y. Liu, and R. Zhang, "Artificial noise aided secrecy information and power transfer in OFDMA systems," *IEEE Trans. Wireless Commun.*, vol. 15, no. 4, pp. 3085–3096, Apr. 2016.
[18] A. Salem, K. A. Hamdi, and K. M. Rabie, "Physical layer security with RF energy harvesting in af multi-antenna relaying networks," *IEEE Trans. Commun.*, vol. 64, no. 7, pp. 3025–3038, Jul. 2016.
[19] V. N. Vo, T. G. Nguyen, C. So-In, and D.-B. Ha, "Secrecy performance analysis of energy harvesting wireless sensor networks with a friendly jammer," *IEEE Access*, vol. 5, pp. 25196–25206, 2017.
[20] Y. Bi and H. Chen, "Accumulate and jam: Towards secure communication via a wireless-powered full-duplex jammer," *IEEE J. Sel. Topics Signal Process.*, vol. 10, no. 8, pp. 1538–1550, Dec. 2016.
[21] E. Everett, A. Sahai, and A. Sabharwal, "Passive self-interference suppression for full-duplex infrastructure nodes," *IEEE Trans. Wireless Commun.*, vol. 13, no. 2, pp. 680–694, Jan. 2014.
[22] M. Duarte *et al.*, "Design and characterization of a full-duplex multi-antenna system for WiFi networks," *IEEE Trans. Veh. Technol.*, vol. 63, no. 3, pp. 1160–1177, Mar. 2014.
[23] C. Zhang *et al.*, "Secrecy outage analysis on underlay cognitive radio system with full-duplex secondary user," *IEEE Access*, vol. 5, pp. 25696–25705, 2017.
[24] W. Tang, S. Feng, Y. Ding, and Y. Liu, "Physical layer security in heterogeneous networks with jammer selection and full-duplex users," *IEEE Trans. Wireless Commun.*, vol. 16, no. 12, pp. 7982–7995, Dec. 2017.
[25] S. Haddad, A. Özgür, and E. Telatar, "Can full-duplex more than double the capacity of wireless networks?" in *Proc. IEEE Int. Symp. Inf. Theory (ISIT)*, Jun. 2017, pp. 963–967.
[26] I. Nikoloska, N. Zlatanov, and Z. Hadzi-Velkov, "Capacity of a full-duplex wirelessly powered communication system with self-interference and processing cost," *IEEE Trans. Wireless Commun.*, vol. 17, no. 11, pp. 7648–7660, Nov. 2018.
[27] Y. Zeng and R. Zhang, "Full-duplex wireless-powered relay with self-energy recycling," *IEEE Wireless Commun. Lett.*, vol. 4, no. 2, pp. 201–204, Apr. 2015.
[28] D. Bharadia, E. McMilin, and S. Katti, "Full duplex radios," *SIGCOMM Comput. Commun. Rev.*, vol. 43, no. 4, pp. 375–386, Aug. 2013.
[29] N. Zlatanov, E. Sippel, V. Jamali, and R. Schober, "Capacity of the Gaussian two-hop full-duplex relay channel with residual self-interference," *IEEE Trans. Commun.*, vol. 65, no. 3, pp. 1005–1021, Mar. 2017.
[30] T. M. Cover and J. A. Thomas, *Elements of Information Theory*. Hoboken, NJ, USA: Wiley, 2012.
[31] J. Xu and R. Zhang, "Throughput optimal policies for energy harvesting wireless transmitters with non-ideal circuit power," *IEEE J. Sel. Areas Commun.*, vol. 32, no. 2, pp. 322–332, Feb. 2014.
[32] N. Zlatanov, R. Schober, and Z. Hadzi-Velkov, "Asymptotically optimal power allocation for energy harvesting communication networks," *IEEE Trans. Veh. Technol.*, vol. 66, no. 8, pp. 7286–7301, Aug. 2017.
[33] J. V. Michalowicz, J. M. Nichols, and F. Bucholtz, "Calculation of differential entropy for a mixed Gaussian distribution," *Entropy*, vol. 10, no. 3, pp. 200–206, 2008.
[34] T. M. Cover and A. A. El Gamal, "Capacity theorems for the relay channel," *IEEE Trans. Inf. Theory*, vol. IT-25, no. 5, pp. 572–584, Sep. 1979.
[35] S. Boyd and L. Vandenberghe, *Convex Optimization*. Cambridge, U.K.: Cambridge Univ. Press, 2004.
[36] J. J. Fahs and I. C. Abou-Faycal, "Using Hermite bases in studying capacity-achieving distributions over AWGN channels," *IEEE Trans. Inf. Theory*, vol. 58, no. 8, pp. 5302–5322, Aug. 2012.

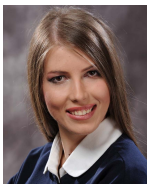

Ivana Nikoloska (S'14) received the bachelor's and master's degrees from Ss. Cyril and Methodius University, in 2014 and 2016, respectively. She is currently pursuing the Ph.D. degree with Monash University, Melbourne, Australia. From 2015 to 2016, she was a Research Associate with the Faculty of Electrical Engineering and Information Technologies, Ss. Cyril and Methodius University, where she was involved in research projects funded by the Alexander von Humboldt Foundation. Her research interests include wireless communication, information theory, and artificial intelligence.

Nikola Zlatanov (S'06–M'15) was born in Macedonia. He received the Dipl.Ing. and master's degree in electrical engineering from Ss. Cyril and Methodius University, Skopje, Macedonia, in 2007 and 2010, respectively, and the Ph.D. degree from the University of British Columbia (UBC), Vancouver, Canada, in 2015.

He is currently a Lecturer (USA equivalent to Assistant Professor) with the Department of Electrical and Computer Systems Engineering (ECSE), Monash University, Melbourne, Australia. His current research interests include wireless communications, information theory, and machine learning. He received several scholarships/awards/grants for his work, including a UBC's Four Year Doctoral Fellowship in 2010, a UBC's Killam Doctoral Scholarship and a Macedonia's Young Scientist of the Year in 2011, the Vanier Canada Graduate Scholarship in 2012, the Best Journal Paper Award from the German Information Technology Society (ITG) in 2014, the Best Conference Paper Award at ICNC in 2016, an ARC Discovery Project, and an ARC DECRA in 2018.

Zoran Hadzi-Velkov (M'97–SM'11) received the Dipl. Ing. degree (Hons.) in electrical engineering, the Magister Ing. degree (Hons.) in communications engineering, and the Ph.D. degree in technical sciences from the Ss. Cyril and Methodius University, Skopje. From 2001 to 2002, he was a Visiting Scholar with the IBM Watson Research Center, Yorktown Heights, NY, USA. From 2012 to 2014, he was a Visiting Professor with the Institute for Digital Communications, University of Erlangen–Nuremberg, Germany. He is currently a Professor of telecommunications with Ss. Cyril and Methodius University. He was a recipient of the Alexander von Humboldt Fellowship for experienced researchers in 2012, the Annual Best Scientist Award from Ss. Cyril and Methodius University in 2014. From 2012 to 2015, he was the Chair of the Macedonian Chapter of the IEEE Communications Society. He served on the technical program committees for numerous international conferences, including the IEEE ICC and the IEEE GLOBECOM. From 2012 to 2016, he served as an Editor for the IEEE COMMUNICATIONS LETTERS.

Rui Zhang (S'00–M'07–SM'15–F'17) received the B.Eng. degree (Hons.) and the M.Eng. degree from the National University of Singapore, Singapore, and the Ph.D. degree from Stanford University, Stanford, CA, USA, all in electrical engineering.

From 2007 to 2010, he was a Research Scientist with the Institute for Infocomm Research, ASTAR, Singapore. Since 2010, he has been with the Department of Electrical and Computer Engineering, National University of Singapore, where he is currently the Dean's Chair Associate Professor with the Faculty of Engineering. He has authored over 300 papers. He has been listed as a Highly Cited Researcher (also known as the World's Most Influential Scientific Minds), by Thomson Reuters (Clarivate Analytics) since 2015. His research interests include UAV/satellite communication, wireless information and power transfer, multiuser MIMO, smart and reconfigurable environment, and optimization methods.

Dr. Zhang was an elected member of the IEEE Signal Processing Society SPCOM Technical Committee from 2012 to 2017 and the SAM Technical Committee from 2013 to 2015. He serves as a member of the Steering Committee of the IEEE WIRELESS COMMUNICATIONS LETTERS. He was a recipient of the sixth IEEE Communications Society Asia–Pacific Region Best Young Researcher Award in 2011, and the Young Researcher Award of the National University of Singapore in 2015. He was a co-recipient of the IEEE Marconi Prize Paper Award in Wireless Communications in 2015, the IEEE Communications Society Asia–Pacific Region Best Paper Award in 2016, the IEEE Signal Processing Society Best Paper Award in 2016, the IEEE Communications Society Heinrich Hertz Prize Paper Award in 2017, the IEEE Signal Processing Society Donald G. Fink Overview Paper Award in 2017, and the IEEE Technical Committee on Green Communications and Computing (TCGCC) Best Journal Paper Award in 2017. His co-authored paper received the IEEE Signal Processing Society Young Author Best Paper Award in 2017. He served for over 30 international conferences as the TPC co-chair or an organizing committee member. He served as the Vice Chair of the IEEE Communications Society Asia–Pacific Board Technical Affairs Committee from 2014 to 2015. He served as the Guest Editor for three special issues in the IEEE JOURNAL OF SELECTED TOPICS IN SIGNAL PROCESSING and the IEEE JOURNAL ON SELECTED AREAS IN COMMUNICATIONS. He served as an Editor for the IEEE TRANSACTIONS ON WIRELESS COMMUNICATIONS from 2012 to 2016, the IEEE JOURNAL ON SELECTED AREAS IN COMMUNICATIONS: Green Communications and Networking Series from 2015 to 2016, and the IEEE TRANSACTIONS ON SIGNAL PROCESSING from 2013 to 2017. He is currently an Editor of the IEEE TRANSACTIONS ON COMMUNICATIONS and the IEEE TRANSACTIONS ON GREEN COMMUNICATIONS AND NETWORKING. He is also a Distinguished Lecturer of IEEE Signal Processing Society and the IEEE Communications Society.

Chapter 4

Deep Reinforcement Learning-aided Random Access

To provide access to the shared wireless channel to a massive number of devices, in this chapter we consider a system model comprised of an access point (AP) and K IoT nodes that sporadically become active in order to send data to the AP. The AP is assumed to have N time-frequency resource blocks that it can allocate to the IoT nodes that wish to send data, where $N < K$. The main problem is how to allocate the N time-frequency resource blocks to the IoT nodes in each time slot such that the average packet rate is maximized. For this problem, we propose a deep reinforcement learning (DRL)-aided random access (RA) scheme, where an intelligent DRL agent at the AP learns to predict the activity of the IoT nodes in each time slot and grants time-frequency resource blocks to the IoT nodes predicted as active. Next, the IoT nodes that are missclassified as non-active by the DRL agent, as well as unseen or newly arrived nodes in the cell, employ the standard RA scheme in order to obtain time-frequency resource blocks. In addition, we leverage expert knowledge for faster training of the DRL agent.

4.1 Introduction

Given its ubiquitous coverage, the 5-th Generation of cellular networks (5G) has great potential to support diverse wireless technologies. These wireless technolo-

gies are expected to be crucial in next generation smart cities, smart homes, automated factories, automated health management systems, and many other applications, some of which can not even be foreseen today [2]. The heterogeneous ecosystem of applications will result in different and often conflicting demands on the 5G radio and, as a result, the air-interface must be capable of supporting both high and low data rates, mobility, (ultra) low latency, as well as many different types of Quality of Service (QoS). In order for this QoS diversity to be achieved, improved medium access control (MAC) protocols have to be developed. As the state of the art MAC protocols for cellular networks have been designed and optimized to support primarily Human-to-Human (H2H) communication, these MAC protocols are not optimal for a massive number of IoT devices, due to the unique characteristics of the IoT traffic.

In IoT networks, communication devices can operate autonomously with little or no human intervention. The amount of data which is generated by the IoT nodes is usually small and the communication activity of these devices is heterogeneous [19]. The heterogeneous communication activity of the IoT nodes makes any attempt to pre-allocate network resources to each IoT node spectrally inefficient [21]. Currently, IoT devices gain access to the channel, and thereby transmit information, by performing grant-based random access (RA) or grant-free RA [20]. In grant-based RA, the nodes attempting to access the channel have to first obtain an access grant from an Access Point (AP) through a four-way handshake procedure [20]. This ensures that the user has exclusive rights to the channel if granted access, thus avoiding any potential collisions, at the expense of large latency and signalling overhead. In grant-free RA, the data is piggy-backed on the first transmission itself along with the required control information, in order to reduce the access latency. However, both schemes suffer from massive packet collisions as the number of IoT nodes requiring access increases. Packet collisions increase latency and energy inefficiency, since collided packets need to be retransmitted, and require heavy exchange of signalling messages. As a result, packet collisions in massive IoT networks can easily become a bottleneck.

One promising research direction for MAC related problems in wireless communication is machine learning. Reinforcement Learning (RL) is one of many machine learning paradigms, where agents mimic the human learning process and

learn optimal strategies by trial-and-error interactions with the environment [24]. RL has been implemented in the development of MAC schemes for cognitive radios [25], where the authors have developed a RL based MAC scheme which allows each autonomous cognitive radio to distributively learn its own spectrum sensing policy. In [26], the authors add intelligence to sensor nodes to improve the performance of Slotted ALOHA. In addition, solving MAC problems with multi agent DDRL has been proposed in [27],[28],[29]. Specifically, in [27], the authors propose a DRL MAC protocol for wireless networks in which multiple agents learn when to access the channel. A DRL MAC protocol for wireless networks in which several different MAC protocols co-exist has been studied in [28]. The authors of [29] have proposed a multi-agent DRL-based MAC scheme for wireless sensor networks with multiple frequency channels. Another distributed MAC scheme has been investigated in [30], where authors embed learning mechanisms to the IoT nodes in order to control IoT traffic and consequently reduce its impact on any cellular network. In [31], [32], [33], the authors reduce the access congestion by adapting the parameters of the access class baring mechanism to different IoT traffic conditions, via DRL. A different approach is proposed in [34], [35], where the authors investigate learning mechanisms to aid the MAC in IoT networks, via dynamic AP selection schemes, in order to avoid overloading a single AP.

In spite of being highly promising, the schemes proposed in [26]-[30] do not necessarily account for the severe device constraints in terms of energy availability and computing power for running on-device optimization and inferences [36]. On the other hand, the schemes in [31]-[33] still rely on RA as a primary access mechanism. In this chapter, we propose a DRL-aided RA scheme which does not require on-device inferences at the IoT nodes and therefore is applicable to devices with computational and energy constraints. In particular, we consider an IoT network comprised of an AP and K IoT nodes that sporadically become active and transmit information towards the AP. Practical applications that subscribe to these assumptions include smart metering, temperature monitoring, air-quality monitoring, emergency reporting etc. In the proposed scheme, the AP is assumed to have N time-frequency resource blocks that it can allocate to the IoT nodes that wish to send data, where $N < K$. The main problem is how to allocate the N time-frequency resource blocks to the IoT nodes in each time slot such that the average packet rate

received at the AP is maximized. For this problem, we propose a DRL-aided RA scheme, where an intelligent DRL agent at the AP learns to predict the activity of the IoT nodes in each time slot and grants time-frequency resource blocks to the IoT nodes predicted as active. Next, the IoT nodes that are missclassified as non-active by the DRL agent, as well as unseen or newly arrived nodes in the cell, employ the standard RA scheme in order to obtain time-frequency resource blocks. In this chapter, we rely on grand-based RA, however, the proposed hybrid scheme is also compatible with grant-free RA. To reduce the amount of live data which needs to be acquired from the IoT network for training the DRL agent, we propose to leverage expert knowledge from the available theoretical models in the literature. Our numerical results show that the proposed algorithm significantly increases the packet rate, and implicitly decreases the energy consumption of the IoT nodes. In addition, as the intelligence is concentrated at the AP, the IoT nodes do not need significant computational power, or energy, for the on-device inferences, and thereby the proposed scheme can be deployed in cells with generic IoT nodes that have limited computational capabilities.

The promising results of the proposed scheme are due to the fact that the conventional RA scheme can not utilize the determinism in the nodes' activity patterns, which usually exists in practice [37]. Our proposed DRL-aided RA scheme fills in this gap. Specifically, the proposed DRL-aided RA scheme uses the DRL algorithm to learn the deterministic components of the nodes' activity patterns in order to allocate time-frequency resources. Moreover, the proposed DRL-aided RA scheme uses the conventional RA scheme to cope with the random components of the nodes' activity patterns and allocate time-frequency resources in the presence of random components. In that sense, the proposed DRL-aided RA scheme operates in the range between the two limiting type of activity patterns. At one end of the range is the absolutely independent and identically distributed (i.i.d.) random activity pattern and at the other end of the range is the absolutely deterministic activity pattern.

The rest of the chapter is organized as follows. Section II provides the network model. Section III presents the proposed DRL-aided RA algorithm. In Section IV, we provide numerical evaluation, and a short conclusion concludes the chapter in Section V.

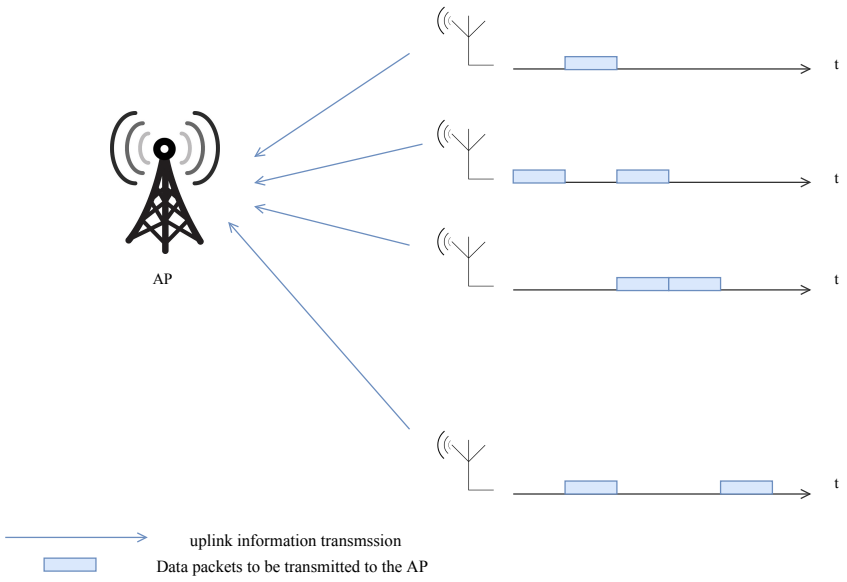

Figure 4.1: Network model.

4.2 System Model And Problem Formulation

In the following, we provide the system model and formulate the underlying problem.

4.2.1 System Model

We consider a network comprised of K IoT nodes and an AP, as illustrated in Fig. 4.1. The locations of the IoT nodes are assumed to be fixed and not to change with time. The transmission time is divided into T time slots of equal duration. At the beginning of each time slot, each IoT node sporadically becomes active in order to sense its environment, generates a data packet from the sensed data, and tries to transmit this data packet to the AP in the same time slot. In order for an IoT node to transmit a data packet to the AP in time slot t, a dedicated time-frequency block, refereed to as resource block (RB), needs to be allocated to the IoT node. Without loss of generality, we assume that all nodes transmit their packets with

identical data rate, which is set to one. We assume that the AP has N RBs available in total, where $N < K$ holds. As a result, in each time slot, the AP needs to perform intelligent resource allocation by allocating the available N RBs to the active IoT nodes only. Otherwise, if the AP allocates a RB to a non-active node, that RB would be wasted and the AP will not receive a packet on the corresponding RB.

4.2.2 Problem Formulation

The AP receives a packet from the k-th IoT node in time slot t if the following two events occur:

- the k-th IoT node is active in time slot t,
- the k-th IoT node has been allocated a RB in time slot t.

Otherwise, the AP will not receive a packet from the k-th IoT node in time slot t. To model this behaviour, let $A_k(t)$ and $I_k(t)$ be binary indicators defined as

$$A_k(t) = \begin{cases} 1 & \text{if node } k \text{ is active in time slot } t \\ 0 & \text{otherwise,} \end{cases} \tag{4.1}$$

$$I_k(t) = \begin{cases} 1 & \text{if a RB has been allocated to node } k \text{ in time slot } t \\ 0 & \text{otherwise.} \end{cases} \tag{4.2}$$

Using these binary indicators, we can obtain the average packet rate, denoted by R, as

$$R = \frac{1}{T}\frac{1}{K}\sum_{t=1}^{T}\sum_{k=1}^{K} A_k(t)I_k(t). \tag{4.3}$$

Our aim is to maximize the average packet rate by solving the following optimization problem

$$\begin{aligned} &\max_{I_k(t)} \frac{1}{T}\frac{1}{K}\sum_{t=1}^{T}\sum_{k=1}^{K} A_k(t)I_k(t) \\ &C1 : I_k(t) \in \{0,1\} \\ &C2 : \sum_{k=1}^{K} I_k(t) \leq N, \end{aligned} \tag{4.4}$$

where the last constraint follows since the AP has N RBs in total in each time slot. If $A_k(t), \forall k,t$ are known, then the optimal solution of (4.4) is known and is $I_k(t) = 1$ if $A_k(t) = 1$ until all N RBs are used up. However, the main problem is that $A_k(t)$ is unknown in practice and needs to be estimated. As a result, a practical algorithm that provides the optimal solution to the maximization problem in (4.4) is difficult in general. Hence, our aim in this chapter is to propose a suboptimal but a practical solution to the recourse allocation problem in (4.4), which provides good performance.

4.3 Proposed Solution

In the following, we discuss the existing solution used in practice and propose our solution.

4.3.1 Existing Solution: The RA Scheme

The existing practical suboptimal solution to the resource allocation problem in (4.4) is the conventional RA scheme [20]. In the RA scheme, each of the K IoT nodes has an identical set of M orthonormal sequences. At the start of each time slot, each active node selects uniformly at random a single orthonormal sequences from its set, and uses that sequences to transmit information to the AP via a dedicated control channel. This transmission, if successful, informs the AP that the considered node is active in the current time slot and thereby needs to be allocated a RB. The AP is able to receive this information from a given active node correctly if no other active node has selected the same orthonormal sequence as the considered node. Otherwise, if two or more active nodes have selected the same orthonormal sequence, collisions occur and the AP is not able to receive the information from these nodes correctly. As a result, the AP will not know that these nodes will be active in time slot t, and consequently the AP will not grant RBs to these nodes. To obtain the packet rate of the RA scheme, note that the probability a collision will occur is given by $(1/M)^n$, where n denotes the number of active nodes [38]. In addition, the RA scheme also fails if the AP does not have enough RBs to grant to all active nodes which have successfully completed the RA procedure and informed the AP that they are active.

The average packet rate achieved by the RA scheme is given by

$$R_{\mathrm{RA}} = \frac{1}{T}\frac{1}{K}\sum_{t=1}^{T}\min\left\{\left(1-\frac{1}{M}\right)^{K^a(t)-1}, \frac{N}{K^a(t)\left(1-\frac{1}{M}\right)^{K^a(t)-1}}\right\}, \tag{4.5}$$

where $(1-1/M)^n$ is the probability that collisions will not occur if n nodes are active, and $K^a(t)$ denotes the number of active nodes at time slot t found as

$$K^a(t) = \sum_{k=1}^{K} A_k(t). \tag{4.6}$$

4.3.2 Proposed Solution: The DRL-Aided RA Scheme

In the proposed DRL-aided RA scheme, the allocation of the N RBs is conducted in two consecutive phases. In the first phase, N_1 RBs are allocated by the AP using the DRL algorithm presented below, where $N_1 \leq N$. Next, in the following phase, $N_2 = N - N_1$ RBs are allocated by the AP using the conventional RA scheme, described in Sec. 4.3.1. To this end, the AP is assumed to host a DRL agent that learns to predict which nodes will be active in a given time slot t. The learning and resource allocation process of the DRL agent, which is repeated in each time slot, is as follows:

- We define a state in time slot t, denoted by $\mathscr{S}_t$. The state $\mathscr{S}_t$ represents a set comprised of the nodes which have been active during the previous t_h time slots, i.e., $t-t_h,...,t-1$, where t_h denotes the history that the agent "remembers".
- Based on the state in time slot t, the DRL agent produces an output set, denoted by $\mathscr{A}_t$ and referred to as the action, comprised of the nodes that have been predicted to be active in time slot t by the DRL agent.
- Based on the set $\mathscr{A}_t$, the following RBs allocations occur:
  - If $|\mathscr{A}_t| \leq N_1$, each node in the set $\mathscr{A}_t$ is allocated a RB.
  - If $|\mathscr{A}_t| > N_1$, then N_1 nodes from the set $\mathscr{A}_t$ are selected uniformly at random and each of these nodes is allocated a RB.

- Based on the allocations of RBs to the nodes predicted as active by the DRL agent, the following occurs in time slot t
  - If a node has been correctly predicted as active, and thereby granted a RB, the node transmits its data packet to the AP on the corresponding RB, and the AP receives this data packet correctly. Consequently, the DRL agent will classify this node as correctly predicted.
  - If a node has been miss-predicted as active by the DRL agent and thereby has been granted a RB, this node stays silent since it is inactive. As a result, the AP will not receive a packet on the corresponding RB. Consequently, the DRL agent will classify this node as erroneously predicted.
  - If a node has been correctly predicted as inactive and thereby has not been granted a RB, the node stays silent.
  - If a node has been miss-predicted as inactive and thereby has not been granted a RB, the miss-predicted active node attempts to obtain a RB using the conventional RA scheme, as described in Sec. 4.3.1. Thereby, the node selects uniformly at random a single orthonormal sequence from its set, and uses that sequence to inform the AP, via the control channel, that the considered node is active and has been miss-predicted in the current time slot. The AP listens to the control channel and detects the nodes which have been miss-predicted as inactive. The AP can detect only those nodes which have selected a unique orthonormal sequence. The other nodes cannot be detected due to collisions of their packets, as explained in Sec. 4.3.1.
- Next, based on the observations, the AP constructs the set $\mathscr{S}_t$ by including the following nodes
  - the nodes which the DRL predicted as active and from which the AP received a packet on the corresponding allocated RB.
  - the nodes which the AP detected as active on the control channel via the RA scheme.

- Based on the observation, the AP computes a reward in time slot t, denoted by r_t, which is equal to K, if all nodes are correctly predicted in time slot t by the DRl agent, or 0 otherwise.
- The system transitions to the next time slot and the whole process described above is repeated.

Implementation of the DRL Agent

The DRL agent is implemented as a deep neural network located at the AP. This deep neural network, in time slot t, has the set $\mathscr{S}_t$ as input and produces as outputs $L = K!$ values, denoted by $Q_e(\mathscr{S}_t|\mathscr{A}_1;\theta)$, $Q_e(\mathscr{S}_t|\mathscr{A}_2;\theta)$, ..., $Q_e(\mathscr{S}_t|\mathscr{A}_L;\theta)$, where $Q_e(\mathscr{S}_t|\mathscr{A}_l;\theta)$ is an estimated average reward the agent will receive in the future if the agent predicts that the set of active nodes in time slot t is $\mathscr{A}_l$, for $l = 1,2...,L$, and θ is a vector comprised of the weights of the neural network. Next, the agent chooses that set $\mathscr{A}$ which corresponds to the largest output value of the neural network, i.e.,

$$\mathscr{A} = \underset{\mathscr{A}}{\text{argmax}}\ Q_e(\mathscr{S}_t|\mathscr{A};\theta). \tag{4.7}$$

The function $Q_e(\mathscr{S}_t|\mathscr{A};\theta)$ obtained at the output of the neural network is an estimate of the function $Q(\mathscr{S}_t|\mathscr{A})$, which is known as the discounted average award. The discounted average award function is defined as

$$\begin{aligned} Q(\mathscr{S}_t|\mathscr{A}) &= E\left\{\sum_{k=t}^{\infty}\gamma^{k-t}r_t\Big|\mathscr{S}_t,\mathscr{A}\right\} \\ &\rightarrow Q(\mathscr{S}_t|\mathscr{A}) + \alpha\left[r + \gamma\underset{\mathscr{A}}{\text{argmax}}\,Q(\mathscr{S}_{t+1}|\mathscr{A}) - Q(\mathscr{S}_t|\mathscr{A})\right], \end{aligned} \tag{4.8}$$

where $0 \leq \gamma \leq 1$ is referred to as the discount factor. In order for the neural network to produce output functions $Q_e(\mathscr{S}_t|\mathscr{A};\theta)$ that are estimates of $Q(\mathscr{S}_t|\mathscr{A})$, the Bellman equation is used and thereby the weights in the neural network θ are

optimized such that the following mean squared error is minimized

$$\mathscr{L} = E\left\{\left(r + \gamma \underset{\mathscr{A}}{\text{argmax}}\, Q_e(\mathscr{S}_{t+1}|\mathscr{A};\theta) - Q_e(\mathscr{S}_t|\mathscr{A};\theta)\right)^2\right\}. \tag{4.9}$$

The above minimization of the mean square error can be implemented iteratively via a stochastic gradient descent (or a variant), where in each iteration the weights in the neural network θ are updated according to

$$\theta \leftarrow \theta - \eta \nabla_\theta \mathscr{L}. \tag{4.10}$$

The reader is kindly referred to [24] and [39], the references therein and the references in this chapter for further details.

Training the DRL Agent Using Expert Knowledge

In order for the training process of the agent to be succesful, the agent needs to obtain a sufficient number of "live" training data samples from the interaction between the AP and the IoT nodes. Let the live data sample at time slot t be obtained as per Subsection 4.3.2. In practice, the acquisition of sufficient number of live samples can be impractical and ultimately prohibitive, due to the excessively long amount of time required to acquire the data. In these cases, transfer learning can be leveraged in order to accelerate the training process. Transfer learning is a recent trend in the ML community where available prior knowledge about the considered problem stemming from theoretical models is embedded in the neural networks [40]-[41]. Transfer learning dramatically reduces the number of live data samples that are needed for the training process to be successful.

The IoT networks research community has provided many theoretical models for the activity of the IoT nodes, such as those in [19], [42]. We choose to leverage the model in [42], where the authors use a Coupled Markov Modulated Poisson Process (CMMPP) to model the activity of the nodes in a IoT cell theoretically. The CMMPP model captures both regular and alarm reporting, as well as the correlated activity behavior among the nodes. Hence, we use the CMMPP model in [42] to train the DRL agent at the AP. To this end, we first synthesize artificial activity patterns of the IoT nodes, according to the CMMPP model, with which we

train the DRL agent. Thereby, during the training process, in each time slot, the DRL agent learns to predict the active nodes from artificial activity patterns as per Subsection 4.3.2. Once the prior knowledge has been transferred, i.e., the DRL agent has been trained using the artificial activity patterns, the DRL-RA scheme starts using the actual live samples from the IoT nodes.

Average Packet Rate

In the following, we derive the average packet rate of the proposed DRL-aided RA scheme. To this end, let $\varepsilon^a(t)$ and $\varepsilon^p(t)$ denote the probability that a node is predicted as active and inactive at time slot t, respectively. Let $\varepsilon^a_{cor.}(t)$ and $\varepsilon^p_{mis.}(t)$ denote the probability that a node is correctly predicted as active and mispredicted as inactive at time slot t, respectively. Finally, let $\varepsilon^a_{cor.,noRBs}(t)$ denote the probability that a node is correctly predicted as active at time slot t, but the AP does not have any RBs left to allocate to the node. For the DRL-aided RA scheme, in each time slot, $K\varepsilon^p_{mis.}(t)$ nodes that are misclassified as inactive, and $K\varepsilon^a_{cor.,noRBs}(t)$ nodes that are correctly classified as active but the DRL agent does not have enough any RBs left to allocate to them, will attempt the RA procedure in order to obtain one of N_2 RBs. The rate of the proposed algorithm is thus given by

$$R_{\text{DRL+RA}} = \frac{1}{T}\frac{1}{K}\sum_{t=1}^{T} \min\left\{ \left(1-\frac{1}{M}\right)^{V^a(t)-1}, \frac{N_2}{V^a(t)\left(1-\frac{1}{M}\right)^{V^a(t)-1}} \right\}, \tag{4.11}$$

where $V^a(t) = K\varepsilon^p_{mis.}(t) + K\varepsilon^a_{cor.,noRBs}(t)$. To find $V^a(t)$, we need to calculate the number of nodes which have not been granted an RB, in spite of being correctly classified as active $K\varepsilon^a_{cor.,noRBs}(t)$. To do so, let ${}^x\mathbf{C}_y$ denote the binomial coefficient, defined as

$${}^x\mathbf{C}_y = \frac{x!}{y!(x-y)!}. \tag{4.12}$$

We can distinguish the following cases: $K\varepsilon^a_{mis.}(t) > N_1$ and $K\varepsilon^a_{cor.}(t) > N_1$; $K\varepsilon^a_{mis.}(t) > N_1$ and $K\varepsilon^a_{cor.}(t) < N_1$; $K\varepsilon^a_{mis.}(t) < N_1$ and $K\varepsilon^a_{cor.}(t) > N_1$; and $K\varepsilon^a_{mis.}(t) < N_1$ and $K\varepsilon^a_{cor.}(t) < N_1$. In the first case, when $K\varepsilon^a_{mis.}(t) > N_1$ and $K\varepsilon^a_{cor.}(t) > N_1$, the following can occur:

- N_1 of the $K\varepsilon^a_{mis.}(t)$ misclassified nodes are granted all N_1 RBs and none of the $K\varepsilon^a_{cor.}(t)$ correctly classified nodes get an RB, which occurs with probability

$$\frac{^{K\varepsilon^a_{cor.}(t)}\mathbf{C}_0 \times ^{K\varepsilon^a_{mis.}(t)}\mathbf{C}_{N_1}}{^{K\varepsilon^a(t)}\mathbf{C}_{N_1}}, \tag{4.13}$$

- $N_1 - 1$ of the $K\varepsilon^a_{mis.}(t)$ misclassified nodes are granted $N_1 - 1$ RBs and one of the $K\varepsilon^a_{cor.}(t)$ correctly classified nodes gets an RB, which occurs with probability

$$\frac{^{K\varepsilon^a_{cor.}(t)}\mathbf{C}_1 \times ^{K\varepsilon^a_{mis.}(t)}\mathbf{C}_{N_1-1}}{^{K\varepsilon^a(t)}\mathbf{C}_{N_1}}, \tag{4.14}$$

- $N_1 - 2$ of the $K\varepsilon^a_{mis.}(t)$ misclassified nodes are granted $N_1 - 2$ RBs and two of the $K\varepsilon^a_{cor.}(t)$ correctly classified nodes get an RB, which occurs with probability

$$\frac{^{K\varepsilon^a_{cor.}(t)}\mathbf{C}_2 \times ^{K\varepsilon^a_{mis.}(t)}\mathbf{C}_{N_1-2}}{^{K\varepsilon^a(t)}\mathbf{C}_{N_1}}, \tag{4.15}$$

$\vdots$

- None of the $K\varepsilon^a_{mis.}(t)$ misclassified nodes are granted RBs and N_1 of the $K\varepsilon^a_{cor.}(t)$ correctly classified nodes get an RB, which occurs with probability

$$\frac{^{K\varepsilon^a_{cor.}(t)}\mathbf{C}_{N_1} \times ^{K\varepsilon^a_{mis.}(t)}\mathbf{C}_0}{^{K\varepsilon^a(t)}\mathbf{C}_{N_1}}. \tag{4.16}$$

Thereby, when $K\varepsilon^a_{mis.}(t) > N_1$ and $K\varepsilon^a_{cor.}(t) > N_1$, the AP does not have enough RBs to allocate to $K\varepsilon^a_{cor.}(t)$ nodes, or to $K\varepsilon^a_{cor.}(t) - 1$ nodes, or to $K\varepsilon^a_{cor.}(t) - 2$ nodes, ... , or to $K\varepsilon^a_{cor.}(t) - N_1$ nodes, each occurring with probability given by (4.13), (4.14), (4.15), and (4.16), respectively. As a result, $K\varepsilon^a_{cor.,noRBs}(t)$ is given

by

$$
\begin{aligned}
K\varepsilon^a_{cor.,noRBs}(t) = K\varepsilon^a_{cor.}(t)&\frac{{}^{K\varepsilon^a_{cor.}(t)}\mathbf{C}_0 \times {}^{K\varepsilon^a_{mis.}(t)}\mathbf{C}_{N_1}}{K\varepsilon^a(t)\mathbf{C}_{N_1}} \\
&+ (K\varepsilon^a_{cor.}(t)-1)\frac{{}^{K\varepsilon^a_{cor.}(t)}\mathbf{C}_1 \times {}^{K\varepsilon^a_{mis.}(t)}\mathbf{C}_{N_1-1}}{K\varepsilon^a(t)\mathbf{C}_{N_1}} \\
&+ (K\varepsilon^a_{cor.}(t)-2)\frac{{}^{K\varepsilon^a_{cor.}(t)}\mathbf{C}_2 \times {}^{K\varepsilon^a_{mis.}(t)}\mathbf{C}_{N_1-2}}{K\varepsilon^a(t)\mathbf{C}_{N_1}} \\
&\vdots \\
&+ (K\varepsilon^a_{cor.}(t)-N_1)\frac{{}^{K\varepsilon^a_{cor.}(t)}\mathbf{C}_{N_1} \times {}^{K\varepsilon^a_{mis.}(t)}\mathbf{C}_0}{K\varepsilon^a(t)\mathbf{C}_{N_1}}.
\end{aligned} \tag{4.17}
$$

By extending this analysis to the other three cases, we obtain $K\varepsilon^a_{cor.,noRBs}(t)$ as

$$
\begin{aligned}
K\varepsilon^a_{cor.,noRBs}(t) = n_1&\frac{{}^{K\varepsilon^a_{cor.}(t)}\mathbf{C}_{n_2} \times {}^{K\varepsilon^a_{mis.}(t)}\mathbf{C}_{N_1-n_2}}{K\varepsilon^a(t)\mathbf{C}_{N_1}} \\
&+ (n_1-1)\frac{{}^{K\varepsilon^a_{cor.}(t)}\mathbf{C}_{n_2+1} \times {}^{K\varepsilon^a_{mis.}(t)}\mathbf{C}_{N_1-n_2-1}}{K\varepsilon^a(t)\mathbf{C}_{N_1}} \\
&+ (n_1-2)\frac{{}^{K\varepsilon^a_{cor.}(t)}\mathbf{C}_{n_2+2} \times {}^{K\varepsilon^a_{mis.}(t)}\mathbf{C}_{N_1-n_2-2}}{K\varepsilon^a(t)\mathbf{C}_{N_1}} \\
&\vdots \\
&+ m_1\frac{{}^{K\varepsilon^a_{cor.}(t)}\mathbf{C}_{m_2} \times {}^{K\varepsilon^a_{mis.}(t)}\mathbf{C}_{N_1-m_2}}{K\varepsilon^a(t)\mathbf{C}_{N_1}},
\end{aligned} \tag{4.18}
$$

where ${}^x\mathbf{C}_y$ is given by (4.12). In (4.18), the constants n_1, n_2, m_1, and m_2 can be found as

$$
n_1 = \begin{cases} K\varepsilon^a_{cor.}(t) - (K\varepsilon^a(t) - N_1), & \text{if } K\varepsilon^a_{mis.}(t) < N_1, \\ K\varepsilon^a_{cor.}(t), & \text{if } K\varepsilon^a_{mis.}(t) \geq N_1, \end{cases}. \tag{4.19}
$$

$$
n_2 = \begin{cases} K\varepsilon^a(t) - N_1, & \text{if } K\varepsilon^a_{mis.}(t) < N_1, \\ 0, & \text{if } K\varepsilon^a_{mis.}(t) \geq N_1, \end{cases}. \tag{4.20}
$$

$$m_1 = \begin{cases} 0, & \text{if } K\varepsilon^a_{cor.}(t) \leq N_1, \\ K\varepsilon^a_{cor.}(t) - N_1, & \text{if } K\varepsilon^a_{cor.}(t) > N_1, \end{cases}. \tag{4.21}$$

and

$$m_2 = \begin{cases} K\varepsilon^a_{cor.}(t), & \text{if } K\varepsilon^a_{cor.}(t) \leq N_1, \\ N_1, & \text{if } K\varepsilon^a_{cor.}(t) > N_1. \end{cases}. \tag{4.22}$$

4.4 Numerical Results

In this section, we compare the performance of the proposed DRL-aided RA scheme with the conventional RA scheme in [20]. To this end, in Section IV-A, we first present the data sets that have been used in the simulations and the hyper parameters of the proposed algorithm are given in Section IV-B. The numerical results are finally given in Section IV-C.

4.4.1 Data Sets

Synthetic Activity Patterns

To demonstrate the effectiveness of the proposed scheme on different traffic types, we first generate synthetic data sets. Specifically, node k is assumed to be active in time slot t with probability $p_k(t)$, where

$$p_k(t) = \begin{cases} 1 - \frac{\delta}{2}, & \text{if } t \text{ is even}, \\ \frac{\delta}{2}, & \text{if } t \text{ is odd}, \end{cases} \tag{4.23}$$

where δ is a constant which controls the determinism of the activity patterns. Thereby, lower values of δ will result in a more periodic activity pattern, and as δ increases, the activity pattern becomes more random.

Real-World Activity Pattern

To demonstrate the effectiveness of the proposed scheme even further, real-world activity patterns are drawn from the publicly available data sets in [43], [44], [45], and [46]. We assume that all nodes operate during the same time period and in the same IoT cell. The data sets in [43]-[46] are comprised of nodes which have different reporting intervals [19]. In particular, the time elapsed between two consecutive data arrivals ranges from one second for some nodes up to 1 hour for others.

4.4.2 Neural Network Hyper-Parameters

To speed-up the training of the DRL agent, we split the neural network into an ensemble of neural networks, such that only subsets of the nodes are included in each network in the ensemble. All networks in the ensemble are identically trained, as described previously. The architecture of each neural network in the ensemble consists of a three-layer, fully connected neural network. The activation functions for the neurons are ReLU functions [47], given by

$$f(x) = \begin{cases} 0, \text{ for } x < 0, \\ x, \text{ for } x \geq 0. \end{cases} \tag{4.24}$$

The discount factor in (4.9) is set to $\gamma = 0.05$. The exploration-exploitation trade-off [47] is controlled via the ε-greedy algorithm, where ε_t is decreasing from $\varepsilon_t = 1$ to $\varepsilon_t = 0.01$ as

$$\varepsilon_{t+1} \leftarrow \varepsilon_t * \varepsilon_{dec.}, \tag{4.25}$$

where $\varepsilon_{dec} = 0.995$. Thereby, the agent chooses the action with the highest $Q_e(\mathscr{S}_t|\mathscr{A};\theta)$ value with probability ε, and randomly chooses an action with probability $1-\varepsilon$. At the start of the training when ε is high, the agent explores the action space via randomly choosing the action. As ε decreases, the agent begins to exploit the accumulated knowledge via choosing the action with the highest $Q_e(\mathscr{S}_t|\mathscr{A};\theta)$ value. The parameters of the proposed algorithm are summarized in Table 5.1.

Table 4.1: Algorithm hyper-parameters

Parameter	Value
No. of hidden layers	3
Discount factor γ	0.05
Learning rate α	0.001
ε	1 to 0.01

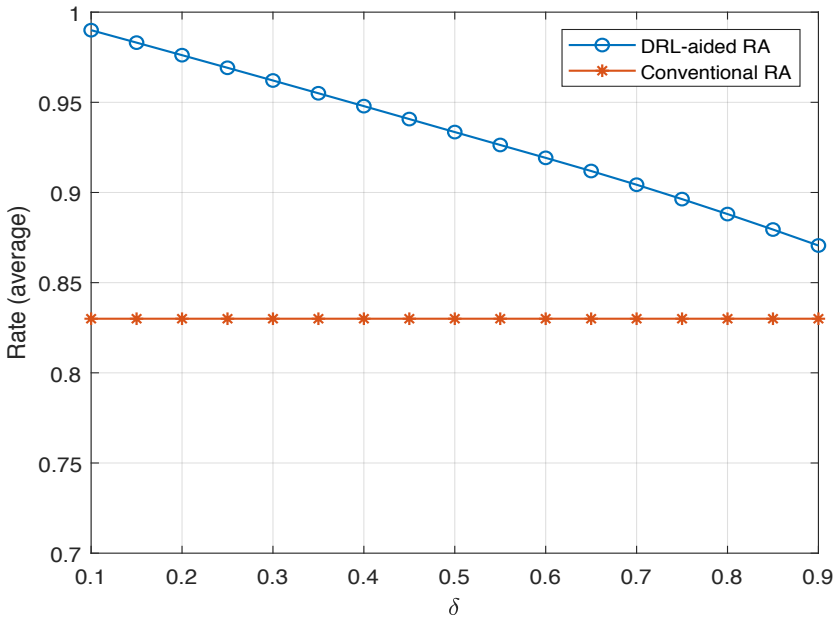

Figure 4.2: Average packet rate as a function of δ for synthetic activity patterns.

4.4.3 Performance Evaluation

Synthetic Data

In Fig. 4.2, we present the average packet rate achieved with the proposed DRL-aided RA scheme on the synthetic activity pattern generated by (4.23) and compare it with the packet rate achieved with the conventional RA scheme for different values of δ. In this example, the number of nodes in the cell is set to $K = 20$

and the number of available RBs at the AP is set to $N = 10$. The number of RBs allocated by the AP via the DRL agent decreases from $N_1 = 7$ for $\delta = 0.1$, to $N_1 = 1$ for $\delta = 0.9$. To determine N_1, we only need to know the probability that a node is correctly classified as active and the probability that a node is misclassified as inactive (see (4.11)-(4.22)), which are obtained from the data samples used for training. In particular, we use these samples to calculate the rate using (4.11) for all values of N_1, and we chose the value which results with the highest rate. In the case of transfer learning, we use only the samples from the real-world activity pattern (not the data used for pre-training). The number of available orthonormal sequences is set to $M = 54$. As Fig. 4.2 illustrates, the average packet rate of the conventional RA scheme is not sensitive to δ. On the other hand, the average packet rate of the proposed DRL-aided RA scheme is a decreasing function of δ. This is due to the amount of randomness in the activity patterns as δ increases. In particular, when δ is low the activity pattern is almost periodic so the DRL agent is able to learn it and then correctly allocate the available RBs, thereby reducing the need for the nodes to attempt RA. Conversely, when δ is high the activity pattern is highly random and the agent is not able to learn it completly. The randomness in the activity patterns increases the probability of missclasification. This forces the nodes which have been misclassified as not active to attempt RA to gain RBs. This example illustrates that the average packet rate of the proposed DRL-aided RA scheme is lower bounded by the average packet rate of the RA scheme. Thereby, the worst possible performance of the proposed DRL-aided RA scheme, obtained for $\delta = 1$, is identical to the performance of the RA scheme.

In Fig. 4.3, we illustrate average packet rate achieved with the proposed DRL-aided RA scheme and compare it with the average packet rate of the conventional RA scheme as a function of the number of nodes in the cell K, for two different values of δ. The number of available RBs at the AP is set to $N = 10$. The number of RBs allocated by the AP via the DRL agent is set to $N_1 = 5$ and $N_1 = 2$ for $\delta = 0.3$ and $\delta = 0.7$, respectivley. The number of available orthonormal sequences is set to $M = 54$. As it can be seen from Fig. 4.3, the packet rate of the proposed DRL-aided RA scheme is significantly higher than the rate of the RA scheme. For example, the proposed scheme can achieve a packet rate of 0.6 when $K = 100$ nodes, whilst the conventional RA scheme can achieve the same packet rate with $K = 50$ nodes

when $\delta = 0.3$. Similarly, when the activity patterns are more random i.e., when $\delta = 0.7$, the proposed scheme can achieve a packet rate of 0.6 for $K = 70$ nodes, whilst the conventional RA scheme achieves the same rate with $K = 50$ nodes.

Real-World Activity Pattern

In Fig. 4.4, we illustrate the instantaneous packet rate in each time slot during a period of 1 hour (3600 s) for the real-world activity pattern. In total our IoT cell is comprised of $K = 222$ nodes, which report 35448 data arrivals during one hour. The number of available RBs at the AP is set to $N = 20$. The number of RBs allocated by the AP via the DRL agent is set to $N_1 = 16$. The number of available orthonormal sequences is set to $M = 54$. Since the minimum duration between two data arrivals in these data sets is 1s, we assume that the duration of a time slot is $t = 1$s. As it can be seen from Fig. 4.4, the proposed DRL-aided RA scheme achieves a packet rate that is significantly higher than the conventional RA scheme in each time slot. This is a consequence of the fact that the agent is able to extract the determinism in the activity pattern, which exists in practice, and correctly predict some of the active nodes. As a result, the number of nodes that attempt the RA procedure is much lower compared to the conventional RA scheme. In the spirit of reproducible science, the codes used for generating this figure are made available on [48].

To illustrate the benefits of transfer learning we present Fig. 4.5, where the percentage of maximum possible reward is illustrated as a function of the percentage of sufficient live samples. The sufficient number of live samples is defined as the number of live samples needed for the DRL agent to obtain the maximum possible reward, and thereby achieve the maximum possible inference accuracy. The maximum reward is defined as the reward obtained by using 100% of live data samples. Fig. 4.5 shows that the maximum reward can be obtained by using 20% of live data samples and 80% of artificial samples. Note that, using an insufficient number of live data samples, and no artificial samples, leads to a reward that is significantly lower than the maximum possible reward, as the agent does not have enough data for the training process. In addition, the obtained reward is significantly lower if only artificial samples, without any live samples, are used which

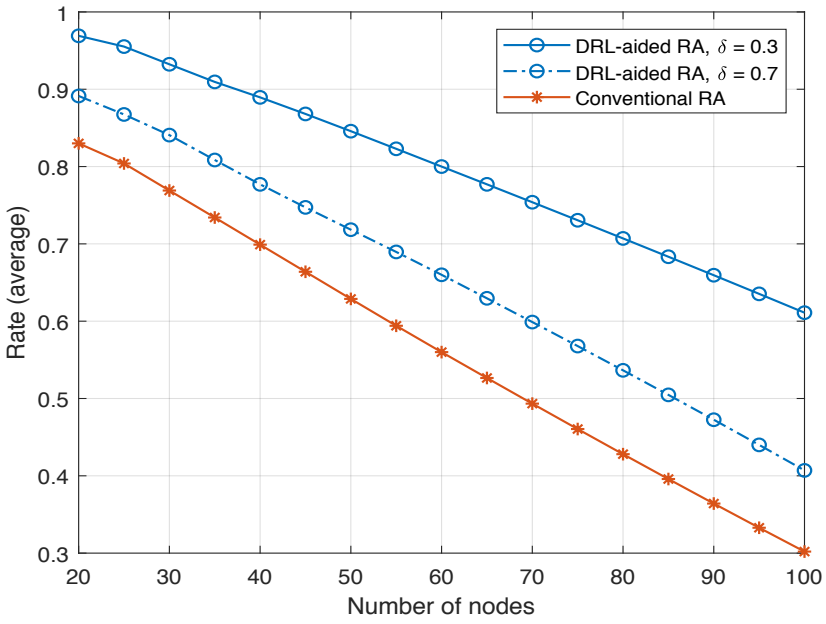

Figure 4.3: Average packet rate as a function of the number of nodes for synthetic activity patterns.

is a consequence of the mismatch between the artificial model and the activity in the IoT cell. Thereby, optimal performance can be achieved by using 20% of live samples and 80% of artificial samples from the theoretical model. This in turn significantly decreases the time required for the agent to be trained, i.e., by up to 80% in our case.

4.5 Conclusion

In this chapter, we proposed a DRL-aided RA scheme for a network comprised of K IoT nodes and an AP. In particular, an intelligent DRL agent placed at the AP learns to predict the activity of the IoT nodes in each time slot and grants time-frequency resource blocks to the IoT nodes predicted as active. The standard RA scheme is used as a back-up access mechanism for potentially misclassified, unseen or new nodes in the cell. In addition, we leverage expert knowledge in order

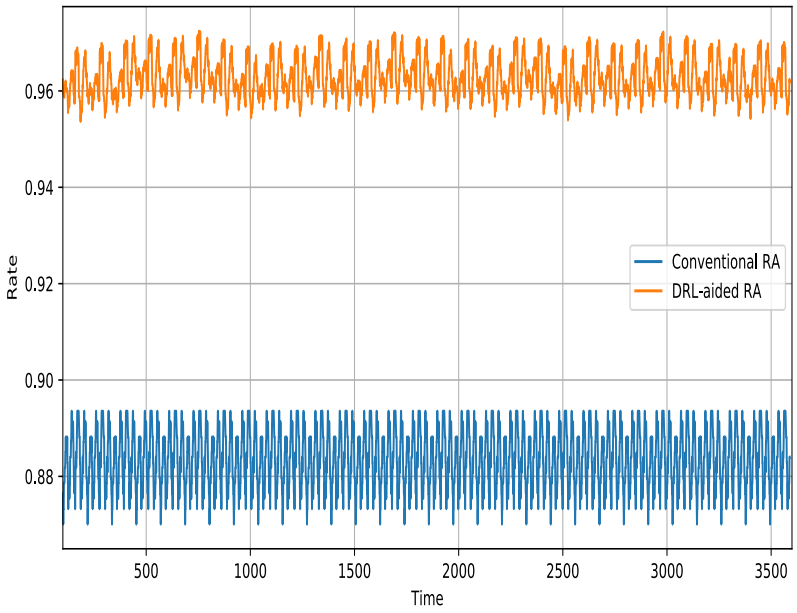

Figure 4.4: Instantaneous packet rate in each time slot during one hour for real-world activity patterns.

to ensure faster training of the DRL agent. By using publicly available data sets, we show signifficant improvements in terms of rate, when the proposed DRL-aided RA scheme is implemented, compared to the conventional RA scheme.

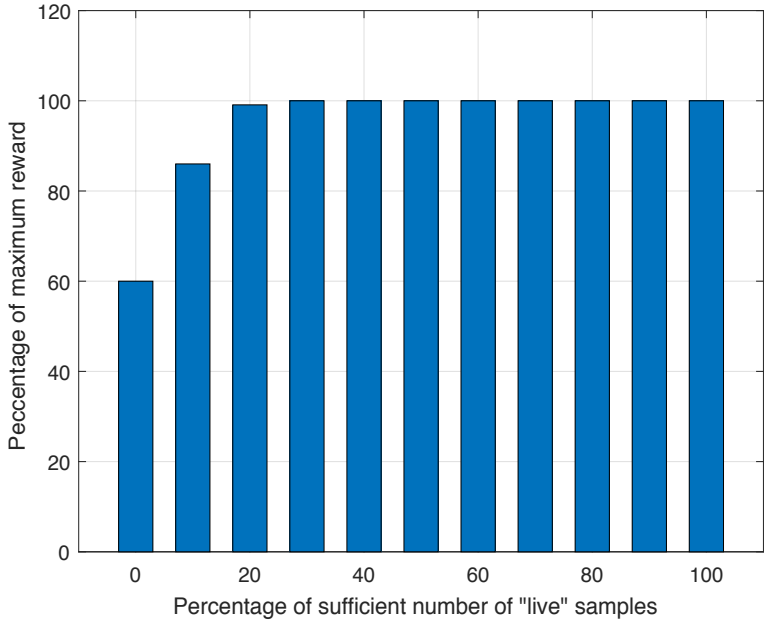

Figure 4.5: Comparison between transfer learning and data driven learning. The percentage of artificial samples can be found as $100 - X$, where X denotes the percentage of sufficient number of live samples.

Chapter 5

Data Selection Scheme For Energy Efficient Supervised Learning At IoT Nodes

In this chapter, we tackle higher level problems in IoT networks. To this end, we consider a system model comprised of an IoT node connected wirelessly to a cloud server. The IoT node is assumed to generate data by sensing its environment and make inferences from the data. To this end, the IoT node can rely on its on-device neural network and make inference locally, which incurs small energy cost but a relatively inaccurate inference, or it can wirelessly transmit the data sample to the cloud so that the cloud makes the inference and feeds it back to the IoT node, which incurs a large energy cost but a more precise inference. For this system model, we propose a scheme that the IoT device can employ to select the data samples that would likely lead to inaccurate inferences if processed locally so that those data samples are transmitted to the cloud. As a result, the amount of transmitted data is significantly reduced and the resources of the device are preserved, whilst the overall inference precision remains high.

5.1 Introduction

AI is set to change many aspect of our lives, ranging from medical diagnosis to natural language processing. This progress has been fuelled mainly by the availability of more data and more computing power [49]. Classical AI is based on the premise that computational nodes have full access to a global dataset and a massive amount of storage and computing power so that they can sift through this data for inference. However, IoT nodes have heavy constrains in terms of memory, computation, and energy. In fact, the memory required to store a deep neural network and its energy consumption may exceed the memory size and battery level of an IoT node [23]. As a result, only simple neural networks can be deployed in such computationally and energy constrained IoT nodes, which leads to relatively inaccurate on-device inferences. On the other hand, a cloud server has practically unlimited memory, large computational power, and uninterrupted power supply. Thereby, a cumbersome neural network can be deployed at the cloud, which leads to more accurate on-cloud inferences compared to the IoT's on-device inferences. However, accessing the cloud's neural network by an IoT node incurs energy cost on the IoT node. Specifically, the IoT node needs to transmit the data sample for which inference is needed to the cloud and then wait to receive the inference information from the cloud. Hence, there is the following energy-accuracy trade-off at an IoT node. On one hand, the IoT node requires frequent transmissions/receptions to/from the cloud in order to improve its inference accuracy. Whereas, on the other hand, the IoT node needs to limit the transmissions to the cloud in order to preserve its energy.

In this chapter, we propose a scheme that the IoT node can employ to select the data samples that would likely lead to inaccurate inferences so that those samples are transmitted to the cloud. As a result, local inferences are made only from data samples that would likely lead to accurate inferences and thereby the overall inference precision of the system is significantly improved for a given energy cost. Our numerical results indicate that the proposed scheme drastically improves the inference accuracy of the system for a given energy constraint compared to the case when the inference is always made locally at the IoT node. Conversely, with our scheme the IoT node can reach the inference accuracy of the cloud but with

fraction of the energy cost, which has a significant impact on the longevity of the IoT node. To the best of our knowledge, such a data selection approach for improving the inference accuracy at computationally constrained wireless devices, such as IoT nodes, has not been proposed in the literature so far. Previous research have focused on increasing the inference accuracy and the energy efficiency of the neural network models that are to be deployed at computationally constrained devices. For example, the authors in [50], [51], and [52] propose compressing highly accurate but slow models into small and computational cheap models. In [53], the authors propose compressing an ensemble of multiple neural networks into a single model. In [54], the authors improve the object detection capacity of small neural networks by using a larger model as a teacher, a method also adopted in [55] for natural language processing. However, the inference accuracy of these models is still smaller than that of a model deployed on a computationally powerful device, such as the cloud. Hence, our data selection scheme can still be applied at IoT nodes employing the models in [50]-[55] in order to increase the overall inference accuracy of the IoT node-cloud system even further.

This chapter is organized as follows. The system model is presented in Section 5.2. In Section 5.3, we present the proposed scheme in detail. The proposed scheme is then numerically evaluated in Section 5.4, and a brief conclusion concludes the chapter in Section 5.5.

5.2 System model

We consider a system model comprised of an IoT node that is connected wirelessly to a cloud[1]. We assume that time is slotted and that in each time slot the IoT node becomes active, senses the environment, and generates a data sample from its sensing. Next, the IoT node uses the data sample to make an inference. To this end, the IoT node has two choices: it can either make the inference locally using its on-device neural network, or it can send the data sample to the cloud, where the neural network at the cloud makes the inference and feeds it back to the IoT node. We assume that the energy cost for making inferences at the IoT node and the cloud are constant during all time slots and are denoted by E_0 and E_C, respectively, where

[1] Note that there can be arbitrary number of hops between the IoT node and the cloud server.

$E_0 < E_C$ holds. The energy cost of the cloud inference is higher than the local inference since the IoT node needs additional energy for sending the data sample to the cloud and then receiving the feedback inference from the cloud. On the other hand, we assume that the average inference accuracy of the neural network at the IoT node is lower than that that at the cloud. Specifically, let $I_0(t) \in \{0,1\}$ and $I_C(t) \in \{0,1\}$ be binary variables defined as

$$I_0(t) = \begin{cases} 1 & \text{if the classification at the IoT node} \\ & \text{of the data sample generated in time slot } t \\ & \text{is correct} \\ 0 & \text{otherwise} \end{cases} \tag{5.1}$$

$$I_C(t) = \begin{cases} 1 & \text{if the classification at the cloud} \\ & \text{of the data sample generated in time slot } t \\ & \text{is correct} \\ 0 & \text{otherwise.} \end{cases} \tag{5.2}$$

Using $I_0(t)$ and $I_C(t)$, $\forall t$, we can find the average inference accuracies of the neural networks at the IoT node and the cloud as

$$A_0 = \lim_{T\to\infty} \frac{1}{T} \sum_{t=1}^{T} I_0(t), \tag{5.3}$$

and

$$A_C = \lim_{T\to\infty} \frac{1}{T} \sum_{t=1}^{T} I_C(t), \tag{5.4}$$

respectively. We assume that $A_0 < A_C$ holds.

We assume that the neural network at the IoT node has M outputs, where M denotes the number of classes, and the i-th output represents the probability that the data sample at the input belongs to class i, for $i = 1,2,...,M$.

For the considered system model, the first choice - making the inference locally - will result in lower energy cost but also lower inference accuracy on average, whereas the second choice - making the inference on the cloud - would results in higher energy cost but also higher inference accuracy on average. Hence, there exists an optimal selection strategy, which in each time slot, selects whether the given data sample should be inferred locally at the IoT node or it should be send to the cloud for on-cloud inference so that the overall inference accuracy of the system is maximized for a given energy constraint.

5.3 Problem Formulation and Solution

In the following, we formulate the problem and provide a solution.

5.3.1 Problem Formulation

Let $b(t) \in \{0,1\}$ be defined as

$$b(t) = \begin{cases} 1, & \text{if cloud inference is selected} \\ 0, & \text{if local inference is selected.} \end{cases} \tag{5.5}$$

Then, the optimal selection strategy can be found as the solution to the following optimization problem

$$\begin{aligned} &\max_{b(t),\forall t} \frac{1}{T}\sum_{t=1}^{T}\Big(b(t)I_C(t) + (1-b(t))I_0(t)\Big) \\ &\text{s.t. } \frac{1}{T}\sum_{t=1}^{T}\Big(b(t)E_C + (1-b(t))E_0\Big) \leq E_{\max}, \end{aligned} \tag{5.6}$$

where E_{max} is the maximum allowed energy cost. The optimal solution to this problem is not known since the inference accuracies $I_C(t)$ and $I_0(t)$ are not known a priori of making the selection. A naive selection strategy, referred to as *the probabilistic scheme*, would be to select $b(i) = 1$ with probability β in each time slot such that $\beta E_C + (1-\beta)E_0 = E_{\max}$ holds. This leads to $\beta = (E_{\max} - E_0)/(E_C - E_0)$

and to an overall inference accuracy, denoted by A, given by

$$A = \frac{E_{\max} - E_0}{E_C - E_0} A_C + \frac{E_C - E_{\max}}{E_C - E_0} A_0. \tag{5.7}$$

However, this probabilistic solution does not distinguish between "good" and "'bad' data samples at the IoT node, i.e., data samples that are more likely to be classified correctly and those that are more likely to be classified incorrectly at the IoT node. In the following, we present a suboptimal solution to the above problem which can distinguish between "good" and "'bad' data samples at the IoT node and thereby yields significant performance gains compared to the probabilistic scheme.

5.3.2 Proposed Selection Scheme

Let $q_i(t)$ be the i-th output at the neural network of the IoT node, which represents the probability that the data sample the IoT node generated in time slot t belongs to class i, for $i = 1, ..., M$. Let $V_q(t)$ be the variance of the outputs of the IoT node's neural network in time slot t, obtained as

$$V_q(t) = \frac{1}{M} \sum_{i=1}^{M} \left(q_i(t) - \frac{1}{M} \sum_{j=1}^{M} q_j(t) \right)^2. \tag{5.8}$$

Next, let $Q_m(t)$ and $Q_{m-1}(t)$ be the highest and the second highest class probabilities at the output of the IoT node's neural network in time slot t, respectively, given by

$$Q_m(t) = \max\{q_1(t), q_2(t), ..., q_M(t)\} \tag{5.9}$$

and

$$Q_{m-1}(t) = \max\big\{\{q_1(t), q_2(t), ..., q_M(t)\} \backslash Q_m(t)\big\}. \tag{5.10}$$

Using the parameters defined above, we now define *the inference confidence metric*, denoted by $C(t)$, as

$$C(t) = V_q(t)\big(Q_m(t) - Q_{m-1}(t)\big). \tag{5.11}$$

The higher $C(t)$ is, the higher the confidence that the data sample at the input of the neural network at the IoT node in time slot t will be correctly classified. The rational for the adopted metric is as follows. The confidence metric is low when the difference between the largest two class probabilities is small and also when the the variance of all class probabilities is small, since in that case all class probability values are almost identical.

Based on the inference confidence metric, $C(t)$, we propose $b(t)$ to be computed as

$$b(t) = \begin{cases} 1, & C(t) < \alpha \\ 0, & C(t) > \alpha \end{cases}, \tag{5.12}$$

where α denotes a weighting parameter found such that the constraint in (5.6) holds. This weighting parameter α can be approximated iteratively in each time slot as $\alpha_e(t) \approx \alpha$, such that $\lim_{t\to\infty} \alpha_e(t) = \alpha$ holds. Specifically, $\alpha_e(t)$ can be found as

$$\alpha_e(t+1) = \alpha_e(t) - \lambda \left(\frac{1}{t} \sum_{j=1}^{t} \left(b(j)E_C + (1-b(j))E_0 \right) - E_{\max} \right), \tag{5.13}$$

where λ is some appropriate constant.

Note that, the proposed scheme is agnostic to the architecture of the neural networks. As a result, it can be employed by IoT nodes where the outputs of their neural networks are class probabilities.

5.4 Experiments

In this section, we provide numerical results of the proposed scheme. To this end, in Subsection 5.4.1, we present the datasets we use in the numerical results and in Subsection 5.4.2, the architectures of the neural networks are presented. The transmission cost model is presented in Subsection 5.4.4 and the Benchmark Schemes are described in Subsection 5.4.3. Finally, the numerical results are given in Subsection 5.4.5.

Table 5.1: Neural networks hyper-parameters

Parameter	Value, edge	Value, cloud
No. of hidden layers	2	2
No. of hidden units	30	1200
Learning rate	0.1	0.1
Batch size	100	100
Activation function	ReLU	ReLU
Dropout	0	0.2
Optimizer	SGD	RMSprop
Loss	Categorical Crossentropy	Categorical Crossentropy

5.4.1 Datasets

We conduct our experiments on MNIST [56], a publicly available dataset comprised of 60000 training images, and 10000 test images.

5.4.2 Architecture of the Neural Networks

The neural network at the cloud is comprised of 2 hidden layers, each with 1200 ReLU hidden units. This neural network is heavily regularized by using Dropout with probability 0.2. Dropout can be seen as using an even larger neural network comprised of an exponentially large ensemble of neural networks. On the other hand, the neural network at the IoT node is comprised of 2 hidden layers, each with 30 ReLU hidden units.

The neural network at the IoT node is trained using the knowledge distillation scheme presented in [50]. In particular, the i-th output of the neural network $q_i(t)$ is produced by using a "softmax" output layer that converts the logit, $z_i(i)$, into the class probability, $q_i(t)$, as

$$q_i(t) = \frac{\exp(z_i(t)/T)}{\sum_{j=1}^{M} \exp(z_j(t)/T)}, \tag{5.14}$$

where T is a temperature. Using a higher value for T produces a softer probability distribution over the classes, and thereby the class probabilities are comparable. Conversely, using a smaller value for T produces a harder probability distribution over the classes, and thereby the class probabilities significantly differ from each

other. This property of the temperature T is used for training the cumbersome neural network in the cloud and than distilling the model into a simpler model for the IoT node. In particular, we train the cloud model by using a high value for the temperature T, which results in a soft probability distribution over the classes. The soft probability distribution is then used to train the distilled neural network. Thereby, the soft predictions of the cumbersome neural network are used as labels for training the distilled neural network in a supervised manner to match those soft predictions. The same high temperature T is used when training the distilled neural network.

5.4.3 Benchmark Schemes

We use the following three benchmark schemes to compare the performance of our scheme.

Benchmark Scheme 1: As Benchmark Scheme 1, we consider the case when all data samples are transmitted to the cloud and thereby all inferences are made using the cloud neural network. This scheme has inference accuracy A_C and energy cost E_C.

Benchmark Scheme 2: As Benchmark Scheme 2, we consider the probabilistic scheme defined in Sec. 5.3.1. This scheme has inference accuracy A given by (5.7) and energy cost $E_{\max}$.

Benchmark Scheme 3: As Benchmark Scheme 3, we consider the case when none of the data samples are transmitted to the cloud and thereby all inferences are made using the distilled neural network at the IoT node. This scheme has inference accuracy A_0 and energy cost E_0.

Note that, Benchmark Schemes 1 and 3 can be considered as natural upper and lower bound on the inference accuracy of our proposed scheme.

5.4.4 Cost Model

In order to quantify the cost of transmission to the cloud, denoted by E, we assume that the IoT node is wirelessly connected to an access point (AP), whilst the AP is connected to the cloud server by means of a fronthaul link. Let the distance between the IoT node and the AP be denoted by d. Then, the signal-to-noise ratio

(SNR) of the link between the IoT node and the AP in time slot t, denoted by $\gamma(t)$, is found as

$$\gamma(t) = Pd^{-L}h(t)/\sigma^2, \tag{5.15}$$

where P denotes transmit power of the IoT node, σ^2 denotes the noise variance at the AP, $h(t)$ is an independently and identically distributed (i.i.d.) small-scale fading power coefficient of the link that follows an exponential distribution with unitary mean, and L is the path loss exponent. We assume that the IoT node and the AP employ type-I Hybrid Automatic Repeat reQuest (HARQ) in order to improve the transmission reliability. Next, we assume that the transmit message to the AP is of size B bits and the allocated spectrum for transmission is fixed to W. Then, the consumed energy for transmission to the AP is given by [57]

$$E = \frac{PB}{W\eta\log_2(1+\theta)}, \tag{5.16}$$

where η denotes the target success probability found as $\Pr(\gamma(t) \geq \theta) = \eta$ and the target threshold θ is given by

$$\theta = \frac{P\log\left(\frac{1}{\eta}\right)}{d^L\sigma^2}. \tag{5.17}$$

Note that, the IoT node requires additional energy in practice for waking up, computation, radio preparation, reception, turning off the radio, post-processing, initiating a turn off sequence, and going to sleep. However, those values are much lower then the energy required for transmission, so for the purposes of this section, we consider them negligible compared to E. Thereby, the energy cost of the cloud is given by $E_C = E$, where E is given by (5.16). On the other hand, the energy cost for an IoT inference is negligible compared to E_C and thereby it assumed to be $E_0 = 0$.

For the considered numerical example, we assume that $d = 100$ m and $L = 3$. In addition, we assume a bandwidth of $W = 100$ kHz. The noise power is set to $\sigma^2 = -90$ dBm. The transmit power of the IoT node is set to $P = 20$ dBm.

5.4.5 Results

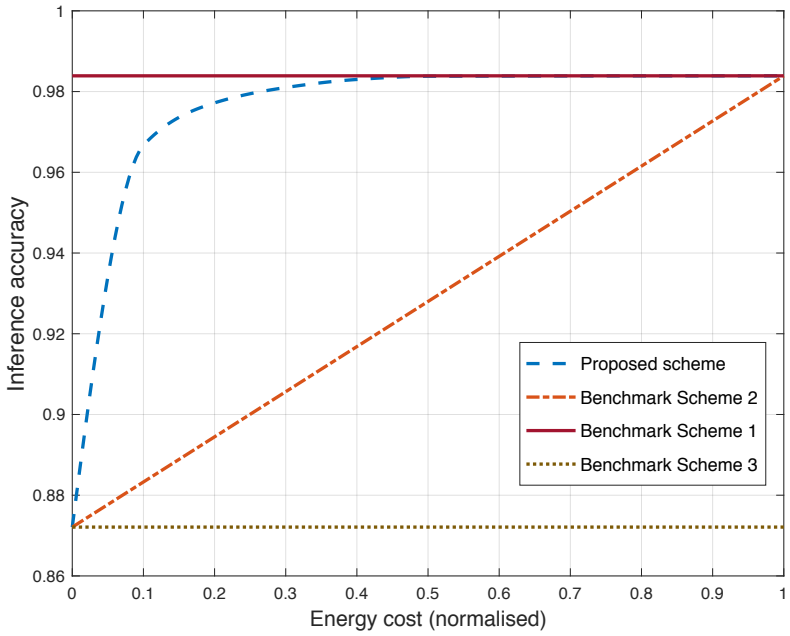

Figure 5.1: Inference accuracy as a function of the normalized energy cost.

In Fig. 5.1, we present the inference accuracy as a function of the normalized energy cost. The normalized energy cost is the incurred energy cost at the IoT node normalized by E_C. Note that the normalized energy costs of Benchmark Schemes 1 and 3 are constant and equal to 1 and 0, respectively. As expected, Benchmark Scheme 1 offers the best performance in terms of accuracy, at the expense of the highest possible energy cost since all inferences are made by the cloud. Conversely, Benchmark Scheme 3 offers the lowest inference accuracy since all inferences are made by the IoT node, but the incurred cost is lowest as well. As it can be seen, the inference accuracy of the proposed scheme is much better then Benchmark Scheme 3 and is comparable to the inference accuracy of Benchmark Scheme 1. It is also interesting to note that the inference accuracy of the proposed scheme converges to the inference accuracy of the cloud for relatively modest energy costs. The reason for this is because higher energy cost results in a lower transmission threshold α, which in turn leads to sending more samples with even higher confidence metric to

the cloud. As a result, at the IoT node are left only samples with very high confidence metric, which the IoT node can easily classify, i.e., classify as accurately as the cloud. In addiction, the proposed scheme significantly outperforms Benchmark Scheme 2, for the same incurred energy cost, since the proposed scheme is able to detect the "bad" data samples that should be transmitted to the cloud compared to Benchmark Scheme 2, which cannot distinguish between "bad" and "good" data samples. In fact, note that due to the uniform probability of transmission, the accuracy of Benchmark Scheme 2 is indeed a linear function of the energy cost as (5.7) suggests.

5.5 Conclusion

In this chapter, we proposed a scheme that the IoT device can employ to select the data samples that would likely lead to inaccurate inferences if processed locally so that those data samples are transmitted to the cloud. As a result, local inferences are made only when the neural network at the IoT node is confident in the respective inference. Consequentially, the overall inference precision of the system is significantly improved for a given energy cost compared to the case when the inference is always made locally at the IoT device. In particular, numerical results indicate that the proposed selection scheme achieves almost the same inference accuracy as the cloud but with a fraction of the energy cost.

Chapter 6

Concluding Remarks and Future Research Directions

In this final chapter, we provide the concluding remarks, and we discuss some future research directions.

6.1 Concluding Remarks

Communication technology has enjoyed unprecedented success in the last few decades, resulting in the vast majority of us humans to be already connected via smartphones or with feature phones. In conjunction, we also use connected cameras that automatically upload pictures to the cloud, or simple wireless sensors that can keep track of temperature and humidity, provide tracking of cargo containers, or measure water or electricity consumption. As the backbone of the IoT, such MTC devices are expected to be the primordial focus of next-generation wireless networks, targeting energy and spectraly efficient connectivity solutions. In this thesis, we targeted both, and we proposed novel communication protocols for WPCNs and MTC networks more broadly. The contributions of this thesis can be summarised as follows.

- We derived the capacity of the fundamental building block of FD WPCNs, and we showed that it is achieved with a relatively simple coding scheme, where the input probability distribution at the EHU is zero-mean Gaussian

and where the ET transmits only one symbol. In addition, we showed that the capacity achieving scheme offers significant gains in terms of data rate compared to HD transmission.

- We derived an upper bound on the secrecy capacity and an achievable secrecy rate that can be achieved with relative low complexity. We also showed that the proposed coding scheme achieves higher secrecy rates compared to the conventional HD-based schemes, even in the case when the channel between the EHU and the ET is worse, on average, than the channel between the EHU and EVE.

- We proposed a DRL-aided RA scheme for a network of K IoT nodes and an AP. We leveraged expert knowledge in order to ensure faster training of the DRL agent. By using publicly available data sets, we showed significant improvements in terms of packet rate, when the proposed DRL-aided RA scheme is implemented, compared to the conventional RA scheme.

- We proposed a data selection scheme that IoT devices can employ in order to select which data samples should be transmitted via the wireless channel, based on inference confidence. We showed that the overall inference precision of the system is significantly improved for a given energy cost compared to the case when the inference is always made locally at the IoT device.

6.2 Future Research

The ideas provided in this thesis create many new research leads worth exploring. Some of them are listed below.

- Investigating the capacity and the secrecy capacity of more complex WPCNs of a massive number of EHUs, ETs and/or EVEs. This requires a new information-theoretical analysis, which may be informed by the results in Chapters 2 and 3. In addition, designing practical coding schemes that achieve the capacity and secrecy capacity for such networks remains an open problem.

- Designing explicit medium access control protocols which account for the semantic content of the packets they are designed to deliver. To this end, the results in Chapters 4 and 5 can be combined in order to design a scheme that grants RBs to devices that are active and also make inaccurate inferences (as opposed to granting RBs to devices that are only active, as in Chapter 4). This inevitably means that the statistical properties of the data must be learnt, in addition to the statistics of the activation of the devices.

- Finally, it would be interesting to consider WPCNs of a massive number of machine-type devices, and apply semantic medium access control protocols. The severity of the energy constraints in this case might force the devices to make local inferences more frequently, especially if a large portion of resources is spent on signalling as is the case with the RA procedure. This might jeopardise the overall inference precision. Thereby, preallocation of RBs as in Chapter 4 might prove vital in order to guarantee reliable operation.

WPCNs and MTC networks will remain vibrant research areas for some time to come. It is my hope that the ideas presented in this thesis will serve as inspiration for future research efforts that will facilitate a data-driven society, enabled by reliable and efficient connectivity solutions.

Bibliography

[1] C. E. Shannon, "A mathematical theory of communication," *Bell system technical journal*, vol. 27, no. 3, pp. 379–423, 1948. → page 1

[2] R. Ratasuk, A. Prasad, Z. Li, A. Ghosh, and M. A. Uusitalo, "Recent advancements in m2m communications in 4g networks and evolution towards 5g," in *2015 18th International Conference on Intelligence in Next Generation Networks*, Feb 2015. → pages 1, 44

[3] D. Gunduz, K. Stamatiou, N. Michelusi, and M. Zorzi, "Designing intelligent energy harvesting communication systems," *IEEE Communications Magazine*, vol. 52, no. 1, pp. 210–216, January 2014. → page 1

[4] C. K. Ho and R. Zhang, "Optimal energy allocation for wireless communications with energy harvesting constraints," *IEEE Transactions on Signal Processing*, vol. 60, no. 9, pp. 4808–4818, Sept 2012. → page 2

[5] S. Bi, Y. Zeng, and R. Zhang, "Wireless powered communication networks: An overview," *IEEE Wireless Communications*, vol. 23, no. 2, pp. 10–18, April 2016. → page 2

[6] L. R. Varshney, "Transporting information and energy simultaneously," in *2008 IEEE International Symposium on Information Theory*, July 2008, pp. 1612–1616. → page 2

[7] K. Han and K. Huang, "Wirelessly powered backscatter communication networks: Modeling, coverage, and capacity," *IEEE Transactions on Wireless Communications*, vol. 16, no. 4, pp. 2548–2561, 2017. → page 2

[8] N. Deng and M. Haenggi, "The energy and rate meta distributions in wirelessly powered d2d networks," *IEEE Journal on Selected Areas in Communications*, vol. 37, no. 2, pp. 269–282, 2018. → page 2

[9] S. Biswas, S. Vuppala, and T. Ratnarajah, "On the performance of mmwave networks aided by wirelessly powered relays," *IEEE Journal of Selected Topics in Signal Processing*, vol. 10, no. 8, pp. 1522–1537, 2016. → page 2

[10] S. Gong, S. Ma, C. Xing, Y. Li, and L. Hanzo, "Multi-antenna aided secrecy beamforming optimization for wirelessly powered hetnets," *IEEE Transactions on Wireless Communications*, 2020. → page 2

[11] E. Everett, A. Sahai, and A. Sabharwal, "Passive self-interference suppression for full-duplex infrastructure nodes," *IEEE Trans. on Wireless Communications*, vol. 13, no. 2, pp. 680–694, Feb. 2014. → page 3

[12] C. R. Anderson, S. Krishnamoorthy, C. G. Ranson, T. J. Lemon, W. G. Newhall, T. Kummetz, and J. H. Reed, "Antenna isolation, wideband multipath propagation measurements, and interference mitigation for on-frequency repeaters," in *IEEE SoutheastCon, 2004. Proceedings.*, March 2004, pp. 110–114. → page 3

[13] M. Duarte, C. Dick, and A. Sabharwal, "Experiment-driven characterization of full-duplex wireless systems," *IEEE Trans. on Wireless Communications*, vol. 11, no. 12, pp. 4296–4307, Dec. 2012. → page 3

[14] B. P. Day, A. R. Margetts, D. W. Bliss, and P. Schniter, "Full-duplex mimo relaying: Achievable rates under limited dynamic range," *IEEE Journal on Selected Areas in Communications*, vol. 30, no. 8, pp. 1541–1553, September 2012. → page 3

[15] M. Duarte, A. Sabharwal, V. Aggarwal, R. Jana, K. K. Ramakrishnan, C. W. Rice, and N. K. Shankaranarayanan, "Design and characterization of a full-duplex multiantenna system for wifi networks," *IEEE Trans. on Vehicular Technology*, vol. 63, no. 3, pp. 1160–1177, March 2014. → page 3

[16] S. Haddad, A. Özgür, and E. Telatar, "Can full-duplex more than double the capacity of wireless networks?" in *Proc. Information Theory (ISIT), 2017 IEEE International Symposium on*, 2017, pp. 963–967. → page 3

[17] C. E. Shannon, "Communication theory of secrecy systems," *The Bell System Technical Journal*, vol. 28, no. 4, pp. 656–715, Oct. 1949. → pages 3, 4

[18] A. D. Wyner, "The wire-tap channel," *The Bell System Technical Journal*, vol. 54, pp. 1355—-1387, 1975. → page 4

[19] V. W. Wong, R. Schober, D. W. K. Ng, and L.-C. Wang, *Key technologies for 5G wireless systems*. Cambridge university press, 2017. → pages 5, 44, 53, 58

[20] 3GPP, "Medium access control (mac) protocol specification," *3GPP TS 38.321 V0.0.3*, May 2017. → pages 6, 44, 49, 57

[21] A. Laya, L. Alonso, and J. Alonso-Zarate, "Is the random access channel of lte and lte-a suitable for m2m communications? a survey of alternatives." *IEEE Communications Surveys and Tutorials*, vol. 16, no. 1, pp. 4–16, 2014. → pages 6, 44

[22] W. Weaver, "Recent contributions to the mathematical theory of communication," *ETC: a review of general semantics*, pp. 261–281, 1953. → page 6

[23] OpenAI, "Artificial intelligence and compute." [Online]. Available: https://openai.com/blog/ai-and-compute/ → pages 6, 66

[24] R. S. Sutton and A. G. Barto, *Reinforcement learning: An introduction*. MIT press Cambridge, 1998, vol. 1, no. 1. → pages 45, 53

[25] M. Bkassiny, S. K. Jayaweera, and K. A. Avery, "Distributed reinforcement learning based mac protocols for autonomous cognitive secondary users," in *Wireless and Optical Communications Conference (WOCC), 2011 20th Annual*. IEEE, 2011, pp. 1–6. → page 45

[26] Y. Chu, P. D. Mitchell, and D. Grace, "Aloha and q-learning based medium access control for wireless sensor networks," in *Wireless Communication Systems (ISWCS), 2012 International Symposium on*. IEEE, 2012, pp. 511–515. → page 45

[27] O. Naparstek and K. Cohen, "Deep multi-user reinforcement learning for dynamic spectrum access in multichannel wireless networks," *arXiv preprint arXiv:1704.02613*, 2017. → page 45

[28] Y. Yu, T. Wang, and S. C. Liew, "Deep-reinforcement learning multiple access for heterogeneous wireless networks," *arXiv preprint arXiv:1712.00162*, 2017. → page 45

[29] S. Wang, H. Liu, P. H. Gomes, and B. Krishnamachari, "Deep reinforcement learning for dynamic multichannel access," in *International Conference on Computing, Networking and Communications (ICNC)*, 2017. → page 45

[30] L. M. Bello, P. Mitchell, and D. Grace, "Application of q-learning for rach access to support m2m traffic over a cellular network," in *European Wireless 2014; 20th European Wireless Conference*. VDE, 2014, pp. 1–6. → page 45

[31] J. Moon and Y. Lim, "Access control of mtc devices using reinforcement learning approach," in *2017 International Conference on Information Networking (ICOIN)*. IEEE, 2017, pp. 641–643. → page 45

[32] ——, "A reinforcement learning approach to access management in wireless cellular networks," *Wireless Communications and Mobile Computing*, vol. 2017, 2017. → page 45

[33] L. Tello-Oquendo, D. Pacheco-Paramo, V. Pla, and J. Martinez-Bauset, "Reinforcement learning-based acb in lte-a networks for handling massive m2m and h2h communications," in *2018 IEEE International Conference on Communications (ICC)*. IEEE, 2018, pp. 1–7. → page 45

[34] Y.-J. Liu, S.-M. Cheng, and Y.-L. Hsueh, "enb selection for machine type communications using reinforcement learning based markov decision process," *IEEE Transactions on Vehicular Technology*, vol. 66, no. 12, pp. 11 330–11 338, 2017. → page 45

[35] A. Mohammed, A. S. Khwaja, A. Anpalagan, and I. Woungang, "Base station selection in m2m communication using q-learning algorithm in lte-a networks," in *2015 IEEE 29th International Conference on Advanced Information Networking and Applications*. IEEE, 2015, pp. 17–22. → page 45

[36] T. Park, N. Abuzainab, and W. Saad, "Learning how to communicate in the internet of things: Finite resources and heterogeneity," *IEEE Access*, vol. 4, pp. 7063–7073, 2016. → page 45

[37] L. Ferdouse, A. Anpalagan, and S. Misra, "Congestion and overload control techniques in massive m2m systems: A survey," *Transactions on Emerging Telecommunications Technologies*, vol. 28, no. 2, p. e2936, 2017. → page 46

[38] M. Vilgelm, S. R. Liñares, and W. Kellerer, "Dynamic binary countdown for massive iot random access in dense 5g networks," *IEEE Internet of Things Journal*, vol. 6, no. 4, pp. 6896–6908, 2019. → page 49

[39] V. Mnih, K. Kavukcuoglu, D. Silver, A. A. Rusu, J. Veness, M. G. Bellemare, A. Graves, M. Riedmiller, A. K. Fidjeland, G. Ostrovski *et al.*,

"Human-level control through deep reinforcement learning," *Nature*, vol. 518, no. 7540, p. 529, 2015. → page 53

[40] T. Inoue, S. Choudhury, G. De Magistris, and S. Dasgupta, "Transfer learning from synthetic to real images using variational autoencoders for precise position detection," in *2018 25th IEEE International Conference on Image Processing (ICIP)*, Oct 2018, pp. 2725–2729. → page 53

[41] A. N. C. Kim, E. Variani and M. Bacchiani, "Efficient implementation of the room simulator for training deep neural network acoustic models," 2019. → page 53

[42] G. C. Madueño, Č. Stefanović, and P. Popovski, "Reliable and efficient access for alarm-initiated and regular m2m in ieee 802.11 ah systems," *IEEE Internet of Things Journal*, vol. 3, no. 5, pp. 673–682, 2016. → page 53

[43] D. Murray and L. Stankovic, "Refit," *available on https://pureportal.strath.ac.uk/en/datasets/refit-electrical-load-measurements-cleaned*, 2016. → page 58

[44] S. De Vito, E. Massera, M. Piga, L. Martinotto, and G. Di Francia, "On field calibration of an electronic nose for benzene estimation in an urban pollution monitoring scenario," *Sensors and Actuators B: Chemical*, vol. 129, no. 2, pp. 750–757, 2008. → page 58

[45] N. Batra, O. Parson, M. Berges, A. Singh, and A. Rogers, "A comparison of non-intrusive load monitoring methods for commercial and residential buildings," *available on arXiv:1408.6595*, 2014. → page 58

[46] "Individual household electric power consumption data set." → page 58

[47] I. Goodfellow, Y. Bengio, A. Courville, and Y. Bengio, *Deep learning*. MIT press Cambridge, 2016, vol. 1. → page 58

[48] "Ra x drl," *https://github.com/ikoloska*. → page 61

[49] J. Chin, V. Callaghan, and I. Lam, "Understanding and personalising smart city services using machine learning, the internet-of-things and big data," in *Industrial Electronics (ISIE), 2017 IEEE 26th International Symposium on*. IEEE, 2017, pp. 2050–2055. → page 66

[50] C. Buciluǎ, R. Caruana, and A. Niculescu-Mizil, "Model compression," in *Proceedings, ACM SIGKDD International Conference on Knowledge Discovery and Data Mining*. ACM, 2006, pp. 535–541. → pages 67, 72

[51] J. Ba and R. Caruana, "Do deep nets really need to be deep?" in *Proceedings, Neural Information Processing Systems (NIPS)*, 2014, pp. 2654–2662. → page 67

[52] A. Mishra and D. Marr, "Apprentice: Using knowledge distillation techniques to improve low-precision network accuracy," *arXiv preprint arXiv:1711.05852*, 2017. → page 67

[53] T. Fukuda, M. Suzuki, G. Kurata, S. Thomas, J. Cui, and B. Ramabhadran, "Efficient knowledge distillation from an ensemble of teachers." in *Proceedings, Interspeech*, 2017, pp. 3697–3701. → page 67

[54] G. Chen, W. Choi, X. Yu, T. Han, and M. Chandraker, "Learning efficient object detection models with knowledge distillation," in *Proceedings, Neural Information Processing Systems (NIPS)*, 2017, pp. 742–751. → page 67

[55] J. Cui, B. Kingsbury, B. Ramabhadran, G. Saon, T. Sercu, K. Audhkhasi, A. Sethy, M. Nussbaum-Thom, and A. Rosenberg, "Knowledge distillation across ensembles of multilingual models for low-resource languages," in *Proceedings, IEEE International Conference on Acoustics, Speech and Signal Processing (ICASSP)*. IEEE, 2017, pp. 4825–4829. → page 67

[56] Y. Lecum, "Mnist." [Online]. Available: http://yann.lecun.com/exdb/mnist/ → page 72

[57] X. Chen, L. Jiao, W. Li, and X. Fu, "Efficient multi-user computation offloading for mobile-edge cloud computing," *IEEE/ACM Transactions on Networking*, vol. 24, no. 5, pp. 2795–2808, 2015. → page 74